UNIVERSITY OF CALGARY

Investigation of Mechanisms for Gravity Drainage in a Hele Shaw Cell

by

John Fredy Martínez Moná

A THESIS

SUBMITTED TO THE FACULTY OF GRADUATE STUDIES

IN PARTIAL FULFILMENT OF THE REQUIREMENTS FOR THE

DEGREE OF MASTER OF SCIENCE

GRADUATE PROGRAM IN CHEMICAL AND PETROLEUM ENGINEERING

CALGARY, ALBERTA

JANUARY, 2020

Abstract

Solvent recovery processes are potentially less energy and greenhouse gas intensive than thermal recovery methods because hydrocarbons are injected instead of steam. To date, an accurate model to predict oil recovery rates is lacking partly because the interplay of the mass transfer and convective mechanisms is still not well understood. In this thesis, a novel Hele-Shaw type apparatus was designed and commissioned to investigate these mechanisms in a controlled flow geometry. The apparatus consists of a Hele-Shaw cell (parallel glass plates) that can be partially filled with bitumen and rotated to set a target initial slope of the bitumen layer. Solvent is fed at the top of the bitumen at a constant volumetric flow rate. It flows along the bitumen surface, sweeps the bitumen that diffuses into this drainage layer, and is collected in sample vials. The flow rate, composition, and properties of the drained liquid are measured over time and photographs of the bitumen profile are taken periodically.

Gravity drainage was measured at ambient conditions for bitumen and toluene at injection flow rates from 0.1 to 2 cm^3/min, gap widths of 0.5 and 1 mm, and initial angles of inclination between 30 and 45°. The following recovery mechanisms were identified: 1) diffusion of bitumen into the drainage layer; 2) falling film flow of the drainage layer; 3) creep flow of the bitumen phase. A two-dimensional numerical model was developed where the bitumen was divided into columns, each with a solvent (drainage) layer and a bitumen layer. The drainage layer flow was modeled as a falling film. The mass transfer of bitumen into each solvent block was determined from Fick's First Law of diffusion with an infinite acting boundary condition. The diffused bitumen was assumed to be swept immediately to the next solvent block. Creep flow of bitumen under its own weight was included to predict the bitumen profiles. After each time step, a material balance was performed and the composition and fluid properties of each block were updated. The model with a single tuning parameter matched all of the bitumen production rates with an average deviation of 7.4%.

Acknowledgements

Getting a graduate degree from the University of Calgary has been by far the biggest and most rewarding challenge of my life and so many people helped and supported me during this process.

Primarily, I have to acknowledge my supervisor, Dr. Harvey Yarranton, for his endless and continuous support, patience, advice and encouragement. Thank you for sharing your knowledge with me and for always believing in me, your comforting words during challenging times were essential to my personal and professional growth. It has been a true privilege to be your student and to be part of your extraordinary research group. You have my most sincere and heartfelt respect, gratitude and admiration.

I owe a great deal of gratitude to the two lab managers of my research group. Florian, thank you for asking me those challenging questions that made possible the set-up of my equipment and the successful completion of my experiments. Your continuous guidance and commitment made me a better engineer and person. Elaine, thank you for your support, for allowing me to work in your lab, for teaching me how to improve my presentation and writing skills and for sharing your life experiences with me.

I am also grateful to Dr. Brij Maini, who helped me from the very beginning with this project. Thank you for guiding me through the process of designing my lab equipment and for your constant advice and feedback to complete the mathematical modeling for my thesis.

I want to acknowledge Dr. Kim Johnston for all her help and advice during my studies. I learned so much from you and I want to thank you for all your supporting words and teachings.

I want to give a special mention to Jose Santos, my colleague and one of my best friends, for his constant support and for always telling me that I should be very proud of myself for my accomplishments.

I want to extend my gratitude to my friends. Daniela and Tatiana, thank you for all these years of support and friendship. Andres and Nicolay, it just would not have been the same without you two. Andrea, you are a wonderful woman and friend. Thanks to previous and current members of the HOPP research group: Jairo, Adel, Sandra, Franklin, Yoshi, Yulman, Javier, Emilio, Nicson, Francisco and Amir. A few others deserve a mention here: Camilla, Marta, Diego, Maria E, Karen and Anderson. I consider myself lucky for meeting all of you at this amazing University.

Thanks to the NSERC Industrial Research Chair in Heavy Oil Properties and Processing, Schlumberger, CNRL, Suncor, CNOOC, VMG and Ecopetrol for funding this project. I also want to thank the staff in the Department of Chemical and Petroleum Engineering for their support.

Finally, I would like to thank my family for all their love and support. There is nothing I want more in life than making my mom, my dad, my brother and my sisters happy.

Dedication

To the five pillars and true loves of my life:

My mom Luz Fabiola, who taught me patience

My dad Fredy, who taught me courage

My sister Diana, the woman I have looked up to all my life, who taught me perseverance

My brother Mauricio, who taught me self-confidence

My sister Marcela, who taught me discipline

Table of Contents

List of Tables

List of Figures and Illustrations

List of Symbols, Abbreviations and Nomenclature

Upper Case Symbols

A : Proportionality constant in diffusivity-viscosity relationship

$\bar{A}$: Average Area of Contact [cm^2]

A_D : Cross sectional area for diffusion [cm^2]

A^* : Bitumen specific parameter in density correlation [kg/m^3]

A_0 : Fitting parameter for dilute gas viscosity

B : Specified Gap between the glass plates of the Hele-Shaw Cell [cm]

B^* : Bitumen specific parameter in density correlation [kg/m^3K]

B_0 : Fitting parameter for dilute gas viscosity

C_{min} : Minimum Concentration of solvent at which oil becomes mobile

C_{max} : Solubility of the solvent in the oil

D_{AB} : Diffusivity of species A in B [cm^2/s]

D_{BA} : Diffusivity of species B in A [cm^2/s]

D_{bs} : Diffusivity of bitumen in solvent [cm^2/s]

D_{sb} : Diffusivity of solvent in bitumen [cm^2/s]

D^* : Bitumen specific parameter in density empirical correlation [1/K]

E_0 : Fitting parameter for dilute gas viscosity

F_0 : Fitting parameter for dilute gas viscosity

F^* : Bitumen specific parameter in density empirical correlation [1/MPa]

$(H/C)_i$: Hydrogen/Carbon ratio of component *i*

K_o : Shape factor for Equation 5.4.

L : Basal Length of the Bitumen Layer in the Hele-Shaw Cell [cm]

MW : Molecular Weight [g/mol]

N_s : Dimensionless parameter for Equation 2.8

P : Pressure

Re : Reynolds number

ΔS_o : Change in Oil Saturation

SG : Specific gravity

T : Temperature

V_{binj} : Volume of injected bitumen [cm^3]

Lower Case Symbols

a_1^* : Fluid specific parameter in effective density correlation [kg/m^3]

a_2^* : Fluid specific parameter in effective density correlation [kg/m^3K]

b_1^* : Fluid specific parameter in effective density correlation [kg/m^3MPa]

b_2^* : Fluid specific parameter in effective density correlation [kg/m^3MPaK]

c_2 : Fluid specific parameter in Expanded Fluid viscosity model

c_3 : Fluid specific parameter in Expanded Fluid viscosity model

g : Gravitational acceleration [cm/s^2]

h : Calculated height of the bitumen in the Hele-Shaw Cell [cm]

h_b : Height of bitumen column [cm]

h_s : Film thickness [cm]

Δh_D : Effective height of the concentration gradient for mass transfer [cm]

$\vec{j}$: Mass flux of component [g/cm^2s]

k : Hele-Shaw cell permeability

m : Cementation factor

m_b : Mass of bitumen recovered [g]

m_{b_out} : Convective mass of bitumen leaving the solvent block [g]

m_{s_out} : Convective mass of solvent leaving the solvent block [g]

$\dot{m}_{C\_out}$: Mass flux between bitumen columns due to creeo flow [g/cm^2]

$\dot{m}_D$: Mass of bitumen diffused [g/s]

$\dot{m}_P$: Diluted bitumen mass flow rate [g/s]

n_b : Bitumen mass flux [$g/cm^2 \cdot min$]

nc : Number of components in a system

q_b : Drainage rate of bitumen

q_s : Solvent flow rate [cm^3/min]

t_{exp} : Time of experiment [h]

Δt : Time step [s]

$\bar{v}$: Average velocity in the solvent layer [cm/s]

v_{creep} : Velocity at which a fluid creeps between parallel plates [cm/s]

$\check{v}_b$: Molar volume of the bitumen at normal boiling [cm³/mol]

w_b : Bitumen mass fraction

w_s : Solvent mass fraction

Greek Symbols

β : Parameter in Expanded Fluid viscosity model

ϕ : Porosity

θ : Initial angle of inclination of the bitumen in the Hele-Shaw cell

θ_{ij} : Binary interaction parameter between in EF viscosity model

ρ_b : Density of bitumen [g/cm^3]

ρ_{mix} : Density of the mixture in the solvent block [g/cm^3]

ρ_s^0 : Compressed state density [kg/m^3]

ρ_s^* : Parameter in Expanded Fluid viscosity model [kg/m^3]

μ : Viscosity of a single fluid [mPa·s]

μ_b : Viscosity of bitumen [g/cm·s]

μ_D : Dilute gas viscosity [mPa·s]

μ_{mix} : Viscosity of the mixture in the solvent block [g/cm·s]

λ_o : Dimensionless parameter for Equation 5.4.

Superscripts

k : Time coordinate index in numerical models

∞ : Infinite dilution

Subscripts

b : Bitumen

i : Horizontal coordinate index in numerical models

j : Vertical coordinate index in numerical models

mix : Of a mixture

s : Solvent

Abbreviations

ARD	: Absolute Relative Deviation
AARD	: Average Absolute Relative Deviation
API	: American Petroleum Institute
ASTM	: American Society for Testing and Materials
CSI	: Cyclic Solvent Injection
CSS	: Cyclic Steam Stimulation
EF	: Expanded Fluid model
ES-SAGD	: Expanding Solvent Steam Assisted Gravity Drainage
LASER	: Liquid Addition to Steam for Enhancing Recovery
MAD	: Maximum Absolute Deviation
MARD	: Maximum Absolute Relative Deviation
SAGD	: Steam Assisted Gravity Drainage
SARA	: Saturates, Aromatics, Resins and Asphaltenes
SAS	: Steam Alternating Solvent
VAPEX	: Vapor Extraction Process

CHAPTER ONE: INTRODUCTION

The estimated worldwide reserves of crude oil is 1729 billion barrels of which 167 billion barrels (10%) are located in Canada (BP, 2019; "Energy Fact Book of Natural Resources of Canada," 2018). Approximately 96% of Canada's proven reserves are heavy oil and bitumen, defined as unconventional crude oils with API gravity in the range of 10-19° for heavy oil and below 10° for bitumen. The lower viscosity heavy oils can be recovered through conventional methods such as cold production, waterflooding and polymer flooding. However, the defining characteristic of a major portion of those fluids is their viscosity which can be as high as one million mPa·s at standard conditions (Gray, 2015) and practically immobile at reservoir pressure and temperature. In this thesis, heavy oil is used to refer to both heavy oil and bitumen unless otherwise noted.

Thermal recovery methods such as Cyclic Steam Stimulation (CSS) and Steam-Assisted Gravity Drainage (SAGD) are used to recover heavy oil and bitumen. In these processes, steam is injected at high temperature to heat up the fluid, reduce the viscosity and drain the now low viscosity oil by means of gravity. SAGD is the most extensively implemented method of heavy oil and bitumen recovery. However, the injection of steam requires the use of large volumes of water, consumes a considerable amount of energy to heat up the water and convert it into steam, and emits a significant amount of greenhouse gases to the atmosphere. In addition, thermal processes are not effective for thin, shallow or carbonate reservoirs.

Solvent-based and solvent-assisted recovery methods are a potential alternative to overcome (partially or totally) the disadvantages of purely thermal recovery methods. In these processes, solvent or a mixture of solvent and steam is injected into the reservoir through an injector well. The injected solvent diffuses into the bitumen, reduces its high viscosity and the low viscosity fluid drains to the producer well by means of gravity. Solvent recovery methods have lower energy requirements and use lower amounts of water, which reduces the greenhouse gas emissions and increases the efficiency. Examples of solvent-assisted recovery methods include Expanding Solvent SAGD (ES-SAGD) and Liquid Addition to Steam for Enhancing Recovery (LASER).

Examples of solvent-based recovery methods include Cyclic Solvent Injection (CSI), Vapour Extraction Process (VAPEX) and N-Solv process. These processes have been pilot tested in the field with mixed to poor results (Bayestehparvin *et al*, 2016, 2019; Castellanos-Diaz *et al.*, 2016; Chen *et al.*, 2018; Dittaro *et al.*, 2013; Gagliano *et al.*, 1994; Gupta and Gittins, 2006; Lin *et al.*, 2014). To date, only LASER (Liquid Addition to Steam for Enhancing Recovery) has been implemented on a commercial scale (Stark, 2013).

In solvent-based recovery methods, mass transfer between the solvent and the bitumen and gravity drainage are the main mechanisms of the process (see Figure 1.1). In this case, sufficient mass transfer rates are required to obtain economical oil rates. In solvent-assisted processes, heat transfer is a significant mechanism and mass transfer is a supplemental mechanism. In this case, the optimization of the combined heat and mass transfer is required. In both cases, the drainage process is further complicated by potential phase changes, such as asphaltene precipitation, when the solvent and heavy oil mix. Asphaltenes are the densest, most aromatic, and most polar fraction of a crude oil and they can form deposits in the reservoir and foul production equipment. Precipitation in the reservoir can upgrade the produced oil quality but may impede flow and oil recovery.

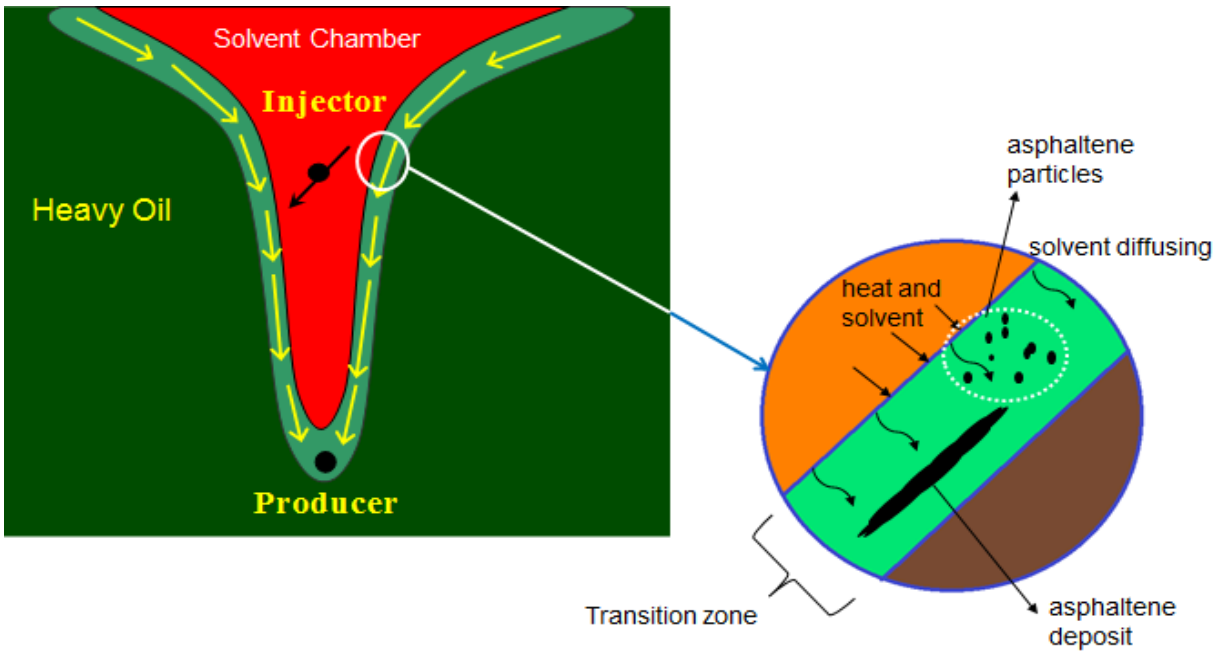

Figure 1.1. Schematic of the mechanisms involved in solvent recovery processes.

A complete and accurate understanding of the above mechanisms is necessary to design and optimize processes to recover heavy oil economically. This thesis focuses on mass transfer controlled (solvent-based) processes. Solvent based recovery methods have been studied at the lab scale using Hele-Shaw cells and sand packs (Butler and Mokrys, 1993; Jiang *et al.*, 2010; Rezaei et *al.*, 2010) and with numerical simulations (Cao, 2014; S. Das, 2005). Diffusion has been previously identified as the primary mass transfer mechanism between solvent and bitumen in the reservoir (Butler and Mokrys, 1989). However, dispersion may have a significant contribution under certain conditions (Boustani and Maini, 2001). Kapadia *et al.*, 2006 developed a mathematical model to calculate dispersion coefficient of butane in bitumen, obtaining values four orders of magnitude greater than previously reported diffusion coefficients. El-Haj *et al.*, 2009 reported dispersion coefficients of butane in heavy oil two orders of magnitude lower than those reported by Kapadia *et al*. Potential effects such as *in-situ* upgrading of bitumen after asphaltene precipitation and the effect on the recovery rates have also been investigated (Haghighat and Maini, 2010; James *et al.*, 2008; Nenniger and Dunn, 2018). Some of the studies reported enhanced oil production rate and some observed decreased production rates due to the potential offset by a reduction of permeability (Das and Butler, 1994). It is challenging to isolate and validate each mechanism because they act simultaneously in a constantly changing geometry.

The most established analytical model for solvent-based heavy oil recovery processes was first developed by Butler and Mokrys (1989) using a Hele-Shaw cell. The model matched Hele-Shaw experiments but under-predicted the production rates from sand-packed experiments (Das and Butler, 1994). Their model holds that the oil production to be proportional to the square root of the drainage height. Yazdani and Maini (2005) suggested a stronger dependency with their experiments in sand packs. Later on, Cuthiell and Edmunds (2013) simulated these sand pack experiments numerically and decreased the exponent of the height in the production rate and pointed out that convective dispersion depends on velocity and not on height. Hence, different authors disagree on fundamental relationships in the models. Other authors have attempted to propose scaling parameters to estimate production rates in the field, but have had poor predictions (Das and Butler, 1998). Finally, although experimental and simulation studies showed that solvents have potential as an alternative for heavy oil recovery, mixed to poor oil recovery rates during

field pilot tests have raised concerns related to the fundamentals behind the process. There appears to be a knowledge gap in the basic understanding of the mechanisms that drive the oil recovery in these processes and this gap translates into poor predictions when scaling lab results to pilot and field recovery rates.

1.1. Objectives

This thesis focuses on the understanding of the mass transfer and drainage mechanisms taking place during gravity drainage experiments for heavy oil and solvent systems. The goal is to investigate the interplay of the mass transfer and drainage mechanisms during solvent-based recovery of heavy oil. To do so, the primary objective of the thesis was to design and commission a Hele-Shaw (parallel glass plate) type apparatus to measure mass transfer and drainage rates in heavy oil and solvent systems with controlled geometries. In Hele-Shaw cells in the literature, the solvent is injected in a port above the production port and a steam chamber evolves around the injector and the interface between the solvent and bitumen has a variable and constantly changing geometry. In the new design, solvent is injected above an inclined plane of bitumen so that the interfacial geometry is well defined and consistent. This set up allows the roles of flow rate and velocity to be examined systematically for example by varying the injection rate and initial angle of inclination of the bitumen plane. A system consisting of a Western Canadian bitumen and toluene at ambient conditions is selected for this study. Toluene was selected to avoid asphaltene precipitation which would complicate the analysis of the process mechanisms. The experiments were performed at ambient conditions to avoid thermal effects.

The other specific objective of the thesis were to:

1. measure the heavy oil recovery rates, bitumen flux, bitumen surface profile, and the density and bitumen content of the produced fluid during gravity drainage experiments. Evaluate the following variables,
    a. gap widths of 0.5 and 1 mm between the glass plates of the Hele-Shaw cell.
    b. solvent injection flow rates from 0.1 and 2 cm^3/min.
    c. initial angles of inclination from 30 and 45 degrees.

2. develop a two-dimensional numerical model of the experiments including mass transfer and gravity drainage mechanisms.
3. identify the mechanisms and assumptions for the model that match the experimental data.

1.2. Thesis Structure

This thesis is divided into six chapters and the remaining five chapters are as follows.

Chapter Two reviews relevant background material for thermal and solvent recovery methods. Previous experimental, numerical and field studies are discussed, and the mass transfer and gravity drainage mechanisms are presented in detail. Previous models for solvent-based recovery processes and fluid property models are presented and discussed.

Chapter Three describes the design of the apparatus and the experimental procedures used in this thesis to collect the gravity drainage data. The tests used to commission the Hele-Shaw apparatus are also presented.

Chapter Four presents the numerical model developed in this thesis for a diffusion limited gravity drainage process in a Hele Shaw apparatus. The introduction into the model of creep flow of bitumen under its own weight is discussed. The density, viscosity and diffusivity models used within the mass transfer calculations are provided. The methodology to fit the model to bitumen recovery data is discussed in detail.

Chapter Five presents the measurements from the gravity drainage experiments. The results from the numerical model presented in Chapter 4 are compared with the experimental data. The roles of diffusive mass transfer, bitumen, and convective drainage mechanisms are examined for a system of toluene/bitumen at ambient conditions. The effects of gap width, toluene injection rate, and the initial inclination angle in the bitumen phase (geometry) are discussed.

Chapter Six provides a summary of findings and conclusions from this thesis. Recommendations for future research with the apparatus are also discussed.

CHAPTER TWO: LITERATURE REVIEW

In this chapter, the relevant background material for solvent based and solvent-assisted heavy oil processes is reviewed. Crude oil is defined and classified. Solvent-assisted and solvent-based recovery methods are described and classified with a focus on the latter. The gravity drainage and mass transfer mechanisms in solvent-based processes are discussed. Previous models for solvent-based recovery processes are reviewed and fluid property models for mixtures of heavy oil and solvent are presented.

2.1. Crude Oil: Definition and Classification

Petroleum is a naturally occurring material composed of thousands of hydrocarbon-based molecules with varying amounts of oxygen, nitrogen, sulfur, hydrogen and metals such as nickel and vanadium. This definition includes petroleum in gas phase (natural gas), liquid (crude oil), or solid (asphalt). Crude oils can be classified based on their viscosity and API gravity as conventional oil, heavy oil, or extra heavy oil, as shown in Table 2.1. When an extra heavy oil is immobile at reservoir conditions, it is commonly referred to as bitumen. In this thesis, heavy oil is used to refer to both heavy oil and bitumen except when discussing a specific bitumen.

Table 2.1. UNITAR Classification of Crude Oil (Gray, 2015).

Classification	API Gravity	Density kg/m^3	Viscosity $mPa{\cdot}s$
Conventional Oil	>20°	>900	$<10^2$
Heavy Oil	10-19°	900-1000	10^2-10^5
Extra Heavy Oil	<10°	>1000	$>10^5$

Although the UNITAR classification gives a general idea of the physical properties of a crude oil, it does not provide any information about its composition which ultimately defines its physical properties and thermodynamic behavior. Crude oil contains millions of different molecules and identifying each individual compound is very difficult (Rodgers and McKenna, 2011). Instead

crude oils are characterized in terms of chemical families, carbon number distributions, or boiling point distributions. The hydrocarbon components of crude oil fall into the following three main chemical classes (Speight and Özüm, 2001):

- Paraffins: saturated hydrocarbons including straight or branched chain alkanes (*n*-paraffins or isoparaffins, respectively). The molecular formula of paraffins is C_nH_{2n+2}.
- Naphthenes or cyclo-paraffins: saturated hydrocarbons with one or more cyclic rings which may have paraffinic side chains. Naphthenes with multiple rings are called fused if the rings share more than one carbon atom. The molecular formula of a single naphthenic ring is C_nH_{2n}.
- Aromatics: unsaturated hydrocarbons with one or more aromatic rings (benzene) in their molecular structure. Aromatic compounds may contain naphthenic rings and/or aliphatic side chains. Like naphthenes, aromatics can include multiple rings and the rings are termed fused if they share more than one carbon atom. The molecular formula for a single aromatic ring is C_nH_n.

As the molecular weight or boiling point of the crude oil fraction increases, the paraffin content decreases and the naphthene, aromatic, heteroatom (S, O, N) and metal (nickel, vanadium, copper and iron) content increases. For components with the same carbon number, alkanes have the lowest boiling point and aromatic and polyfunctional components have the highest boiling points. The relationship between the complexity of the crude oil molecules and the molecular weight and boiling point is illustrated in Figure 2.1 (Altgelt and Boduszynski, 1994).

Heavy oil is commonly characterized as a combination of different chemical families according to differences in polarity and polarizability in different solvents: saturates, aromatics, resins and asphaltenes (Speight, 2007). Saturates, aromatics and resins are adsorption class components. Saturates are a mixture of paraffinic and naphthenic compounds. Aromatics, resins and asphaltenes are a continuum of aromatic and polynuclear aromatic species of increasing molecular weight, density, aromaticity and heteroatom content. Asphaltenes are the heaviest and most polar fraction in the crude oil and are solubility class components, meaning that they are insoluble in paraffinic solvents, such as pentane or heptane, and soluble in aromatic solvents such as benzene or toluene.

Asphaltenes also tend to self-associate into nano-aggregates. The size distribution of the nano-aggregates likely depends on the composition of the oil and temperature but the average nano-aggregate is believed to consist of 5-10 molecules (McKenna *et al*., 2013; Yarranton *et al*., 2013).

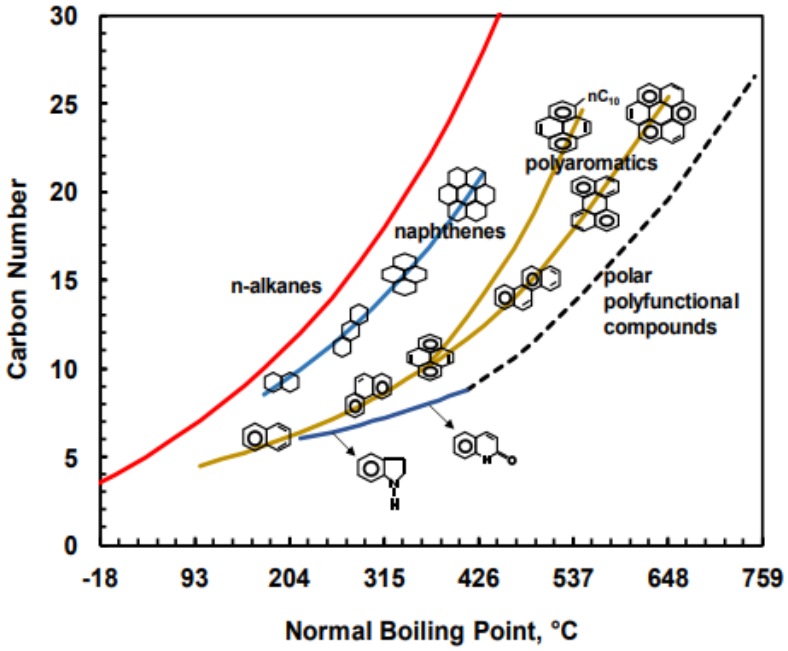

Figure 2.1. Relationship between carbon number, boiling temperature and structure of chemical compounds in crude oil. Adapted from Altgelt and Boduszynski (1994).

Compared to conventional oil, heavy oil has a higher viscosity and a lower API gravity, a higher content of aromatic and polyaromatic components, and a higher content of asphaltenes and heterocompounds. The mutual diffusivity of heavy oil and solvents is relatively low due to the high oil viscosity. These factors make heavy oil a challenging resource to recover and process. For example, the high viscosity of heavy oil, as high as 1,000,000 mPa·s at standard conditions, means that heat or dilution is required to flow the oil. The low mutual diffusivity with solvent leads to slow recovery rates for some processes involving solvent. The high asphaltene content creates a higher potential for coke formation in refining processes compared with conventional oils.

2.2. Heavy Oil Recovery Methods

There are four types of *in situ* recovery methods: cold production, thermal methods, solvent-assisted thermal methods, and solvent-based methods. Cold production involves the co-production of sand and heavy oil and has low recovery factors, typically between 10 and 15% (Kantzas and Brook, 2002). This review focuses on thermal and solvent methods.

2.2.1. Thermal Recovery Methods

Thermal methods are commercially successful and widely used in Canada to recover *in situ* heavy oil (Jimenez, 2008; Kamari *et al.*, 2015). In these methods, heat is supplied to the reservoir by injection of a hot fluid to decrease the viscosity of the heavy oil. Additional mechanisms such as rock and fluid expansion and compaction may occur (Zhao *et al.*, 2014). The two most successful methods used currently in the oil and gas industry are Cyclic Steam Stimulation (CSS) and Steam Assisted Gravity drainage (SAGD).

Cyclic Steam Stimulation (CSS)

In this method, steam is injected through a vertical well at high pressure (typically 10 MPa) for several days or weeks to heat the oil up to 200-300°C (Alvarez and Han, 2013). The well is then shut-in for a specific period, typically between one and two weeks (the "soaking" period), during which the steam condenses and allows uniform heat distribution into the formation. Finally, the well is put on production and the now mobile heavy oil, condensed steam, and gas to flow to the surface. Production is maintained until reaching an economic limit and then a new cycle of injection, soaking and production is started. The cycles are repeated until the ratio of produced oil to injected steam is considered uneconomic. Although the ultimate oil recovery is relatively low (typically between 10 and 40%), this method is used because it has quick payout (Kamari *et al.*, 2015).

Steam Assisted Gravity Drainage (SAGD)

The SAGD method was proposed by Roger Butler (Butler *et al.*, 1981) and first tested with a horizontal well pair in Cold Lake, Alberta (Bezaire and Markiw, 1979). As shown in Figure 2.2, a horizontal producer is located near the bottom of the heavy oil formation and a horizontal injector

is placed a few meters above the producer. Steam is injected into the formation through the upper well, creating a steam chamber that expands upwards and laterally. The heat from the steam reduces the heavy oil viscosity and the mobilized oil drains by gravity along with the condensed steam to the producer well. SAGD is best suited for reservoirs with thick pay-zones (> 15m), high vertical permeability, and no presence of thief zones (Edmunds and Chhina, 2001; Al Bahlani and Babadagli, 2008). SAGD is a mature commercial technique and has been successfully applied in a variety of fields (Jimenez, 2008).

Although CSS and SAGD have been applied successfully, they are unsuitable for reservoirs with a gas cap, a thin pay-zone, bottom aquifers, and low rock thermal conductivity. With a gas cap, the steam migrates to the gas zone and heat is lost to the overburden. In thin zones, there is excessive heat loss to the overburden and underburden. With bottom aquifers and low rock thermal conductivity, the energy efficiency is too low (Karmaker and Maini, 2003). In addition, SAGD has high operating costs from the production of steam and treatment of emulsions, and generates significant greenhouse gas emissions (Das, 1997; Luhning *et al.*, 2003).

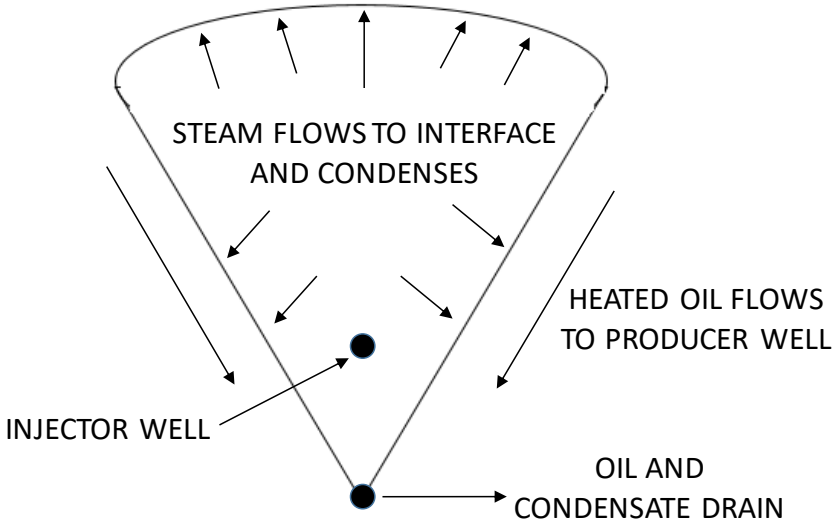

Figure 2.2. Schematic of Steam-Assisted Gravity Drainage. Adapted from Butler *et al*. (1981)**.**

2.2.2. Solvent-Based Recovery Methods

Solvent-based (and solvent-assisted) recovery methods aim to reduce the heavy oil viscosity with the injection and mutual dissolution of a solvent with the heavy oil. Some of the advantages of these recovery methods are better energy efficiency, cost effectiveness, produced oil quality, and lower greenhouse gas emissions (James *et al.*, 2008). However, few of these processes have yet achieved commercial success. The diffusion and dispersion of solvent into heavy oil is much slower than heat conduction limiting the production rates. Also, solvent is relatively expensive and solvent recovery is a critical economic factor. The solvent-based recovery processes that have been tested in the field include Cyclic Solvent Injection (CSI), vapor extraction (VAPEX), and N-Solv.

Cyclic Solvent Injection (CSI)

CSI is the solvent-based equivalent to Cyclic Steam Stimulation (CSS). In CSI, a vertical well is used for injection of a solvent or a mixture of solvents. The solvent increases the reservoir pressure and diffuses into the heavy oil by mass transfer and convective dispersion and reduces the oil viscosity during the soak period. Then the well is reopened to production and the low viscosity oil flows to the surface. The cycle of solvent injection, soaking, and production is repeated until reaching an economic limit.

CSI was first introduced in the 1970s (Allen, J.C., 1977; Allen *et al.*, 1976) when it was patented as a solvent injection process for heavy oil recovery using propane, butane, or a solvent mixture. In the 1980s, field studies were performed to evaluate the feasibility of CO_2 injection in a CSI process. Bardon *et al.* (1986) conducted a CSI pilot with CO_2 in the Camurlu Field in Turkey, running the first two cycles with an improved but short-lived response. In the third cycle, the CO_2 injection was increased by a factor of 10 and the production response was much better. They attributed the good response to an enhanced pressure build up caused by the increase in the injection of the solvent.

Lim *et al.* (1995) studied the injection of ethane in a 3D physical model saturated with Cold Lake bitumen. According to their results, the bitumen viscosity could be reduced by a factor of 1000 with the solubilization of solvent gas at ambient temperature and reservoir pressure. In the first

cycle they noticed a rapid decline in oil production, but in subsequent cycles the oil production increased due to the effect of gravity drainage. Additional experimental tests have been performed to evaluate the potential of CSI (Ahadi and Torabi, 2018; Alshmakhy and Maini, 2012; Dong *et al.*, 2006; Jiang *et al.*, 2014; Qazvini Firouz and Torabi, 2014; Shi and Kantzas, 2008; Sun *et al.*, 2015; Zhang and Kantzas, 2014). Final recovery factors depend on the pressure drop across the core, mobility ratio, type of solvent and core properties like length and porosity. The main drawback of CSI is the slow solvent diffusion in the heavy oil and fast reduction in the diluted oil production rate (Das and Butler, 1998).

Jia *et al.* (2015) simulated the mass transfer between solvent and heavy oil in the transition zone during the CSI process and developed a diffusion-convection model. The solution showed that when the reservoir pressure was not uniform, convective mass transfer improved solvent dissolution and a considerable amount of solvent remained in the reservoir at the end of the production period which is difficult to retrieve in the short term.

Vapor Extraction Process (VAPEX)

The vapor extraction process (VAPEX) is the solvent-based analogue to SAGD. In this process, solvent is injected in the vapor phase into a horizontal well where it diffuses/disperses into the heavy oil. The mixture of oil and solvent has a low enough viscosity to drain to the producing well by gravity. VAPEX was first introduced by Butler and Mokrys (1991). Since then, numerous experimental and simulation studies have been performed to understand and model the VAPEX process. Some experimental studies are summarized below. VAPEX modelling will be discussed later in this chapter.

Butler and Mokrys (1993) injected propane into a 2D sand-packed model and recovered 66% of the bitumen in 7 hours, higher than the recovery of 60% in 8 hours with injection of hot water and propane. They also noticed a significant reduction in the viscosity of the oil when propane was injected. Ethane injection showed poor response with only 26% recovery in 7 hours (Butler and Mokrys, 1993). One of the highlights of the results was the potential for *in-situ* upgrading of the bitumen when asphaltenes precipitated. Das and Butler (1994) further investigated asphaltene

deposition during VAPEX. Propane was injected into a Hele-Shaw cell filled with Peace River bitumen and regular patterns of precipitation were noticed. Production rates increased by at least 37% after the onset of precipitation, suggesting that a significant reduction in viscosity is achieved by deasphalting. However, part of the increased production potential could be offset by a reduction of permeability (Das and Butler, 1994).

Several studies have reported enhanced oil production with asphaltene precipitation (James *et al.*, 2008; Ardali *et al.*, 2009; Nenniger and Dunn, 2018; Rezaei and Chatzis, 2008) while others have observed decreased production rates (Haghighat and Maini, 2010; Luo *et al.*, 2008). Luo *et al.* (2008) studied asphaltene precipitation during VAPEX in a sand-packed high pressure physical model with propane and butane as solvents. When asphaltenes precipitated in a high permeability medium, the oil still drained readily by gravity and production rates were enhanced due the lower oil viscosity. However, in a low permeability medium, asphaltene deposition plugged the formation and production rates were reduced. They also noticed that reducing the operating pressure prevented asphaltene precipitation, but decreased the solubility of the solvent in the bitumen. Propane performed better than butane in terms of oil recovery, suggesting that lighter solvents suit VAPEX better than heavier solvents (Butler and Mokrys, 1993; Luo et *al.*, 2008). Ardali *et al.* (2009) reported an increased performance of VAPEX after asphaltene precipitation and concluded that an operating pressure close to the dew point and low permeability increased the probability of plugging (Ardali *et al.*, 2009). They also reported that the presence of connate water reduced asphaltene adsorption and lowered the chances of formation damage.

N-Solv

N-Solv was introduced by Nenniger (2008). It used the same well configuration as VAPEX but is a condensing process in which the solvent is injected at pressures and temperatures close to the saturation point, such that heat transfer to the oil causes condensation of the solvent when it contacts the heavy oil. Hence, the mass transfer occurs between heavy oil and liquid solvent instead of a gaseous solvent. Both heat transfer and dilution reduce the viscosity of the heavy oil and accelerate the extraction (Nenniger and Nenniger, 2005).

N-Solv benefits from faster mass transfer and some heat transfer. Liquid-liquid diffusion is higher than gas-liquid diffusion which is limited by the solubility of the gas in the liquid. James (2009) studied butane diffusion in heavy oil using glass micromodels and the interface advance velocity was four times higher in a solvent-condensing process compared to a non-condensing process. The improved rate was attributed to enhanced viscosity reduction due to heat transfer and a much higher concentration gradient in the condensing process (James, 2009). Enhanced oil recovery rates during experimental condensing-solvent processes have also been reported by other authors (Jiang *et al.*, 2010; Rezaei and Chatzis, 2007; Rezaei *et al.*, 2010). Cao (2014) performed numerical simulations using CMG and confirmed the extraction mechanisms of N-Solv (concentration gradient, surface renewal and sweep efficiency).

The presence of non-condensable gas (NCG) during N-Solv makes it more difficult for the solvent to contact heavy oil and hinders the heat transfer process (Nenniger and Dunn, 2008). Hence, solvent purity during the N-Solv process is a key parameter to ensure successful performance. The main concern with N-Solv is solvent migration into thief or non-targeted zones. Since N-Solv requires injection of large volumes of solvent, recovery of the solvent with the produced heavy oil is critical for the successful economic performance of the process. Evaluation of solvent migration requires field trials (Cao, 2014). N-Solv Corporation tested the process in the Dover lease between 2014 and early 2017, reporting a production of 25000 bbl. of heavy oil produced. The project also reported upgrading of heavy oil from 8° API to 14° API and an 80% reduction in greenhouse gas emissions (GHG). According to the report, 20% of the solvent was left behind (Bayestehparvin *et al.*, 2016, 2019).

2.2.3. Solvent-Assisted Thermal Methods

Solvent-assisted processes partially replace steam with solvent. These processes retain the benefits of heat transfer and reduce the energy requirements and greenhouse gas emissions of the process. The solvent-assisted thermal methods that have been field tested include Expanded Solvent Steam Assisted Gravity Drainage (ES-SAGD), Liquid Addition to Steam for Enhancing Recovery (LASER), and Steam Alternating Solvent (SAS).

Expanded Solvent Steam Assisted Gravity Drainage (ES-SAGD)

Expanded Solvent Steam Assisted Gravity Drainage (ES-SAGD) was first introduced in 2003 (Nasr *et al.*, 2003). In this process, a hydrocarbon solvent is co-injected with steam at a low concentration to improve the efficiency of SAGD. The solvent (or mixture of different solvents) is designed to condense at a similar temperature to steam at reservoir pressure. Mass and heat transfer occur simultaneously at the interface between the vapor chamber and the heavy oil. Among the advantages of ES-SAGD over SAGD are the higher diluted heavy oil flow rate, lower energy requirement after the decrease in the production of steam, and decrease in the water disposal requirement. The election of a proper solvent or mixture of solvents depends on availability, cost and saturation temperature (Deng *et al.*, 2010).

Although experimental and numerical studies have shown ES-SAGD as a good method to increase heavy oil recovery rates from SAGD after injection of solvents with intermediate carbon numbers (C_4 to C_8) (Akinboyewa *et al.*, 2010; Ardali *et al.*, 2012; Ayodele *et al.*, 2010; Boak and Palmgren, 2007; Ghasemi and Whitson, 2014; Govind *et al.*, 2008; Yazdani *et al.*, 2012), field implementation has shown mixed results. Some pilot tests have shown increases in hydrocarbon production, however, given the slow mass transfer rate between solvent and heavy oil, it is not clear if the increase in production is related with an increase in heavy oil production or simply because the injected solvent was being recovered (Dickson *et al.*, 2011; Dickson *et al.*, 2013a-b; Dittaro *et al.*, 2013; Khaledi *et al.*, 2014; Orr, 2009).

Liquid Addition to Steam for Enhancing Recovery (LASER)

In the Liquid Addition to Steam for Enhancing Recovery (LASER) process, a liquid hydrocarbon solvent is injected as an additive to the steam into a vertical well operating in cyclic steam stimulation mode. This process is expected to increase the oil recovery by at least 5% and reduce the greenhouse gas emissions by 25% (Stark, 2013). This method has been experimentally studied, numerically validated, and pilot tested by Imperial Oil (Léauté and Carey, 2007; Léauté, 2002). Although LASER operates in cyclic steam stimulation mode, at the later stage, the main mechanism acting for oil recovery is gravity drainage (Gates and Chakrabarty, 2008; Nasr and Ayodele, 2006). The percentage of the injected solvent that can be recovered is critical because it

defines the economic performance of solvent recovery methods. During the pilot at Cold Lake, 80% of the diluent was recovered in one cycle. However, after a second cycle with a diluent recovery factor of 53%, the repeatability and sustainability of LASER was not clear (Stark, 2013).

Steam Alternating Solvent (SAS)

The Steam Alternating Solvent (SAS) process uses the same well configuration as SAGD and steam and solvent are injected alternately. Alternating steam and solvent injection allows for a combination of the advantages of SAGD and VAPEX to decrease the energy requirements of the recovery process. First, steam is injected to heat the heavy oil, reduce the viscosity, and start the production process. When the heat losses become significant, the injection is then switched to solvent for diffusion into the heavy oil and further reduction of viscosity. The temperature of the chamber then decreases and injection is switched back to steam and the cycle repeats until it is no longer economical (Zhao, 2007).

The economic performance of SAS is determined by the energy intensity and oil production, which can be optimized through solvent selection and the duration of the steam and solvent injection periods (Zhao, 2004; Zhao, 2007). Experimental and numerical studies showed a decrease in energy intensity while maintaining similar rates of SAGD. In a subsequent laboratory study, Zhao *et al.* (2005) injected a mixture of methane and propane and reduced the energy input by 47%; however, the average oil production rate was lower compared to SAGD. Similar to LASER and other solvent recovery methods, SAS economic performance is highly dependent on the recovery of the injected solvent.

2.3. Mechanisms Involved in Solvent-Based Heavy Oil Recovery Methods

The two main mechanisms in solvent-based recovery processes are mass transfer and gravity drainage. Solvent-assisted processes also involve heat transfer. This thesis focuses on mass transfer and gravity drainage and heat transfer will not be reviewed further.

2.3.1. Gravity Drainage

Gravity drainage is the flow of denser reservoir fluids downward in the reservoir (Ahmed, 2010); for example, heated bitumen is denser than the surrounding steam and will drain downwards. The efficiency of gravity drainage increases as permeability increases and the oil viscosity decreases. During Solvent-Based extraction processes like VAPEX and N-Solv, mass transfer acts to reduce the viscosity of the oil and the low-viscosity mixture drains by means of gravity to the producer well. The relatively low viscosity solvent/oil mixture can be considered as a falling liquid film that moves with a velocity profile represented in Figure 2.3 when the fluid is flowing under laminar flow regime (Bird *et al.*, 2006). The falling film concept has been well studied and is used in this thesis. Details on the formulation will be presented and discussed in Chapter 4.

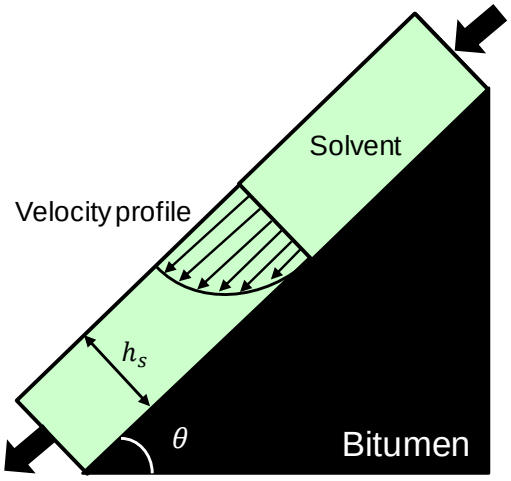

Figure 2.3. Schematic of a falling film of solvent flowing down an inclined plane of bitumen.

2.3.2. Mass Transfer

Mass transfer in the reservoir is governed by diffusion and dispersion. In the experiments performed in this thesis, diffusion occurs between a liquid solvent and heavy oil in an unpacked Hele-Shaw cell (no porous medium) and dispersion is assumed to be negligible since the drainage velocity was constant during the experiments. Therefore, diffusion is discussed in detail while dispersion is only reviewed briefly.

Diffusion

Diffusion is the net transport of matter within a single phase in the absence of external mechanical mixing or convection (Poling *et al.*, 2001). In solvent-based or assisted recovery processes where the solvent is in the liquid phase, a concentration gradient exists between the solvent and the heavy oil that causes molecules of solvent to transfer into the heavy oil and molecules of heavy oil to transfer into the solvent. In a typical mass transfer experiment, as shown in Figure 2.4, a column of Substance A is placed on top of a column of Substance B in a closed vessel. At the beginning, a well-defined interface separates the fluids. As time passes, molecules of Substance A move across the interface to the bottom, and molecules of Substance B move across the interface to the top. In other words, Substance A is diffusing into Substance B and *vice versa*. If the medium is considered isotropic (*i.e.*, no preferential paths) and the system isothermal and isobaric with no external force or field gradients and no reactions, the only driving force of diffusion is the concentration gradient.

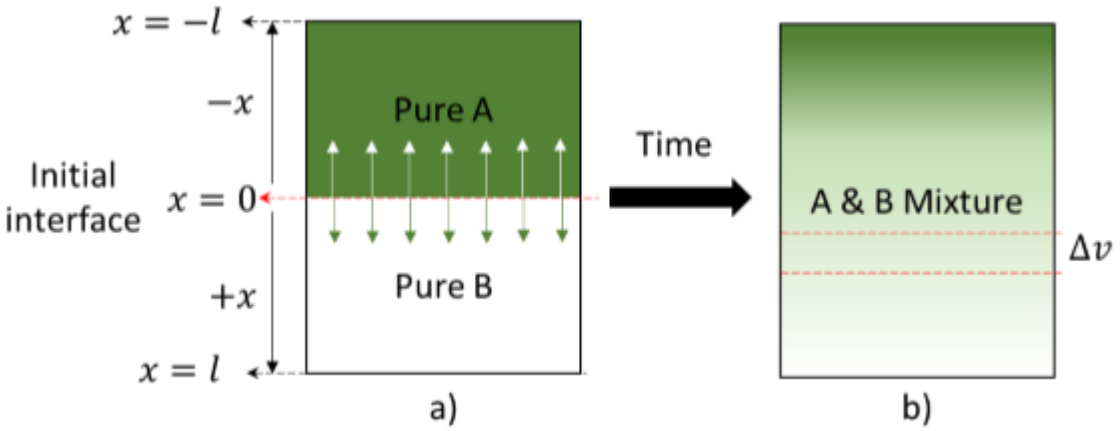

Figure 2.4. Schematic of a mass transfer experiment for an isotropic medium under isothermal and isobaric conditions with no external force or field gradients. a) initial condition; b) after some time.

A mass balance is performed on a control volume Δv, obtaining the following continuity equation after neglecting mass transfer due to flow and reactions (Bird *et al.*, 2006):

$$\frac{d(\rho \cdot w_A)}{dt} = -(\nabla \cdot \overrightarrow{J_A}) \tag{2.1}$$

where w_A is the mass fraction of component *A*, t is time, ρ is the density of the mixture and j_A is the mass flux. Diffusive mass transfer is governed by Fick's First Law, which states that the rate of transfer of a diffusing substance through a unit cross-sectional area is proportional to the concentration gradient (Bird *et al.*, 2006) and is given by:

$$\overrightarrow{J_A} = -\rho D_{AB} \nabla w_A \tag{2.2}$$

where D_{AB} is the diffusivity between components *A* and *B* in cm²/s, defined as the proportionality constant between the mass flux and the concentration gradient (Bird *et al.*, 2006). Depending on the system, diffusivity can be treated as a constant or as a function of concentration (Crank, 1975). Assuming one-dimensional, isothermal, isobaric diffusion system without reaction and without bulk flow, and combining Equations 2.1 and 2.2, the continuity equation simplifies to the following (Bird *et al.*, 2006):

$$\frac{\partial(\rho \cdot w_A)}{\partial t} = \frac{\partial}{\partial x}\left(\rho D_{AB} \frac{\partial w_A}{\partial x}\right) \tag{2.3}$$

where x is the position along the path of diffusion. If D_{AB} and ρ are constant, Equation 2.3 reduces to Fick's Second Law, given by:

$$\frac{\partial C_A}{\partial t} = D_{AB} \frac{\partial^2 C_A}{\partial x^2} \tag{2.4}$$

where C_A is the concentration of component *A*. The solution to Equations 2.3 or 2.4 depends on the nature, geometry, initial condition and boundary conditions of the system.

In Figure 2.1, Substance B is diffusing upwards and Substance A is diffusing downwards across the plane $x = 0$. Considering a one-dimension diffusion process, the mass fluxes of each substance are given by:

$$\overrightarrow{J_B} = -D_{BA} \frac{dC_B}{dx} \tag{2.5}$$

$$\overrightarrow{J_A} = -D_{AB} \frac{dC_A}{dx} \tag{2.6}$$

where D_{BA} is the diffusivity, a measure of how fast Substance B diffuses through Substance A and D_{AB} is a measure of how fast Substance A diffuses through Substance B. If there is no volume change upon mixing in either side of the plane $x = 0$, it can be proved that (Crank, 1975):

$$D_{AB} = D_{BA} \tag{2.7}$$

This equality implies that a single mutual diffusivity describes the behavior of a binary system with no volume change upon mixing. The mutual diffusivity is a function of the concentration of each component, temperature and pressure (Crank, 1975; Oballa and Butler, 1989).

Figure 2.5 shows the different types of diffusivity for a binary mixture of A (*n*-octane) and B (*n*-dodecane). The mutual diffusivity (D_{AB} or D_{BA}) represents the diffusion of each component in a binary mixture (line in Figure 2.2). The limiting values for the mutual diffusivity are the infinite dilution diffusivities. When the concentration of *A* tends to zero, the mutual diffusivity of A goes to the infinite dilution diffusivity of A in B, D_{AB}^{o}, which represents the diffusion of a molecule of A in a medium of pure B. Similarly, D_{BA}^{o} is the infinite dilution diffusivity of a molecule of B in pure A. The self-diffusion coefficients (symbols in Figure 2.5) represent the diffusivity of a given molecule in its own medium. Although the self-diffusion coefficient cannot be correlated to the mutual diffusivity, the mutual diffusivity must be lower than the maximum self-diffusion coefficient and higher than the minimum self-diffusion coefficient (Crank, 1975; Cussler, 2009; Oballa and Butler, 1989).

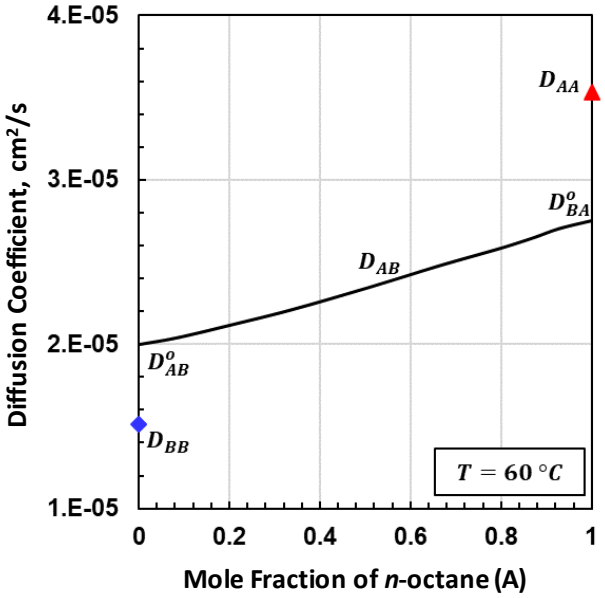

Figure 2.5. Mutual diffusivity, self-diffusivity and infinite diffusivity in a binary mixture of *n*-octane and *n*-dodecane. Adapted from Poling *et al.* (2001).

Dispersion

Dispersion is defined as an increased mixing caused by uneven fluid flow or concentration gradients resulting from fluid flow (Perkins and Johnston, 1963). This phenomenon was first described and studied by Taylor (1954), who performed experiments in capillary tubes and approximated a solution to the mass transfer profile of a pulse of brine injected into a flowing stream of water. Figure 2.6 illustrates the concept of dispersion in capillary tubes. A small amount of soluble material (represented by the black squares) is introduced into the flowing stream at time t_0. The material spreads gradually under the influence of the parabolic velocity profile created by wall effects. At time t_1, the material has adopted the shape of the velocity profile and a transverse concentration gradient has been created by the uneven movement of the fluid causing dispersion of the slug in the direction of the arrows. This form of dispersion is referred to as Taylor dispersion.

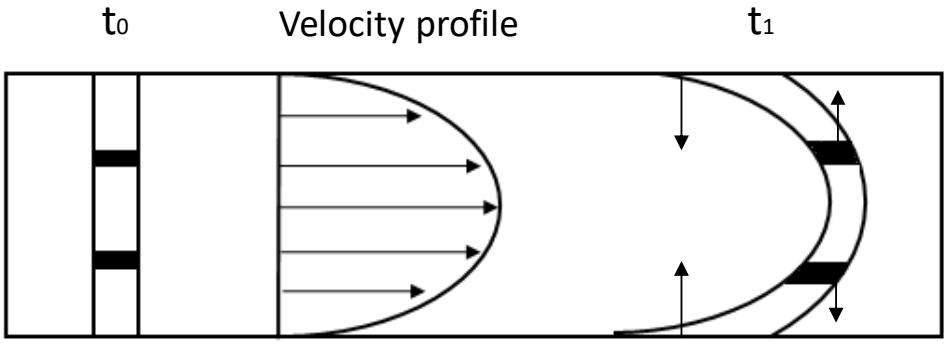

Figure 2.6. Concentration distribution due to velocity profile in capillary tubes. Adapted from Boustani and Maini (2001)and Taylor (1954).

Boustani and Maini (2001) suggested that a similar form of dispersion is created in a Hele-Shaw cell due to the velocity profile created when the fluid at the transition zone drains by gravity faster than the layer closer to the untouched heavy oil. Similarly, a velocity profile could be created from the center of the Hele-Shaw cell towards the walls and enhancing dispersion in that direction. (Boustani and Maini, 2001). Details of Hele-Shaw cells are discussed in Chapter 3.

An additional form of dispersion occurs in the case of fluid flow in porous media. Transverse dispersion is caused by the tortuosity of the porous medium and can be explained as a stream-

splitting mechanism (Perkins and Johnston, 1963) shown in Figure 2.7. Initially, Streams 1 and 2 are injected into the porous medium and the molecules are distributed across the flow channel until they reach Region a, where some molecules from Stream 1 transfer to Stream 2 and *vice-versa*. At Regions b and c, the streams split again and molecules continue flowing in different directions. The partition of the streams is highly dependent on the average flow rate (Blackwell, 1962). Transverse dispersion is also dependent on particle shape, particle size distribution, permeability, heterogeneity of the porous medium and viscosity (Perkins and Johnston, 1963).

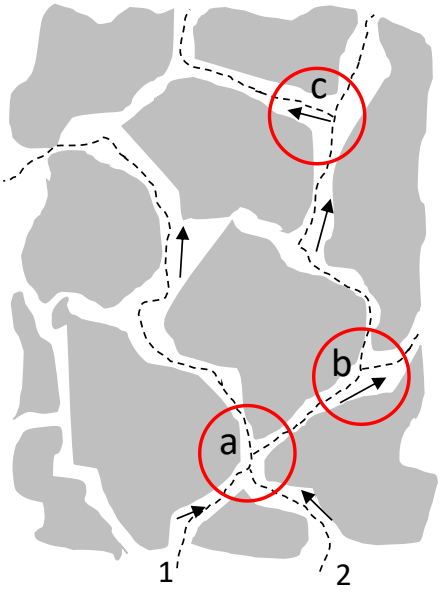

Figure 2.7. Microscopic dispersion in porous media. Adapted from Blackwell (1962).

2.4. Solvent-Based Heavy Oil Recovery Models

To date, the main analytical model for solvent-based heavy oil recovery processes is VAPEX model developed by Butler and Mokrys (1989) and furthered by others (Das and Butler, 1998; Dunn *et al.*, 1989). No other analytical models were found in the literature for solvent-based cyclic processes or for solvent-assisted steam processes.

Figure 2.8 shows a schematic of the vapor extraction process. The solvent in the vapour chamber diffuses/disperses directly into the bitumen creating a layer of lower density and viscosity liquid

that drains by gravity to the producer well. Depending on the type of solvent, asphaltene particles could precipitate, creating asphaltene deposits but giving a partially upgraded produced oil. Butler and Mokrys (1989) modeled the VAPEX process analogously to Butler's previously developed SAGD model (Butler *et al.*, 1981) by replacing the heat transfer contribution with a mass transfer contribution. The key assumptions are: 1) that the interface between the drainage layer and the undiluted bitumen moves at a constant velocity (*U*); 2) the mass occupying the space "swept" by the movement of the interface is equal to the mass that drains by gravity and is produced.

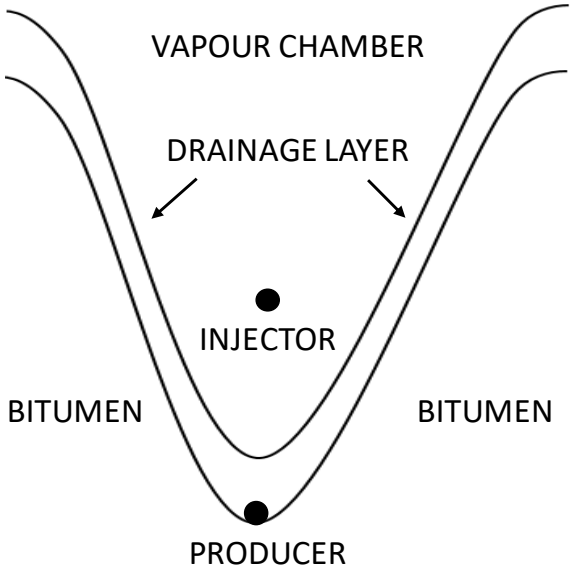

Figure 2.8. Schematic of the VAPEX process. Adapted from Pourabdollah and Mokhtari (2013).

Figure 2.9 shows a schematic of the mass transfer and gravity drainage components. To account for mass transfer, the concentration profile is integrated across the drainage layer, and the mixture in the layer moves at a velocity (*v*) towards the exit of the process. The bitumen drainage rate is given by (Butler and Mokrys, 1989):

$$q_b = \sqrt{2kg\phi\Delta S_o N_s h} \tag{2.8}$$

where q_b is the drainage rate, k is the Hele-Shaw cell permeability, g is the gravitational acceleration, ϕ is the porosity (equal to one for Hele-Shaw cells), ΔS_o is the change in oil saturation

(also equal to one in Hele-Shaw cells), h is the height of the draining layer and N_s is a dimensionless parameter related to the properties of the solvent and the heavy oil given by:

$$N_s = \int_{C_{min}}^{C_{max}} \frac{\Delta\rho D_s(1-C_s)}{\mu C_s} dC_s \tag{2.9}$$

where C_{min} is the minimum concentration of solvent at which oil becomes mobile, C_{max} is the solubility of the solvent in the oil, $\Delta\rho$ is the density difference between the oil and the solvent, D_s is the diffusivity, C_s is the solvent concentration and μ is the mixture viscosity. Since N_s is related only to physical characteristics of the heavy oil-solvent system, at constant pressure and temperature, it is expected to be constant (Butler and Mokrys, 1989). Das (1995) calculated the VAPEX parameter (a modified version of N_s) for numerous experiments in Hele-Shaw cell and confirmed the parameter to be constant within experimental error (Das, 1995). A scaling procedure was outlined to convert the Hele-Shaw results to reservoir conditions (Butler and Mokrys, 1991; Das, 1995). The drainage rate in a porous medium is given by:

$$q_b = \sqrt{2kg\phi^m \Delta S_o N_s h} \tag{2.10}$$

where m is the cementation factor, a measurement of the consolidation of the rock.

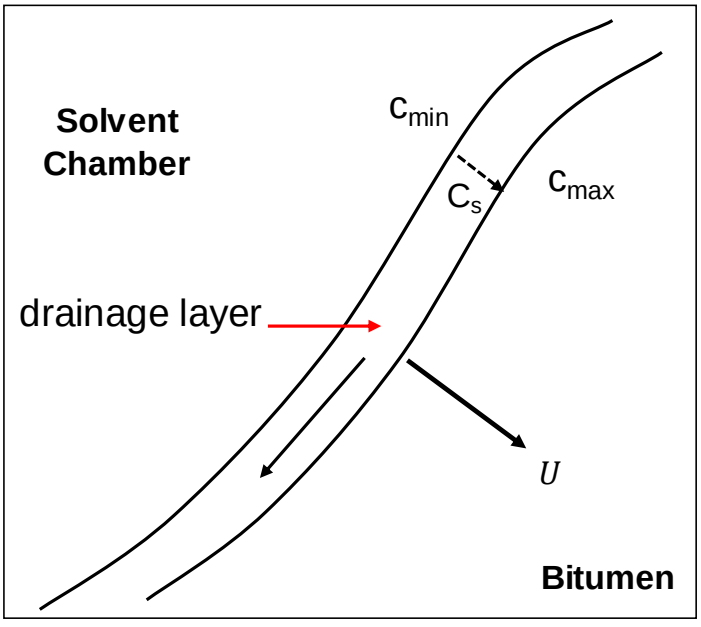

Figure 2.9. Representation of Mass Transfer and Drainage for VAPEX process. Adapted from Butler and Mokrys, 1989.

Das and Butler, (1994) found that this model under-predicted the production rates from sand-packed reservoir models for a propane VAPEX test by a factor of ten. This result suggested that the surface area for diffusion was higher and dispersion in porous media contributed to better mixing of solvent and heavy oil (Das, 1997; Das and Butler, 1998). Boustani and Maini (2001) investigated the mechanisms of VAPEX in a Hele-Shaw cell with Dover heavy oil and propane as the solvent. They determined the diffusivity of propane in heavy oil using a correlation (Hayduk *et al.*, 1973) and calculated N_s for a concentration equal to the solubility of propane in heavy oil using Eq. 2.9. They compared this analytical value with the experimental value of N_s calculated by fitting the gravity drainage data with Eq. 2.8. Figure 2.10 shows that the experimental N_s is two orders of magnitude greater than the analytical N_s, again suggesting that a second mechanism like dispersion is contributing to the drainage rate. The discrepancy between experimental and predicted rates decreased when a Taylor dispersion coefficient was included in the prediction of N_s.

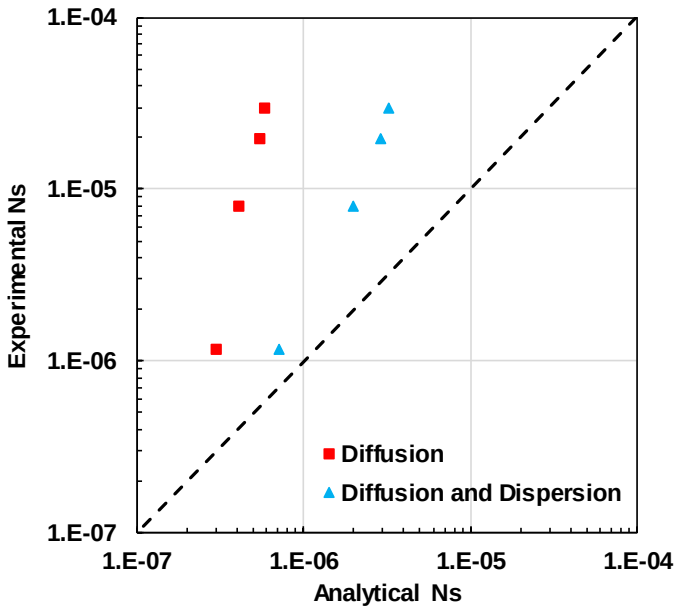

Figure 2.10. Comparison between analytical and experimental values of $\boldsymbol{N_s}$ parameter. Adapted from Boustani and Maini (2001).

Kapadia *et al.,* (2006) developed a mathematical model to describe VAPEX in a block of a porous medium to determine the dispersion coefficient of butane in Cold Lake bitumen. They chose the dispersion coefficient by matching previous published experimental results to the simulations, obtaining a value four orders of magnitude higher than previously reported diffusion coefficient of butane in heavy oil (Kapadia *et al.*, 2006). El-Haj *et al.* (2009) followed a similar methodology of comparing predicted and experimental production rates and obtained dispersion coefficients of butane in heavy oil two orders of magnitude lower than Kapadia *et al.* The dispersion coefficient is a function of solvent mass fraction, viscosity of the heavy oil, and permeability (El-Haj *et al.*, 2009; Kapadia *et al.*, 2006).

Yazdani and Maini (2005) studied VAPEX in a cylindrical annulus filled with different sand packs, using two different samples of heavy oil and injecting *n*-butane at a constant rate. Their results suggested the oil production rate to have a stronger dependency on the chamber height, contrary to Equation 2.10 which suggests that flow rate is proportional to the square root of the chamber height. They attributed this dependency to the higher convective dispersion in porous media (Yazdani and Maini, 2005). Their conclusion was challenged by Cuthiell and Edmunds (2013) who simulated the experiments numerically and found the solvent fraction in the produced oil increased as height increased, and as a consequence the production rate was higher. After removing the solvent mixing effect from the simulations, the exponent of the height in the production rate equation decreased from the range 1.1-1.17 to 0.86. They pointed out that convective dispersion depends on velocity and that there is no obvious dependence on height (Cuthiell and Edmunds, 2013).

Das and Butler (1998) proposed a scaling parameter for VAPEX given by:

$$a = \sqrt{2kg\phi^m \Delta S_o N_s} \tag{2.11}$$

where a is the VAPEX parameter which includes the properties of the system such as permeability, porosity, density, and viscosity (at the system temperature and pressure). The heavy oil flow rate is given by:

$$q_b = 2La\sqrt{h} \tag{2.12}$$

In Equation 2.12, the flow rate of heavy oil is multiplied by the length of the horizontal well and by a factor of two (the original equation considers the flow from one side of the VAPEX chamber). Since N_s is constant at fixed temperature and pressure, the results from one sand pack can be scaled to another a follows:

$$\frac{a_1}{a_2} = \sqrt{\frac{k_1 \phi_1^{m_1} \Delta S_{o_1}}{k_2 \phi_2^{m_2} \Delta S_{o_2}}} \tag{2.13}$$

Figure 2.11 shows that the flow rates from different sand packs predicted from this scaling method are up to ten times lower than experimental flow rates, indicating the model under-predicts the heavy oil flow rates. However, the results confirm that the heavy oil flow rate is proportional to the square root of the permeability of the porous medium.

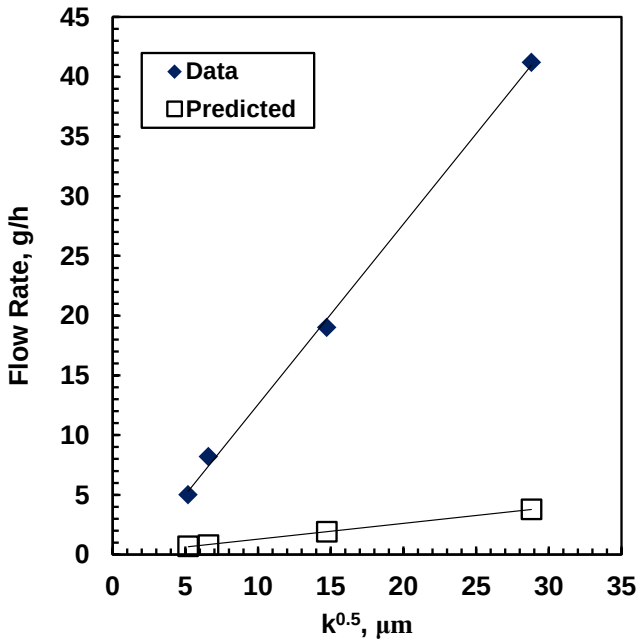

Figure 2.11. Comparison between predicted and experimental heavy oil flow rates using Peace River Bitumen and Butane in sand packs of different permeabilities at 21°C. (adapted from Das and Butler, 1998).

Nenniger and Dunn (2008) compiled a set of drainage rates from published data and developed a correlation to predict heavy oil production rates for solvent-based gravity drainage. The correlation is given by:

$$m = 43550\left(\frac{k\phi}{\mu}\right)^{0.51} \tag{2.14}$$

where m is the mass flux in g/m^2·h, k is the permeability of the medium in Darcies, ϕ is the porosity of the medium and μ is the heavy oil viscosity in mPa·s. The product $k\phi$ was previously identified as the grain size parameter (Yazdani and Maini, 2005). Nenniger and Dunn explained the dependence of the mass flux on the heavy oil viscosity as the representation of a "concentration shock mechanism" in which solvent penetration is shallow and surface renewal is fast. They concluded the correlation apparently resolved discrepancies between Hele-Shaw results and porous media results and contradicted previous experimental evidence that the drainage rate is proportional to the square root of the drainage height. As mentioned by the authors, the results were inconsistent with Butler's VAPEX model. However, they acknowledge limitations of the correlation in regards to accounting resistances to mass transfer like the presence of non-condensable gases or heterogeneities in the permeability (Nenniger and Dunn, 2008).

2.5. Properties of Mixtures of Heavy Oil and Solvent

The properties that are relevant for mass transfer and gravity drainage in the experiments performed in this thesis are density, viscosity, and diffusivity. Accurate determination of these properties is essential to model these experiments and solvent based processes in general. Methods to predict these properties from typically available data are reviewed below.

2.5.1. Density

The density of mixtures of solvent and bitumen can be modeled using cubic equations of state. Mehrotra and Svrcek (1985) modeled density of Alberta bitumen saturated with CO_2 and ethane using Peng-Robinson EoS with Lee-Kesler critical property correlations (Kesler and Lee, 1976). They matched the density of Athabasca bitumen to within 3.6% (Mehrotra and Svrcek, 1985).

Kokal and Sayegh (1990) modeled the density of an Alberta bitumen and determined the volume translation parameter for pure components below the critical temperature (Eq. 2.15) and above the critical temperature (Eq. 2.16) given by:

$$c = \bar{v} - \frac{RT_c}{P_c} Z_{RA}^{[1+(1-T_r)^{2/7}]} \tag{2.15}$$

$$c = \frac{RT_c}{P_c}(0.307 - Z_{RA}) \tag{2.16}$$

where c is the volume translation parameter, $\bar{v}$ is the liquid molar volume, R is the universal gas constant, Z_{RA} is the Racket compressibility factor, and T_c and P_c are the critical temperature and pressure, respectively. For mixtures, the volume translation parameter can be calculated using the following mixing rule:

$$c = \sum x_i c_i \tag{2.17}$$

where x is the mole fraction and subscript i refers to the component in the mixture.

Another approach to model the density of mixtures of heavy oil and solvents is to correlate the solvent and oil densities separately and use an excess volume based mixing rule to calculate the density of the mixture. Saryazdi *et al.* (2013) modeled the density of diluted bitumen mixtures with a deviation of less than 1% using a symmetric excess volume based mixing rule. The mixing rule includes a binary interaction parameter that can be fitted to the experimental data, or can be assumed to be zero in the case of a regular solution. The same approach will be used in this thesis and is presented in detail in Chapter 4.

2.5.2. Viscosity

Heavy oil viscosities are measured usually over range of temperatures at atmospheric pressure. Solvent viscosities are usually available in the literature. Measured mixture viscosities are usually sparse or not available. Hence, the viscosity of mixtures of heavy oil and solvent must be predicted. The methods available to predict these viscosities over a range of temperatures and pressures are: the Modified Walther model, the Corresponding States model, Friction Theory, and the Expanded Fluid model. The EF model is used in this thesis because it was designed specifically for heavy oils and has been shown to provide accurate results from mixtures of heavy oil and solvent

(Motahhari *et al.*, 2011; Ramos-Pallares *et al.*, 2016). It is presented in detail in Chapter 4. The other models are summarized briefly below.

Modified Walther Model

This method is an empirical correlation to model the viscosity of liquids, particularly hydrocarbons and crude oils. Walther (1931) related the viscosity to the temperature using logarithmic functions as follows:

$$\log(\log(\vartheta + c)) = b_1 + b_2 \log(T) \tag{2.18}$$

where ϑ is kinematic viscosity, T is temperature, b_1 and b_2 are fluid specific parameters and c ranges from 0.7 to 1. Several authors have fitted the Modified Walther equation to match viscosity data of crude oils and mixtures, including Athabasca and Peace River (Badamchi-Zadeh *et al.*, 2009a; Badamchi-Zadeh *et al.*, 2009b; Mehrotra and Svrcek, 1986, 1988), Cold Lake (Eastick and Mehrotra, 1990; Mehrotra, 1990) and Lloydminster heavy oil (Li *et al.*, 2013).

Yarranton *et al.*, 2013 included a third parameter into the correlation to account for changes in viscosity with pressure. The model was used to predict viscosity of characterized crude oils using a GC assay. Correlations were developed using the molecular weight of pseudo-components and obtained an average relative deviation of 44% in the predicted viscosity for crude oils from Canada, the Gulf of Mexico, the Middle East, Asia, and Europe. In this method, the GC assay must be extrapolated to account for the C_{30}^{+} fraction. This fraction makes up more than 70 wt% of a heavy oil. Hence, the viscosity prediction for heavy oils is highly sensitive to the extrapolation procedure (Ramos-Pallares *et al.*, 2017). The accuracy of the method improved to a deviation of 5% after tuning to a single viscosity measurement.

Corresponding States Model

This method is based on the corresponding states principle which states that for any compound, a given property can be related to that of a well-known reference substance in a corresponding state; that is at the same reduced temperature and pressure (Pedersen et *al.*, 1984). A reduced property is the value of the property divided by the value of the property at the critical point. In other words, two components at the same reduced temperature and pressure will have the same reduced

viscosity. Reduced properties for different species are all expected to follow the same relationship to their reduced temperature and pressure. Hence, the viscosity of one species can be determined from the viscosity of another. Typically, a substance with well-established viscosity behavior is selected as a reference fluid. The viscosity of any other substance is determined as follows (Hanley, 1976):

$$\mu_i(\rho, T) = \mu_o \left[\rho\left(\frac{\rho_{c,o}}{\rho_{c,i}}\right), T\left(\frac{T_{c,o}}{T_{c,i}}\right)\right]\left(\frac{M_i}{M_o}\right)^{1/2}\left(\frac{\rho_{c,i}}{\rho_{c,o}}\right)^{2/3}\left(\frac{T_{c,i}}{T_{c,o}}\right)^{1/2} \quad (2.19)$$

where μ is the viscosity, ρ is density, T is temperature and M is molecular weight. subscript i refers to any substance in the group, subscript o refers to the reference substance, and subscript c refers to the property evaluated at the critical point.

The original formulation was modified to predict viscosity of pure hydrocarbons and mixtures and by choosing methane as the reference substance; the viscosity of ethane, propane, butane, carbon dioxide and nitrogen were predicted. However, large deviations were observed at higher densities. Further modifications of the corresponding states model improved prediction for pure hydrocarbons and binary mixtures (Baltatu, 1982; Ely and Hanley, 1981; Pedersen and Fredenslund, 1987). However, tuning seems necessary to accurately match crude oil viscosity (Svrcek and Mehrotra, 1987; Lindeloff *et al*., 2004). The method is challenging to apply to heavy oils because heavy oil viscosities fall in a region where data are not available for reference fluids.

Friction Theory

This method describes the viscosity of a fluid as the result of an addition between a dilute gas viscosity contribution and a residual viscosity contribution which comes from friction between layers (Quiñones-Cisneros *et al.*, 2000):

$$\mu = \mu_G + \mu_F \quad (2.20)$$

where μ is the viscosity, μ_G is dilute gas viscosity and μ_F is the friction contribution. Dilute gas viscosity is calculated from a correlation (Chung *et al.*, 1988) and the friction contribution term is assumed to be a function of repulsive and attractive van der Waals pressure terms calculated from a cubic equation of state (EoS) such as Peng-Robinson (PR) or Soave-Redlich-Kwong (SRK). This model requires a high number of parameters. A version of the model with only one adjusted

parameter was proposed by Quiñones-Cisneros *et al.* (2001a) and was further developed to predict the viscosity of natural gas (Zéberg-Mikkelsen *et al.*, 2002) and crude oils with molecular weight less than 200 g/mol (Quiñones-Cisneros *et al*., 2001b, 2003). A two parameter version was developed by Quiñones-Cisneros *et al.* (2004, 2005) and fitted viscosity data of heavy oils with molecular weights up to 443 g/mol with an accuracy of 7.5%.

2.5.3. Diffusivity

The mutual diffusivity of liquid hydrocarbons and heavy oil are available in the literature and a detailed description of the measurement technique and modeling approaches can be found elsewhere (Grimaldos, 2018). The main observations on the diffusivities are summarized here.

Oballa and Butler (1989) used a free diffusion method to determine concentration profiles for toluene and heavy oil systems at ambient conditions. They used the Boltzmann-Transformation approach to calculate a concentration dependent diffusivity (Oballa and Butler, 1989). They found a non-physical maximum in the diffusivity at a heavy oil volume fraction of approximately 50%, as shown in Figure 2.12.

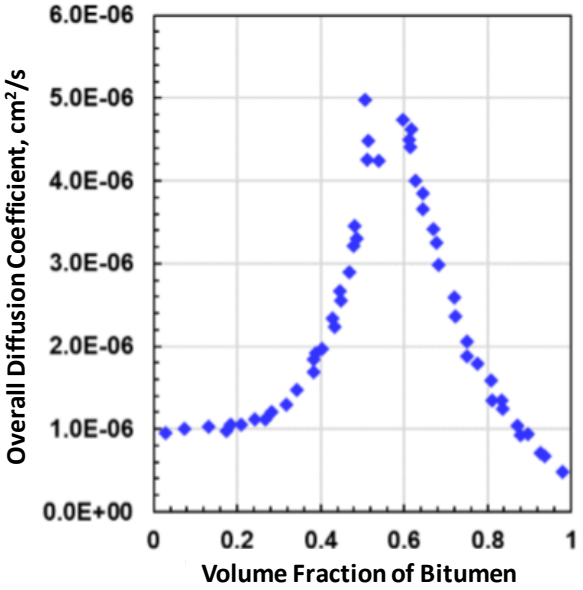

Figure 2.12. Diffusivity dependence on concentration for a toluene/heavy oil system at ambient conditions. Adapted from Oballa and Butler (1989).

A similar counterintuitive concentration dependence of the diffusivity was reported by Fadaei *et al.*, (2013) for toluene in Athabasca atmospheric residue as well as for other systems (Salama and Kantzas, 2005; Wen *et al.*, 2004; Wen and Kantzas, 2005). The counterintuitive concentration dependency is almost certainly related to the data analysis method. Zhang *et al.* (2007) and Zhang and Shaw (2007) noted that the Boltzmann-Transformation approach considered spatial density gradients to be negligible which might affect diffusivity calculations in a system of solvent/heavy oil where density gradients are high in early times (Zhang and Shaw, 2007; Zhang *et al.*, 2007).

Diedro *et al.* (2015) obtained concentration profiles using an x-ray technique and used the slope and intercept method to determine diffusivity of liquid dimethyl ether, propane, pentane and toluene into Peace River and Grosmont Bitumen at ambient temperature (22°C). They also determined diffusivity of vapour dimethyl ether and propane into the same samples of bitumen. For solvents in vapour phase, the pressures were close to the saturation pressure. They reported a monotonic change of diffusivity with concentration and concluding that for solvent concentrations below 50% volume the diffusivity could be considered constant. However, Fayazi *et al.* (2017) used the slope and intercept technique to determine the concentration dependence of diffusion of toluene into heavy oil and obtained abnormal trends. The inconsistent results using this latter technique may occur because, according to the conditions of the method, the plot of concentration as a function of distance on a semi-probability paper must lead to a curve with a straight line in the low and high concentration regions (Sarafianos, 1986). However, in hydrocarbon solvent and heavy oil systems, the plot is not linear in those regions.

Grimaldos (2018) measured concentration profiles during diffusion in solvent (toluene, *n*-pentane, and *n*-heptane) and heavy oil systems at ambient conditions. A cylindrical diffusion cell was partially filled with heavy oil and a column of solvent was placed above the heavy oil. The system was left to diffuse for a specified time and then displaced through a density meter to measure density over a series of height intervals. At each height, the solvent content was determined from the measured density and the known density of the components. Finally, a numerical model was developed and tuned to match the concentration profiles and the diffusivity was determined. The calculated diffusivities increased monotonically with solvent concentration. The model with the

proposed correlations matched measured concentration profiles within 2% for heavy oil and predicted toluene-heavy oil concentration profiles (on the same dataset) with a maximum absolute deviation of 3% (Grimaldos, 2018). This model is used in this thesis and the correlations will be presented and discussed further in Chapter 4.

2.6. Summary

Solvent recovery methods are a promising alternative to reduce the high costs of steam production and greenhouse gas emissions associated with thermal recovery methods. However, even after numerous experimental and numerical studies, pilot tests have had mixed to poor oil recovery rates. There are a number of uncertainties with these processes including the rate of diffusion, the complex interactions between solvent and heavy oil, the effect of *in-situ* asphaltene precipitation, and the potential loss of solvent to untargeted or thief zones. The uncertainty in the loss of solvent is a critical issue because the economic performance of a solvent recovery process is highly dependent on the recovery of the injected solvent.

While it is well accepted that mass transfer and gravity drainage are key mechanisms in solvent-based and solvent-assisted processes, there appears to be a gap in the basic understanding of these mechanisms and the interplay between them at different conditions. Unrealistic diffusion coefficients must be used in simulations of solvent-based recovery methods to match measured results (Das, 2005). The available models do not accurately predict oil recovery rates and cannot be used to scale up lab experiments to the field. The success of solvent recovery processes depends on understanding these mechanisms in order to accurately predict solvent and oil recovery rates.

CHAPTER THREE: EXPERIMENTAL METHODS

This chapter presents the materials and experimental methods used in this thesis. The design and commissioning of a new Hele-Shaw type apparatus and the experimental procedure for the gravity drainage experiments are discussed in detail, including the treatment of collected data and images.

3.1. Materials

The Western Canadian bitumen sample used in this thesis (WC-B-A3) was provided by CNOOC Petroleum North America ULC (originally Nexen). The sample was obtained from a JACOS SAGD process and had been dehydrated to a residual water content of less than 1 wt%. Properties such as molecular mass, density, viscosity, and the SARA composition of the WC-B-A3 bitumen are listed in Table 3.1. Details for the measurements are presented later. Toluene, Certified ACS, of ≥99.5% purity was purchased from Fisher Scientific and was used for all gravity drainage experiments. Nitrogen was Industrial Grade (99.998% purity) and was purchased from Praxair Canada.

Table 3.1. Physical properties and composition of WC-B-A3 bitumen sample.

Property	Units	WC-B-A3 Bitumen
Density at 20°C, 0.1 MPa	g/cm³	1.009
Viscosity at 20°C, 0.1 MPa	mPa·s	358,000
Molecular Weight	g/mol	570
Saturates	wt%	19.5
Aromatics	wt%	41.7
Resins	wt%	18.5
C5-asphaltenes	wt%	20.1
Toluene Insolubles	wt%	0.1

3.2. Bitumen Fractionation and Property Measurements

SARA Fractionation

The bitumen sample (WC-B-A3) was fractionated into saturates, aromatics, resins, and *n*-pentane insoluble asphaltenes using a modified ASTM D4124 separation method (Alboudwarej *et al.*, 2002). Asphaltenes and any toluene insoluble components were precipitated with *n*-pentane and removed from the bitumen. This material was redissolved in toluene to separate the toluene insoluble components. The maltenes (de-asphalted oil) were fractionated into saturates, aromatics, and resins using liquid chromatography. The SARA fractionation was performed at the University of Calgary by Elaine Baydak and the repeatability of the compositions was 0.9 wt% (Rodriguez-Leon, 2018). The assay is provided in Table 3.1.

Molecular Weight

The molecular weight of the bitumen sample (WC-B-A3) was measured with a Jupiter Model 833 Vapor Pressure Osmometer. A detailed explanation of this equipment and the procedure to measure the molecular weight can be found elsewhere (Alboudwarej *et al.*, 2002). The molecular weight measurement was performed at the University of Calgary by Elaine Baydak and was repeatable to ±50 g/mol based on a 95% confident interval. The molecular weight is reported in Table 3.1.

Density and Viscosity Measurements

The density and viscosity for Athabasca bitumen sample WC-B-A3 were measured from 50 to 175°C and 0.1 to 10 MPa using an in-house capillary viscometer equipped with an Anton Paar DMA-HPM density meter. A detailed explanation of the apparatus and procedure can be found elsewhere (Motahhari and Yarranton, 2013; Ramos-Pallares, 2017). The viscosity and density measurements were performed at the University of Calgary by Florian Schoeggl. The measured densities were fitted with an empirical correlation from (Saryazdi *et al.*, 2013) and the measured viscosities were fitted with the Expanded Fluid viscosity correlation (Yarranton and Satyro, 2009). The correlations are presented in Chapter 4. The values at 20°C and 0.1 MPa were determined from the fitted correlations and are reported in Table 3.1.

3.3. Gravity Drainage Experiments

3.3.1. Apparatus

A new Hele-Shaw (parallel glass plates) type apparatus was designed to perform gravity drainage experiments of solvent/bitumen systems. Figure 3.1 shows a complete side view of the experimental setup and Figure 3.2 shows a frontal view of the Hele-Shaw cell. The main components are the Hele-Shaw cell, a displacement pump, two cylinders equipped with pistons to contain toluene (for injection during the experiment) and the bitumen (for injection during the filling process prior to the experiment), a sampling vessel to collect samples, a compressed nitrogen cylinder, an LED light, a camera and a computer. Details of the components are as follows:

- The Hele-Shaw cell has a 20 cm by 20 cm viewing area. The gap thickness can be set between 0.5 and 3 mm. In this thesis, only gap widths of 0.5 and 1 mm were used.
- The Demi 2510S pump delivers metered flow rates in the range of 0.2 to 10 cm^3/min and has an accuracy of ±1% of the set point. The operating pressure range is 10 to 2500 psi.
- The piston-equipped cylinders containing solvent (toluene) and bitumen have a maximum fluid capacity of 400 cm^3.
- The sampling vessels are 7.4 cm^3 glass vials.
- Nitrogen injection is used to prevent liquid build-up in the Hele-Shaw cell when flow backs up at the outlet (see Section 3.3.3).
- The camera is a Microsoft LifeCam cinema HD with high-precision glass element lens for sharp image quality and a resolution of 1280x720 pixels.
- The LED light is located behind the Hele-Shaw cell during the experiments to improve the quality of the pictures.
- The computer is equipped with LabVIEW and NI Vision assistant software to analyze the images.
- An Anton Paar DMA 4500M density meter is used to measure the density of the samples collected in the vials at room pressure and 20°C. The instrument was calibrated using air, toluene, and reverse osmosis water. The precision and repeatability of the density meter are ±0.00001 g/cm^3 and ±0.00005 g/cm^3, respectively.

- A Mettler Toledo AB204 Analytical Balance is used to measure the mass of the empty and filled glass vials. The balance has an accuracy of 0.0001 g.

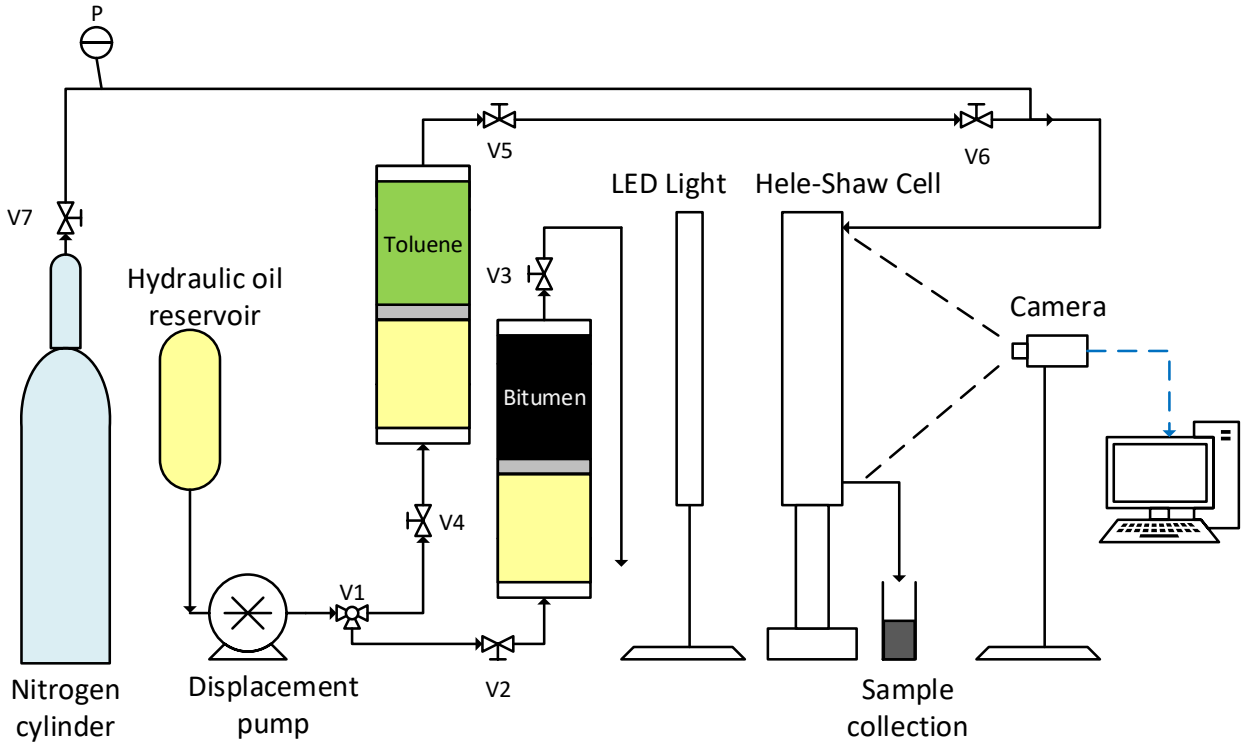

Figure 3.1. Schematic of the gravity drainage apparatus (side view of Hele-Shaw cell).

The novelty of the set-up is that the Hele-Shaw cell can be rotated to create a nearly fixed geometry for the drainage process; that is, an interface with an initially constant slope. To initialize an experiment, the apparatus is rotated into the filling configuration and partially filled with bitumen such that when rotated into the drainage configuration, the bitumen is positioned with the target angle of inclination. The gap width, defined as the space between the two parallel glass plates, is narrow enough and the bitumen sufficiently viscous that it does not move on its own in the time interval of a typical gravity drainage experiment (approximately 4 hours).

After the initially immobile bitumen interface is set, a fixed volumetric flow rate of solvent is introduced at the top of the bitumen interface. In this thesis, toluene is the solvent. Toluene flows along this interface, accumulates the bitumen that diffuses into the flowing layer, drains by gravity

and is collected from the bottom of the interface in a sampling vessel. The liquid flow rate, density, bitumen and toluene content of the drained liquid are measured over time. The interface profile is also measured over time from images captured periodically with the CCD camera.

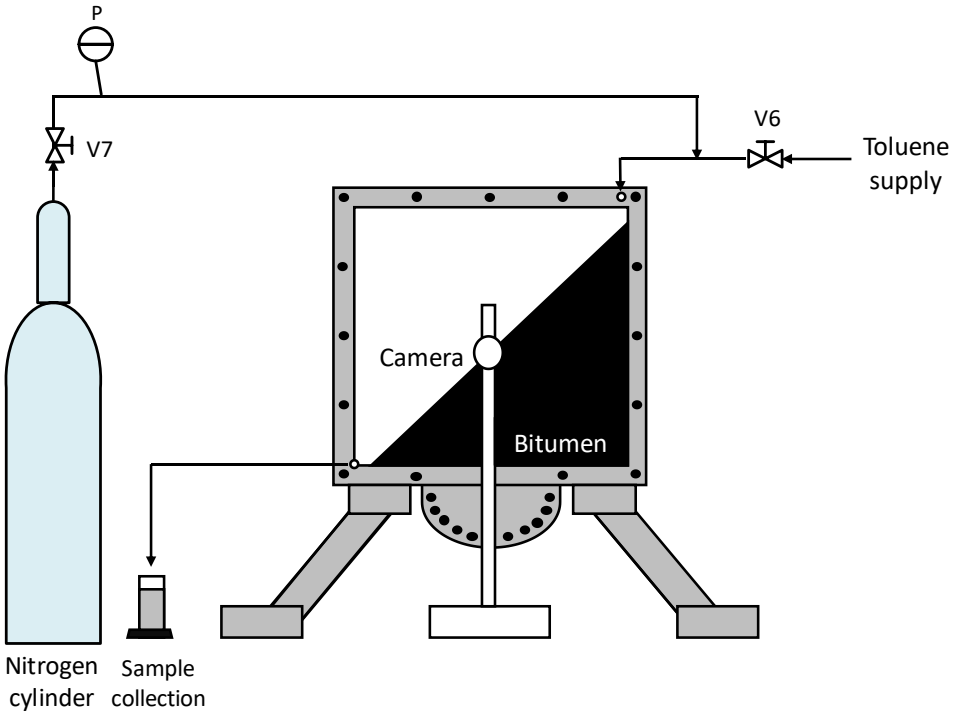

Figure 3.2. Schematic of the gravity drainage apparatus (frontal view of Hele-Shaw cell) set in the drainage configuration.

3.3.2. Experimental Procedure

Initial Preparation

The Hele-Shaw cell is assembled at the specified gap width (either 0.5 or 1.0 mm). The filling angle is set so that when the cell is rotated into the drainage configuration after filling, the bottom of the cell will be horizontal and the bitumen/toluene interface will have the specified angle of inclination (30 to 45º). The required volume of bitumen is determined from the initial geometry of the bitumen zone in the drainage configuration. The zone to be occupied by the bitumen is triangular and is given by:

$$V_b = \frac{hLB}{2} = \frac{L^2 B\ tan\theta}{2} \quad (3.1)$$

where B is the specified gap between the glass plates in cm, h is the calculated height of the bitumen in cm and L is the basal length of the bitumen layer in cm, and θ is the initial angle of inclination. Figure 3.3 Illustrates the calculation of the volume of the cell to be occupied by the bitumen.

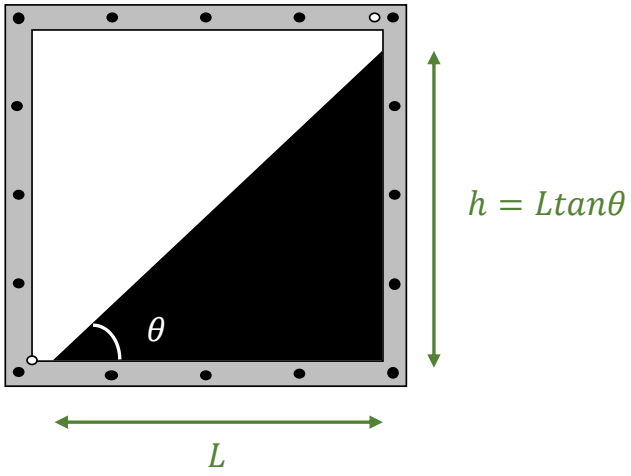

Figure 3.3. Calculation of the volume of the Hele-Shaw cell occupied by the bitumen.

The bitumen and toluene cylinders are filled with excess volumes of each fluid. The bitumen cylinder is wrapped with electrical heating tape and heated at 40°C for 24 hours in order to expel any air bubbles from the bitumen and to avoid high pressures during injection. It is cooled to the ambient temperature (21ºC) before the start of the experiment.

Filling Procedure

A complete schematic of the filling process is shown in Figure 3.4. The bitumen cylinder is connected to the hydraulic oil supply and to the Hele-Shaw cell and Valves V1, V2 and V3 are opened. The maximum injection rate is set to 1 cm³/min to avoid high injection pressures (above 100 psi) and the bitumen is displaced into the Hele-Shaw cell. When bitumen is first observed in the cell, the injected volume is reset to zero at the pump and the injection continues until the target volume in the cell has been reached. The volume is calculated as described above and the pump

displacement volume is used as a check. The two volumes were within 0.8 cm³ (6%) of each other in all cases. Then the pump is turned off and after the pressure drops to atmospheric pressure, Valves V1, V2 and V3 are closed.

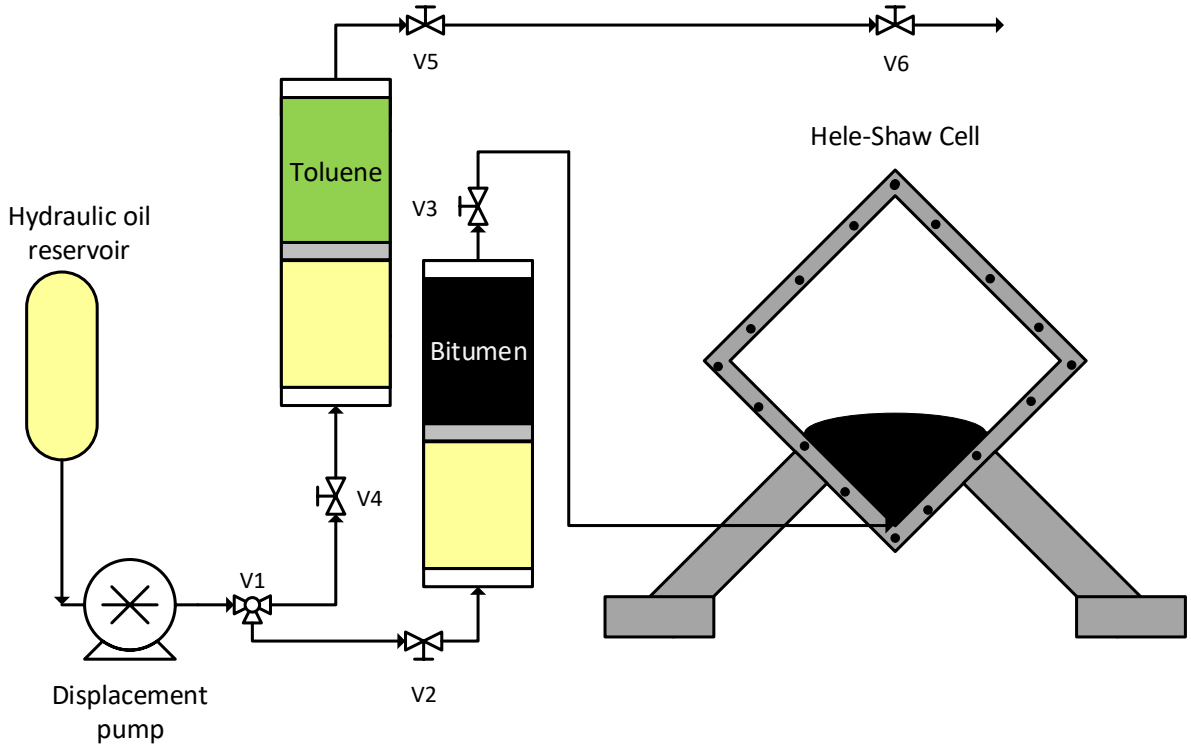

Figure 3.4. Schematic of the gravity drainage apparatus in the filling configuration.

During the bitumen injection, a meniscus forms at the interface between the bitumen and the air inside the cell, as shown schematically in Figure 3.3. The cell is left in the rotated position for approximately 24 hours or until the meniscus has completely flattened. A flat meniscus is required to obtain a bitumen/toluene interface of constant slope when rotated into the drainage configuration. Finally the cell is disconnected from the cylinder, but kept in the rotated position until the gravity drainage experiment starts.

Gravity Drainage Procedure

Before starting the gravity drainage procedure, the sample collection vials are weighed and labelled. The image capture rate for the LabVIEW software was set to one image per 10 minutes in order to have enough pictures at the end of each experiment to see the progression of the profiles and to calculate the contact area between the bitumen and the flowing layer (toluene) over time.

After the meniscus has completely flattened, the Hele-Shaw cell is positioned between the camera and LED light and connected to the diluent cylinder and the nitrogen cylinder. A sample collection vial is positioned at the cell outlet and the cell is rotated to the horizontal position to start the diluent injection. Before starting the pump, Valves V1, V4, V5 and V6 are opened to allow hydraulic oil to flow to the cylinder and toluene to flow to the cell. The toluene flow rate is set and toluene is displaced to the Hele-Shaw cell inlet. Once the first drop of toluene is seen in the cell, the injected volume is reset to zero in the pump to have an accurate measure of the total injected volume. Then the image-capture program is started and the outlet mixture of toluene and bitumen is collected in the sample vial. New vials are added whenever the previous one is full and the time to collect each sample is recorded. The nitrogen injection rate is adjusted with Valve V7 to prevent liquid build-up inside the cell at the outlet.

When the target time of the experiment is complete (approximately 4 hours), the pump is turned off to stop the toluene injection, the last vial is removed from the outlet of the cell, the image-capture program is stopped, and Valves V1, V4, V5 and V6 are closed. The Hele-Shaw cell is disassembled and cleaned with toluene.

Sample Analysis

The vials with samples are weighed. A sub-sample of 3 cm^3 is taken from each vial with a syringe and injected into the density meter to obtain a density measurement. The vials are weighed again and left open in a fume hood to evaporate all of the toluene until the mass is constant. The composition of the sample is determined from the mass of evaporated toluene and the residual mass of bitumen. The original mass of bitumen and toluene in each vial is determined from the

mass before subsampling and the composition measured after the subsampling. The bitumen mass flux during the time each sample was collected is calculated as follows,

$$n_{b,i} = \frac{m_{b,i}}{\bar{A}_i t_i} \tag{3.2}$$

where n_b is the bitumen mass flux in g/cm²·min, m_b is the recovered bitumen mass in g, t is the time in which the vial was receiving fluids from the process in min, $\bar{A}$ is the average area of contact between the solvent and the bitumen during the filling of the vial in cm², and *i* indicates the sample number. The procedure to calculate the contact area between the bitumen and the solvent will be explained in the next section.

Image Analysis

Figure 3.5 shows the typical progression of the bitumen profile in one experiment, with one image taken at the beginning of the experiment and subsequent pictures after 2 and 3 hours of solvent injection and gravity drainage. To extract information from the images, a script was developed using NI Vision Assistant software with the following steps:

- the image is rotated so that the bottom edge of the bitumen is horizontal.
- an image mask is obtained; that is, a region of interest (the viewing area of the Hele-Shaw cell) is selected and the remaining portion of the picture is eliminated.
- the region of interest is calibrated from the number of pixels to centimeters.
- the bitumen is then captured by the software as a single 'particle'.
- the particle analysis function in the software is used to calculate the perimeter, width and height of the bitumen.

The contact length between the bitumen and the flowing layer (mostly toluene) is then calculated from the perimeter less the basal length and height of the bitumen. The contact area is the product of the contact length and the gap width. To calculate the bitumen mass flux associated with each sample, the average contact area is determined as follows:

$$\bar{A}_i = \frac{A_i(beginning\ of\ filling) + A_i(end\ of\ filling)}{2} \tag{3.3}$$

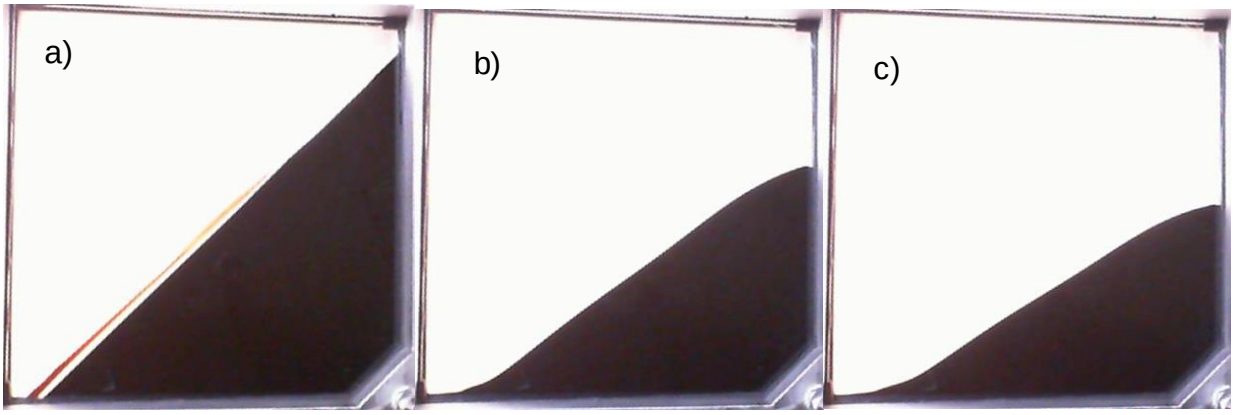

Figure 3.5. Typical progression of bitumen profiles during gravity drainage experiments in this thesis: a) 0 h, b) 2 h and c) 3 h.

3.3.3. Design Checks

The following factors may prevent the collection of representative, accurate, and usable data during gravity drainage experiments using the new apparatus:

- settling of the initially inclined bitumen layer independent of the toluene induced gravity drainage,
- liquid build-up in the Hele-Shaw cell at the outlet.

Each factor is discussed below.

Bitumen Settling

The inclined bitumen layer is denser than the surrounding air and will settle over time. The settling rate is low because the bitumen is viscous and the gap width is small. To determine if the settling rate was likely to be significant for the gravity drainage experiments, the Hele-Shaw cell was filled with bitumen as described previously and left for four hours without any toluene injection. Figure 3.6 shows the bitumen profile at the beginning of the test and after four hours. The displacement rate was calculated to be 0.2 cm/h, much lower than the gravity drainage rate with toluene between 2.5 and 3 cm/h. Hence, bitumen settling was not expected to be an issue during the gravity drainage experiments.

However, the bitumen settling rate was later found to be much higher when a film of solvent was present on top of the bitumen layer. As will be discussed later, the capillary forces were much lower in this situation and the bitumen settling rate increased. Therefore, in order to match the bitumen profiles in the modeling, the bitumen self-displacement by gravity was taken into account in the interpretation and modeling of the data (see Chapter 4).

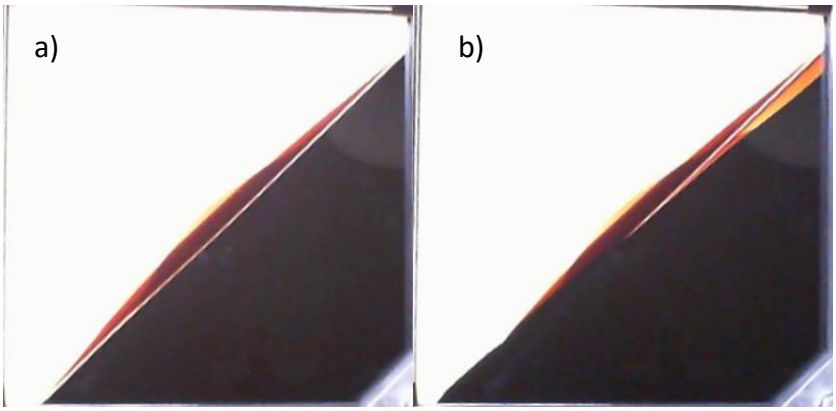

Figure 3.6. Bitumen profile progression without solvent injection. a) 0 h and b) 4 h.

Liquid Build-Up

During the first gravity drainage experiment, some liquid accumulation was observed at the outlet of the Hele-Shaw cell because the atmospheric pressure inside the cell was insufficient to flow all of the draining liquid through the outlet at same rate as the feed flow rate. Therefore, a nitrogen cylinder was connected to the entry port of the cell and nitrogen was injected to slightly increase the pressure inside the cell to flow out all of the accumulating liquid at the outlet. The nitrogen flow rate was set high enough to prevent the liquid build-up and low enough to avoid forcing the solvent to drip to the bitumen away from the inlet.

3.3.4. Repeatability

Figures 3.7, 3.8, and 3.9 show the bitumen mass flux, profiles, and product properties, respectively, over time for two gravity drainage experiments performed with a gap width of 0.5 mm and a toluene flow rate of 1 cm³/min. The bitumen mass fluxes were within 0.0022 g/cm²min of each other except for one outlier. The repeatabilities of the diluted bitumen density rate and bitumen content were ±0.0006 g/cm^3 and ±0.4%, respectively. The repeatabilities of the bitumen production rate and cumulative bitumen production (not shown here) were ±0.0013 g/min and ±3%, respectively. See Appendix A for details.

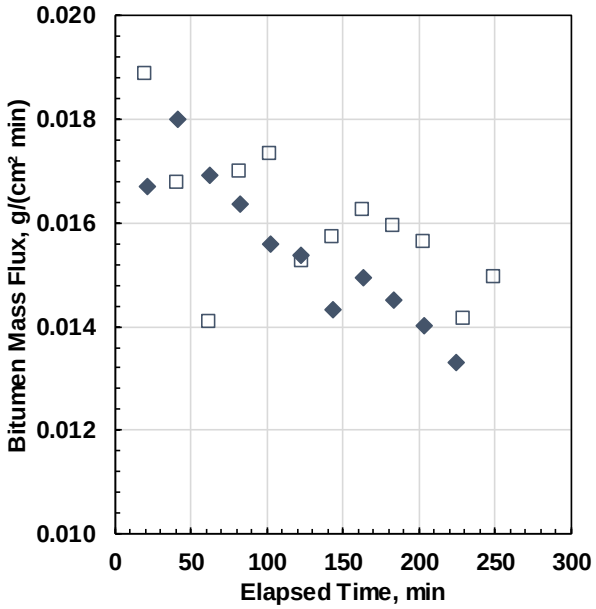

Figure 3.7. Bitumen mass flux over time for two gravity drainage experiments with a gap width of 0.5 mm and toluene flow rate of 1 cm³/min.

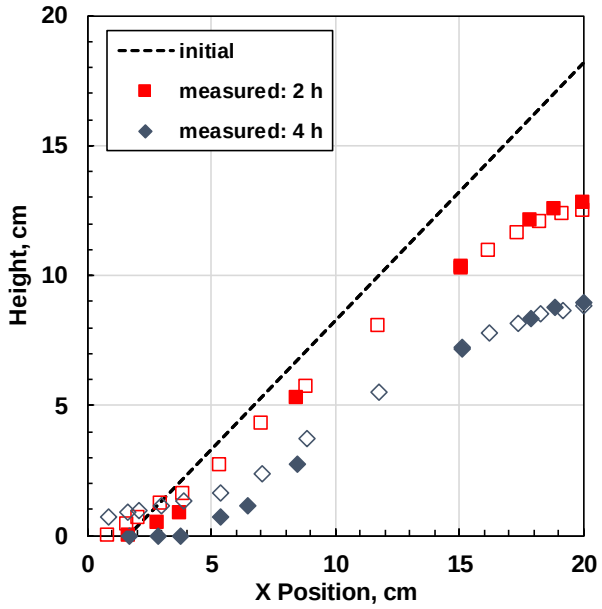

Figure 3.8. Bitumen profiles over time for two gravity drainage experiments with a gap width of 0.5 mm and toluene flow rate of 1 cm³/min.

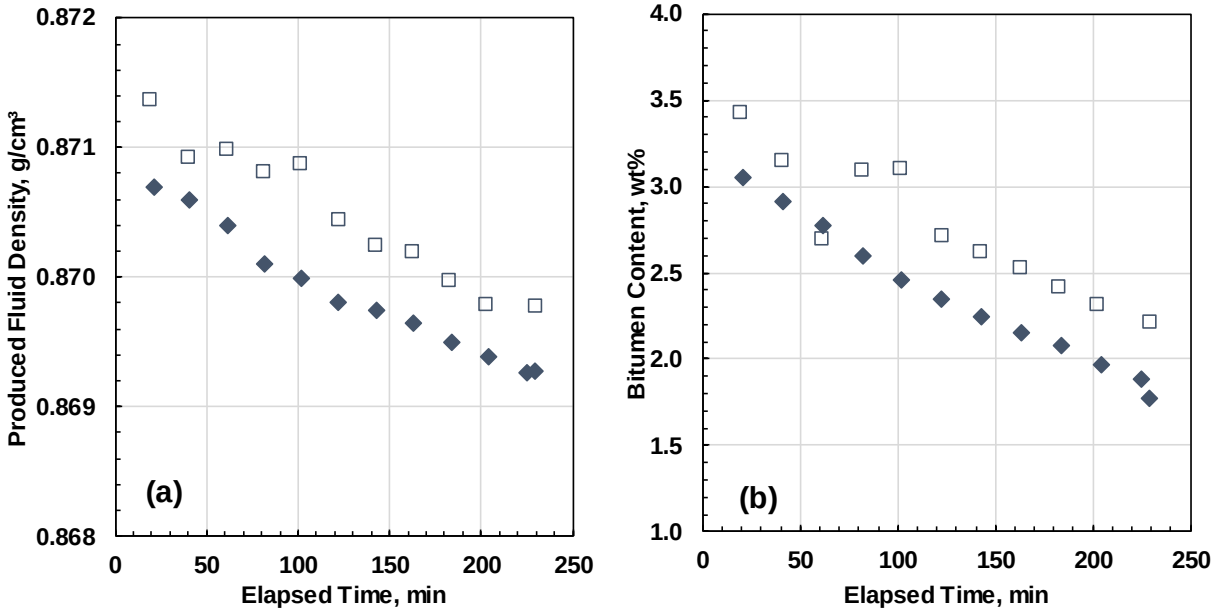

Figure 3.9. Produced fluid properties over time for two gravity drainage experiments with a gap width of 0.5 mm and toluene flow rate of 1 cm³/min. a) Density and b) Bitumen content.

3.3.5. Drainage Layer Velocity Measurement

The velocity of the drainage layer was assessed to determine the appropriate drainage layer flow model. The drainage layer was not detectable in the experiments with bitumen. Therefore, the velocity of the drainage layer was measured using toluene with a dye (Oil Blue N) flowing over a teflon spacer. The spacer was set in the Hele-Shaw cell at 35° and the toluene was injected at different rates. The velocity of the solvent layer was determined from the time it took a small pulse of toluene to travel down the known length of the spacer. The velocity was assumed to be the average velocity of the drainage layer. The repeatability of the velocity measurement was ±3%.

CHAPTER FOUR: MODELING GRAVITY DRAINAGE EXPERIMENTS

In this chapter, a numerical model for gravity drainage in a Hele-Shaw cell is developed for a system of bitumen and liquid solvent. The model assumptions and boundary conditions are defined and discussed. A complete description of the model is provided and its limitations are established. Density, viscosity and diffusivity models used within the numerical mass transfer and gravity drainage model are described in detail. An algorithm to fit the experimental data is explained.

4.1. Development of Gravity Drainage Model

Figure 4.1a shows a general schematic of gravity drainage for a flowing solvent layer over stationary bitumen in a Hele Shaw apparatus. During the gravity drainage process, bitumen diffuses upwards into the flowing layer where it is swept away to the outlet of the apparatus. At the same time, solvent diffuses downwards into the bitumen. Over time, as bitumen is swept away by the flowing layer, the height of the bitumen column decreases (Figure 4.1b). The process continues until the bitumen is depleted.

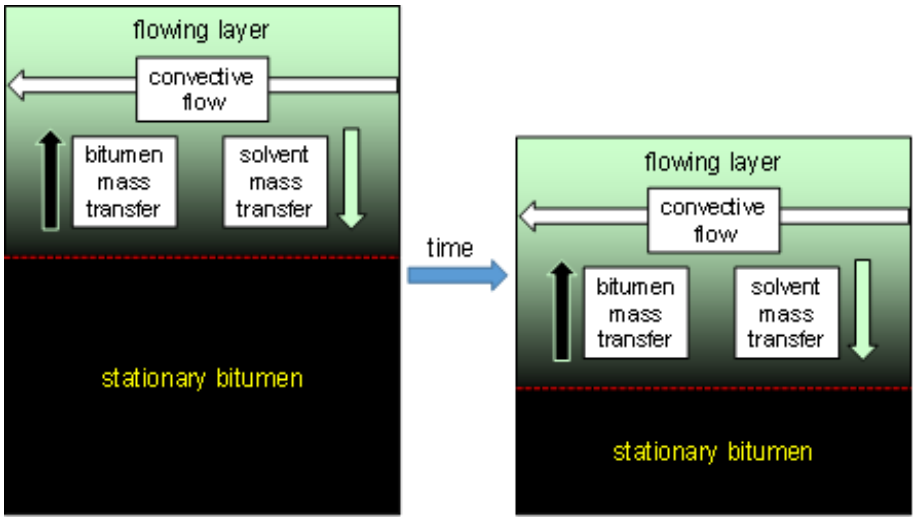

Figure 4.1. Schematic of gravity drainage process in a Hele-Shaw geometry: a) initial condition; b) after some time. The bitumen is shown as a horizontal layer for convenience but in reality is inclined.

Figure 4.2 shows the gravity drainage process at the bitumen-solvent interface. Both bitumen and solvent are diffusing but the diffusing bitumen is swept away so that the height of the bitumen layer decreases during the mass transfer process. A key feature is that the bitumen diffuses into solvent much more rapidly than the solvent into bitumen. For example, the diffusivity of bitumen into pure toluene is approximately 60 times higher than the diffusivity of toluene into pure bitumen (Grimaldos, 2018). Therefore, to simplify the problem, it was assumed that the penetration rate of the solvent is less than or equal to the depletion rate of the bitumen. In other words, the height of the bitumen layer decreases as fast as the solvent diffuses into the bitumen and therefore the diffusion of solvent into bitumen can be neglected. Grimaldos, (2018) showed that toluene diffused through bitumen less than 1 cm in 5 days at ambient conditions; that is, a penetration rate of approximately 0.2 cm/day. The typical rate at which the height of the bitumen layer decreased in the experiments in this thesis was between 2.5 and 3 cm/h. Hence, the assumption was reasonable for the conditions examined in this thesis.

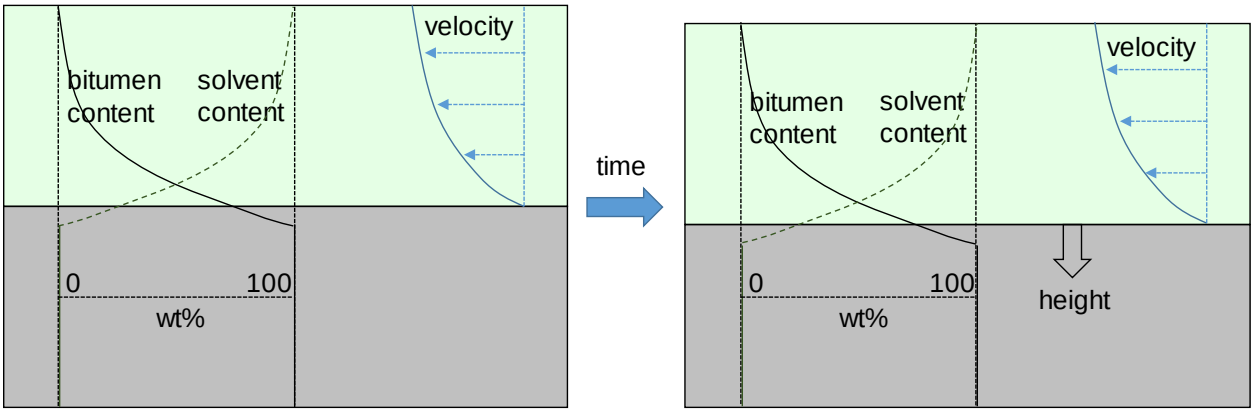

Figure 4.2. Schematic illustration of concentration and velocity profiles near bitumen solvent interface in gravity drainage process and change in height of bitumen over time. The gray area at the bottom is the immobile fluid.

Figure 4.3 is a schematic of a discretized model for the gravity drainage process neglecting solvent mass transfer. The fluid is divided into columns, each containing a solvent block and a bitumen block. At each time step, a material balance is performed on each solvent block accounting for the convective flow of bitumen and solvent in and out of the block and the mass transfer of bitumen into the block. An additional creep flow term between parallel glass plates is introduced in the

bitumen blocks to account for movement of the bitumen phase due to the difference in the height of adjacent columns. At the end of each time step, the composition of the solvent block and the height of the bitumen block are updated and the convective, creep, and diffusive mass flow rates are calculated for the next time step. The approach used to determine the convective, creep and diffusive mass flow rates are outlined below and then the model implementation is discussed.

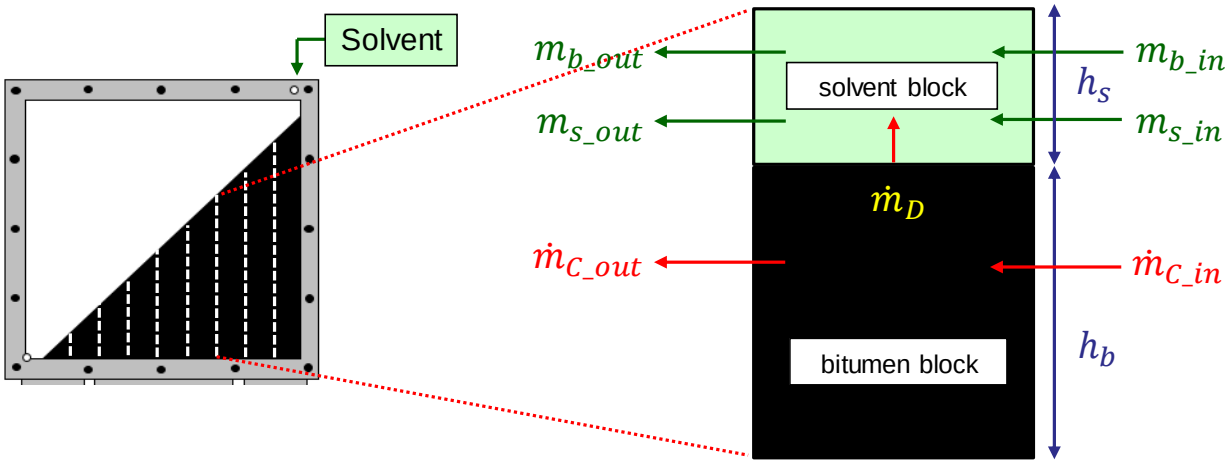

Figure 4.3. Modeling approach for the Hele-Shaw drainage process.

4.1.1. Convective Mass Flow Rates

Figure 4.2 shows that the composition of the liquid in the flowing layer changes with height and therefore that the density and viscosity vary with height and there will be vertical mass transfer of solvent and bitumen. The most extreme variations are expected near the boundary between the stationary layer and the flowing layer where the concentration gradients are high. This “boundary” region has a relatively high bitumen content and therefore a high viscosity and a low flow rate. Above the boundary region, if there is sufficient solvent flow rate, there will be a layer of fluid where there is relatively little change in properties with height and a much higher flow rate. It was assumed that the boundary region of extreme property changes is small relative to the total height of the flowing layer. One consequence of this assumption is that the model is only valid at sufficiently high flow rates. This threshold will be discussed in Chapter 5.

Another related assumption is that all of the flowing layer moves at the average velocity of a falling film (flow of a liquid down an inclined flat plane). This assumption is discussed further in Section 5.4.1. The lateral diffusion of solvent and bitumen is assumed to be negligible compared to the convective transfer. Vertical diffusion within the flowing layer is also assumed to be negligible because the concentration gradients within the flowing region are small. Furthermore, the bitumen that enters the solvent block is assumed to be immediately swept away by the solvent. Hence, the masses of bitumen and solvent leaving a solvent block by convective flow in one time step are given by:

$$m_{b\_out} = \dot{m}_D \Delta t + m_{b\_in} \tag{4.1}$$

$$m_{s\_out} = \rho_{mix} \bar{v} h_s B w_s \Delta t \tag{4.2}$$

where m_{b_out} and m_{s_out} are the convective masses leaving the solvent block in g, $\dot{m}_D$ is the mass of bitumen diffused from the bitumen block underneath the solvent block in g/s, m_{b_in} is the mass of bitumen entering the solvent block in g, ρ_{mix} is the density of the mixture in the solvent block in g/cm^3, $\bar{v}$ is the average velocity in the solvent layer in cm/s, h_s is the height of the solvent layer, B is the gap width between the glass plates in cm, Δt is the time step in s, and w_s is the solvent mass fraction in the solvent block. The film thickness (height of the solvent block) is given by (Bird *et al.*, 2006):

$$h_s = \sqrt[3]{\frac{3\mu_{mix} q_s}{\rho_{mix} g B \sin\theta}} \tag{4.3}$$

where μ_{mix} is the viscosity of the mixture in g/cm·s, q_s is the solvent flow rate in cm^3/min, g is gravitational acceleration in cm/s^2 and θ is the inclination angle. The average velocity is given by (Bird *et al.*, 2006):

$$\bar{v} = \frac{\rho_{mix} g h_s^2 \sin\theta}{3\mu_{mix}} \tag{4.4}$$

Equations 4.3 and 4.4 are valid only when the flow regime is laminar and the fluid layers move smoothly over one another in the direction of flow (Bird *et al.*, 2006). The flow regime can be established by calculating the Reynolds number given by:

$$Re = \frac{4 h_s \bar{v} \rho_{mix}}{\mu_{mix}} \tag{4.5}$$

The flow is considered to be laminar when *Re* is less than 1500 and this was the case for the conditions examined in this thesis (*Re<350* for all cases). Restrictions related to the flow regime are discussed in more detail in Chapter 5.

4.1.2. Diffusive Mass Flow Rate of Bitumen

The continuity equation for the mass transfer of bitumen into a solvent block is given by:

$$\frac{D(\rho \cdot w_b)}{Dt} = -(\nabla \cdot j_b) + r_b \tag{4.6}$$

where w_b (= *1-* w_s) is the bitumen mass fraction, ρ is the density of the mixture in g/cm³, j_b is the mass flux of bitumen in g/cm².s, and r_b is the rate of bitumen mass addition per unit volume due to reaction in g/cm³·s. The mass flux of bitumen is given by:

$$j_b = -\rho D_{bs} \nabla w_b \tag{4.7}$$

where D_{bs} is the diffusivity of bitumen in solvent in cm²/s. As discussed previously, the mass transfer of solvent was neglected. The assumptions made to simplify the continuity equation are listed below.

<u>One Dimensional Diffusion:</u> The inclination of the bitumen plane determines the direction of flow when the solvent and bitumen are in contact. It is expected that diffusion dominates in the direction perpendicular to flow and convective transfer dominates in the direction of flow. Therefore, the lateral diffusion of solvent and bitumen is assumed to be negligible in the direction of flow compared to the convective transfer and is neglected. This assumption has been applied in available literature of liquid-liquid diffusion because it considerably simplifies the continuity and the mass flow equations. After applying this assumption, the gradient operator (∇) of Equation 4.7 becomes a partial derivative with respect to the direction of diffusion (perpendicular to flow). In this case, ∇w_b becomes $\partial w_b / \partial h$.

<u>Isothermal System:</u> In this thesis, all experiments were run at ambient conditions at a stable, uniform temperature of 20 ± 2°C. Therefore, the system is considered to be isothermal with no heat transfer.

No Natural Convection: In all of the experiments, the liquid with lower density was always on top of the liquid with higher density, *i.e.*, the solvent was always on top of the bitumen. Therefore, in the direction of mass transfer, there was no possibility of creating an inverse density gradient that could cause natural convection within the Hele-Shaw cell. In addition, possible natural convection caused by precipitation of asphaltenes when the solvent is partially miscible with the bitumen (such as *n*-pentane or *n*-heptane) was avoided by performing all experiments with toluene as the solvent. The same assumption has been applied in all the available literature of liquid-liquid diffusion.

Pseudo-Binary System: Heavy oil and bitumen are mixtures of millions of chemical compounds (McKenna *et al.*, 2013) and therefore it is a multi-component fluid. However, modeling a multi-component system is virtually impossible since other phenomena such as reverse diffusion, osmotic diffusion, and diffusion barriers can occur (Bird *et al.*, 2006). Therefore, for the sake of simplicity, the bitumen was assumed to be a single pseudo-component and the solvent-bitumen system was treated as pseudo-binary. The same assumption has been applied in previous studies that involve diffusion in heavy oil or bitumen.

No Chemical Reactions: The only solvent used in this thesis is toluene and it does not react with the bitumen at the temperatures of the gravity drainage experiments. Reactions have been shown to only occur above 250°C (Gray, 2015)). Hence, the reaction terms r_b and r_s are neglected in the continuity equations.

Zero Excess Volume of Mixing: If there is a volume change because of mixing, a convection term must be introduced into the bitumen and solvent mass flux equations or a new frame of reference must be used (Crank, 1975). Therefore, to further reduce the complexity of the model, the volume change upon mixing was neglected. If there is no volume change upon mixing on either side of the interface, it can be shown that (Crank, 1975):

$$D_{sb} = D_{bs} \tag{4.8}$$

Hence, the behavior of the binary system of bitumen and solvent can be described using a single mutual diffusivity. The diffusivity is a function of the composition, temperature, and pressure

(Crank, 1975; Oballa and Butler, 1989). Most of the studies on the diffusion of liquid solvent in bitumen have assumed no excess volume of mixing (Grimaldos, 2018).

No Forced Convection: The only force that causes the movement of the flowing layer in the Hele-Shaw cell is gravity, and bitumen is assumed to be a solid that is partially soluble in the solvent. There are no external sources of mixing such as a stirrer. Additionally, since there is no excess volume upon mixing, then there is no mass velocity related to different diffusion rates between solvent and bitumen (Crank, 1975). Therefore, the velocity term in the continuity equation (perpendicular to the solvent flow) is neglected.

The above assumptions were applied and Equations 4.6 and 4.7 were combined to obtain the following expression for the mass transfer in the Hele-Shaw cell:

$$\frac{\partial(\rho \cdot w_b)}{\partial t} = \frac{\partial}{\partial h}\left(\rho D_{bs} \frac{\partial w_b}{\partial h}\right) \tag{4.9}$$

The mass flow rate of the bitumen is then given by:

$$\dot{m}_D = -A_D \frac{\partial}{\partial h}(\rho D_{bs} w_b) \tag{4.10}$$

where A_D is the cross sectional area (area of contact between the flowing layer and the bitumen layer) in cm².

In liquid-liquid systems, the density gradient is very high during the experiment, requiring a relationship between density and bitumen concentration in Equation 4.10. The numerical procedure would then become complex and impractical. An alternative is to discretize the fluid column and solve the mass flow equations with a constant density in each block. The mass flow equation for bitumen diffusion with a constant density is given by:

$$\dot{m}_D = -A_D \rho D_{bs} \frac{dw_b}{dh} \tag{4.11}$$

Equation 4.11 describes the mass flow of bitumen across the interface during the gravity drainage experiment.

4.1.3. Creep Flow Rate of the Bitumen Layer

The analysis of the photographs taken during gravity drainage experiments showed flattening in the bitumen layer over time. As will be discussed in Chapter 5, the flattening was consistent with creep flow of the bitumen with negligible capillary pressure forces acting in opposition. Creep flow is movement of a fluid when it is subject to different pressure gradients (like a hill slumping under its own weight).

Figure 4.4 shows the schematic of how creep flow is acting in the bitumen layer and how the effect is included in the model. The column in the middle of Figure 4.4 has a lower height compared to the column in the right and therefore the hydrostatic pressure in the middle column at any height is less than the column to the right. Consequently there is a pressure gradient between the two columns which drives flow into the bitumen column with the lower height. The velocity at which the bitumen creeps between parallel glass plates (Hele-Shaw cell) is given by:

$$v_{creep} = \frac{B^2}{12\mu_b}\left(\frac{\Delta P}{\Delta x}\right) \tag{4.12}$$

where μ_b is the viscosity of the bitumen in g/cm·s and $\Delta P/\Delta x$ is the pressure gradient. The pressure gradient is the difference in the hydrostatic pressure at any height within the column divided by the column width and is given by:

$$\frac{\Delta P}{\Delta x} = \frac{\rho_b g \Delta h}{\Delta x} \tag{4.13}$$

where ρ_b is the density of bitumen in g/cm³, and Δh is the height difference between adjacent columns in cm. Substituting the pressure gradient (Equation 4.13) into the creep flow velocity (Equation 4.12), and multiplying by the area and density, the mass flux from one column to the adjacent column to the left is given by:

$$\dot{m}_{C\_out} = \frac{B^2}{12\mu_b}\left(\frac{\rho_b g \Delta h}{\Delta x}\right) h_b B \rho_b \tag{4.14}$$

where h_b is the height of the column in cm. The total mass that creeps between adjacent columns is the mass flux calculated from Equation 4.14 multiplied by the time step Δt.

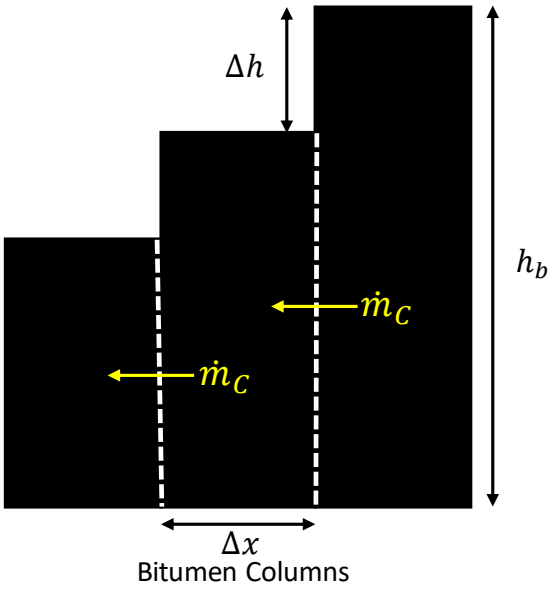

Figure 4.4. Schematic of the creep flow in the bitumen phase during gravity drainage experiments.

4.2. Numerical Model for Gravity Drainage

The fluid is divided into columns of equal width each containing a bitumen block and a solvent block. The bitumen blocks contain only bitumen at all times. The solvent block initially contains only solvent. The initial height of each bitumen block is calculated based on the total bitumen volume, the position of the column, and the initial inclination angle. The initial height of each solvent block is calculated using the injection flow rate and Equation 4.3. The average velocity of the solvent column is calculated using the calculated solvent block height, the initial inclination angle and Equation 4.4. The initial bitumen concentration in the solvent columns is set to zero. The density and viscosity of each solvent block and the diffusivity of each bitumen column are initialized based on the known properties of the solvent and the known bitumen diffusivity in the solvent.

A mass balance is applied to each solvent and bitumen blocks in every time step as shown in Figure 4.5. The bitumen flow and solvent convective mass flow rates exiting each block are calculated from Equations 4.1 and 4.2, respectively. The diffusive mass flow rate is calculated form Equation 4.11 and the creep mass flow rate is calculated from Equation 4.14. The mass fractions of solvent

and bitumen, density, and viscosity of each solvent block are updated. The diffusivity of the bitumen is updated. The height of each block, the inclination angle, the diffusion area, and the average velocity of the solvent layer are recalculated. Then, the next time step is initiated. The model initialization, discretized equations, and fitting algorithm are described below.

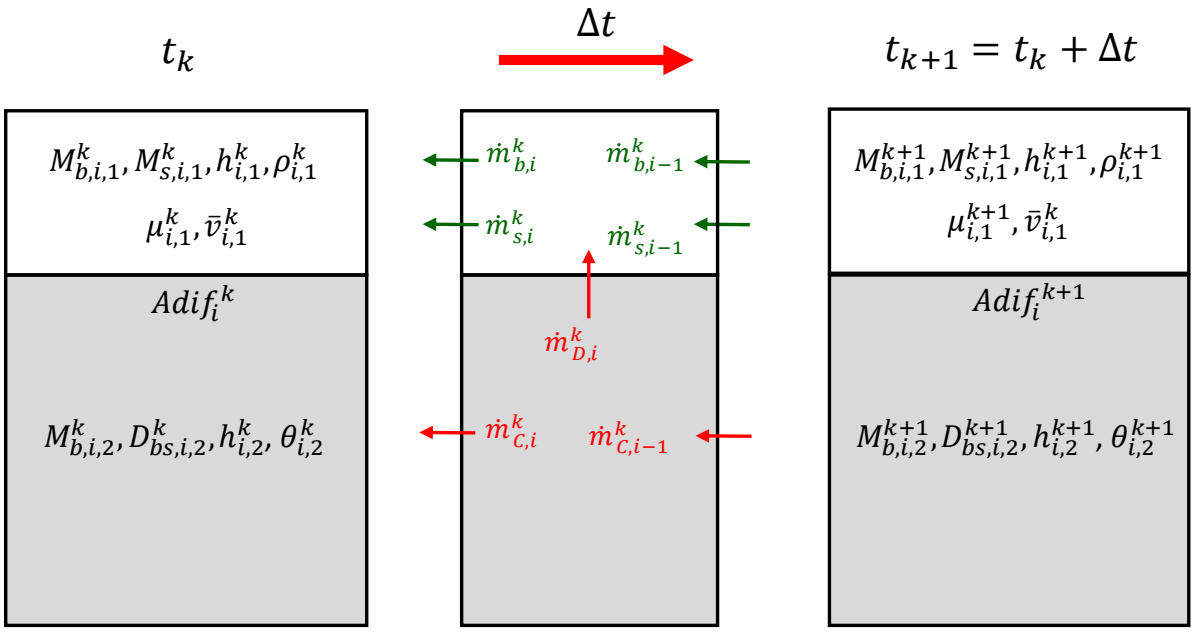

Figure 4.5. Single column within numerical model for gravity drainage experiments.

4.2.1. Initialization

The model is divided into columns designated from 1 to *n* in the horizontal direction. Each column has two blocks: a solvent block (1) on top and a bitumen block (2) below. The horizontal index starts at 1 corresponding to maximum bitumen height (right hand side of the Hele Shaw cell in Figure 4.3). The value of a quantity in a given block is specified as follows: $X^k_{i,j}$ where *X* is the quantity, *i* is the horizontal index, *j* is the vertical index (1 or 2), and *k* is the time index. Bitumen and solvent are indicated by subscripts *b* and *s*, respectively.

The initialization of the program requires setting the volume, mass, height, density, and viscosity of each bitumen and solvent block, as well as the area for mass transfer. The bitumen diffusivity and velocity of the solvent must also be defined. The total bitumen mass, basal length of the bitumen, angle of inclination are model inputs. The density and viscosity of the bitumen and solvent are also model inputs. The bitumen diffusivity is calculated from a correlation to viscosity as will be discussed later.

The bitumen has a triangular shape, as shown in Figure 4.6. Initially, there is no solvent in the bitumen and the height of the first bitumen column is calculated as follows:

$$h_{1,2}^{1} = \frac{2V_{binj}}{BL} \tag{4.15}$$

where h is height in cm, V_{binj} is the total volume of injected bitumen in cm³, and L is the basal length of the bitumen layer in cm. The heights of the other bitumen layers are given by:

$$h_{i,2}^{1} = h_{1,2}^{1} - (i-1)\frac{L}{n}\tan\theta \tag{4.16}$$

where n is the number of bitumen columns and θ is the initial angle of inclination. The initial bitumen volume in each column is calculated from the product between its area and the gap width as follows:

$$V_{b,i,2}^{1} = B\frac{L}{n}\left(L - i\frac{L}{n}\right)\tan\theta + \frac{\left(\frac{L}{n}\right)^{2} B\tan\theta}{2} \tag{4.17}$$

where V is volume in cm³. The initial mass of bitumen in each bitumen block is given by:

$$M_{b,i,2}^{1} = V_{b,i,2}^{1}\rho_{b} \tag{4.18}$$

where M is mass in g and ρ is density in g/cm³.

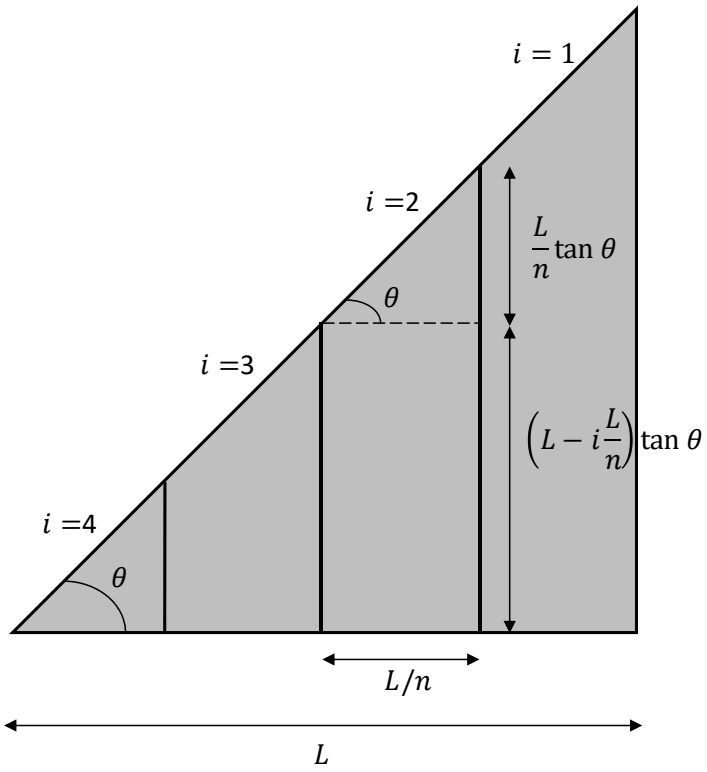

Figure 4.6. Trigonometric relations in the bitumen layer when n = 4.

Initially, there is no bitumen in the solvent layer. The initial thickness of the solvent layer is the same in all blocks and is calculated from Equation 4.3 as follows:

$$h_{i,1}^{1} = \sqrt[3]{\frac{3\mu_s q_s}{\rho_s g B \sin\theta}} \tag{4.19}$$

The volume of solvent in each solvent block is given by:

$$V_{s,i,1}^{1} = Bh\frac{L}{n} \tag{4.20}$$

The mass of solvent in each solvent block is given by:

$$M_{s,i,1}^{1} = V_{s,i,1}^{1}\rho_s \tag{4.21}$$

The mass of bitumen in the solvent blocks and the mass of solvent in the bitumen columns are set equal to zero at time $k = 1$:

$$M_{b,i,1}^{1} = M_{s,i,2}^{1} = 0 \tag{4.22}$$

The initial velocity of fluid in a solvent block is defined by the average velocity of a falling film (Equation 4.4) using the properties of the pure solvent at time $k = 1$:

$$\bar{v}_{i,1}^{1} = \frac{\rho_s g \sin\theta}{3\mu_s}\left(h_{i,1}^{1}\right)^2 \tag{4.23}$$

where $\bar{v}$ is the average velocity in cm/min, and μ_s is viscosity of the solvent in g/cm·s. Initially, the angle of inclination is the same in all blocks and therefore the velocity is the same in all solvent blocks.

4.2.2. Discretized Mass Balances

The mass balances for each component in the solvent layer over a time step are given by:

$$M_{b,i,1}^{k+1} = M_{b,i,1}^{k} + \dot{m}_{D,i}^{k}\Delta t + \dot{m}_{b,i-1}^{k}\Delta t - \dot{m}_{b,i}^{k}\Delta t \tag{4.24}$$

$$M_{s,i,1}^{k+1} = M_{s,i,1}^{k} + \dot{m}_{s,i-1}^{k}\Delta t - \dot{m}_{s,i}^{k}\Delta t \tag{4.25}$$

and the mass balance of bitumen in the bitumen layer over a time step is given by:

$$M_{b,i,2}^{k+1} = M_{b,i,2}^{k} - \dot{m}_{D,i}^{k}\Delta t + \dot{m}_{C,i-1}^{k} - \dot{m}_{C,i}^{k} \tag{4.26}$$

where $\dot{m}$ is mass flow rate. The subscript *D* indicates the bitumen mass flow rate from mass transfer and the subscript *C* indicates bitumen mass flow rate from creep flow; the other mass flow rates are from convection. The convective mass flow rate into the first block (1,1) is set to zero.

The discretized convective mass flow rates of bitumen and solvent exiting a solvent block (*i*,1) are given by:

$$\dot{m}_{b,i,1}^{k} = \dot{m}_{D,i}^{k-1}\Delta t + \dot{m}_{b,i-1,1}^{k} \tag{4.27}$$

$$\dot{m}_{s,i,1}^{k} = \rho_{mix,i,1}^{k} w_{s,i,1}^{k} \bar{v}_{i,1}^{k} h_{i,1}^{k} B\Delta t \tag{4.28}$$

where *w* is mass fraction. The discretized diffusive mass flux equation (Equation 4.11) exiting a bitumen block (*i*,2) is given by:

$$\dot{m}_{D,i}^{k} = A_{D,i}^{k}\rho_b D_{bs,i,2}^{k}\left(\frac{1 - w_{b,i,1}^{k}}{\Delta h_{D,i,1}^{k}}\right) \tag{4.29}$$

where $\dot{m}_D$ is the bitumen mass flow in g/min, A_D is the cross-sectional area in cm², D_{bs} is the diffusivity of the bitumen in the solvent in cm²/min, and Δh_D is the effective height of the concentration gradient for mass transfer. The final ratio in Equation 4.29 represents the concentration gradient for mass transfer. This gradient is not known and is approximated from the

difference in bitumen concentration between the bitumen and solvent block divided by the effective height for mass transfer. This height will be used as a fitting parameter. The calculation of diffusivity is discussed later.

The discretized creep mass flow rate equation (Equation 4.14) exiting a bitumen block (i,2) is given by:

$$\dot{m}_{C,i}^{k} = \frac{B^2}{12\mu_b}\left(\frac{\rho_b g(h_{i,2}^{k} - h_{i+1,2}^{k})}{\Delta x}\right) h_{i,2}^{k} B \rho_b \tag{4.30}$$

where $\dot{m}_C$ is the bitumen mass flow in g/min, $h_{i,2}^{k}$ is the height of the bitumen column in cm, $h_{i+1,2}^{k}$ is the height of the adjacent bitumen column to the left in cm and Δx is the column width (constant for all columns and at all times) in cm.

At each time step, the mass balances are solved and the following variables are updated: mass fractions, fluid properties, fluid velocity, angle of inclination, and block heights. The fluid properties are discussed later. The mass fraction of each component in each solvent block is calculated as follows:

$$w_{b,i,1}^{k} = \frac{M_{b,i,1}^{k}}{M_{s,i,1}^{k} + M_{b,i,1}^{k}} \tag{4.31}$$

$$w_{s,i,1}^{k} = \frac{M_{s,i,1}^{k}}{M_{s,i,1}^{k} + M_{b,i,1}^{k}} \tag{4.32}$$

The bitumen block height is calculated after each time step as follows:

$$h_{i,2}^{k} = \frac{M_{b,i,2}^{k}}{\rho_b \Delta x B} \tag{4.33}$$

The inclination of the bitumen phase is calculated between bitumen columns as follows:

$$\theta_{i,2}^{k} = \tan^{-1}\left(\frac{h_{i,2}^{k} - h_{i+1,2}^{k}}{\Delta x}\right) \tag{4.34}$$

The area available for mass transfer between the bitumen and the solvent blocks is updated as follows:

$$A_{D,i}^{k} = \left(\frac{\Delta x}{\cos\theta_{i,2}^{k}}\right) B \tag{4.35}$$

The velocity of the fluid in the solvent block is calculated as follows:

$$\bar{v}_{i,1}^{1} = \frac{g\left(\rho_{mix,i,1}^{k}\right)\left(h_{i,1}^{1}\right)^{2}\sin\left(\theta_{i,1}^{k}\right)}{3\mu_{mix,i,1}^{1}} \tag{4.36}$$

where subscript *mix* indicated the mixture of bitumen and solvent in the solvent block. The calculation of the mixture density and viscosity are discussed later.

The diluted bitumen mass flow rate is the mass of bitumen and solvent exiting from the last solvent block (*n*,1) divided by the time step and is calculated as follows:

$$\dot{m}_{P}^{k} = \frac{\dot{m}_{b,n,1}^{k} + \dot{m}_{s,n,1}^{k}}{\Delta t} \tag{4.37}$$

where $\dot{m}$ is mass flow rate. The subscript *P* indicates the diluted bitumen mass flow rate. The density of the diluted bitumen is calculated using density mixing rules and will be discussed later. The bitumen profile is estimated using the updated height of the bitumen columns.

4.2.3. Model Algorithm

A schematic of the algorithm to fit experimental data to the numerical model is shown in Figure 4.7. First, the duration of the experiment is set (normally four hours) and the time step and number of blocks are specified. The properties of the solvent blocks and bitumen columns are initialized and density and viscosity in the solvent layer are set as the pure solvent properties. The diffusivity and average velocity are calculated. An initial guess of the effective height for mass transfer, Δh_D, is provided.

The numerical model has two loops. The inner loop calculates the mass flow rates of produced bitumen and solvent, the density of the produced fluid, and the bitumen height profiles over time. At each time step, the mass fluxes from diffusion, creep flow and the convective masses are calculated and the masses of bitumen and solvent in each solvent block are updated. The density and viscosity of the mixture in the solvent blocks and the diffusivity of the bitumen into the solvent layer is recalculated. The average velocity in each solvent block is recalculated. The same procedure is repeated until the elapsed time in the model matches the duration of the experiment.

The outer loop compares the output of the inner loop with the experimental data of bitumen mass flux and density over time. The Δh_D input parameter is updated until the calculated plots match the target measured trends and magnitudes of bitumen mass flux and density over time. In this study, Δh_D was adjusted manually until the average absolute relative deviation of bitumen production over time was minimized.

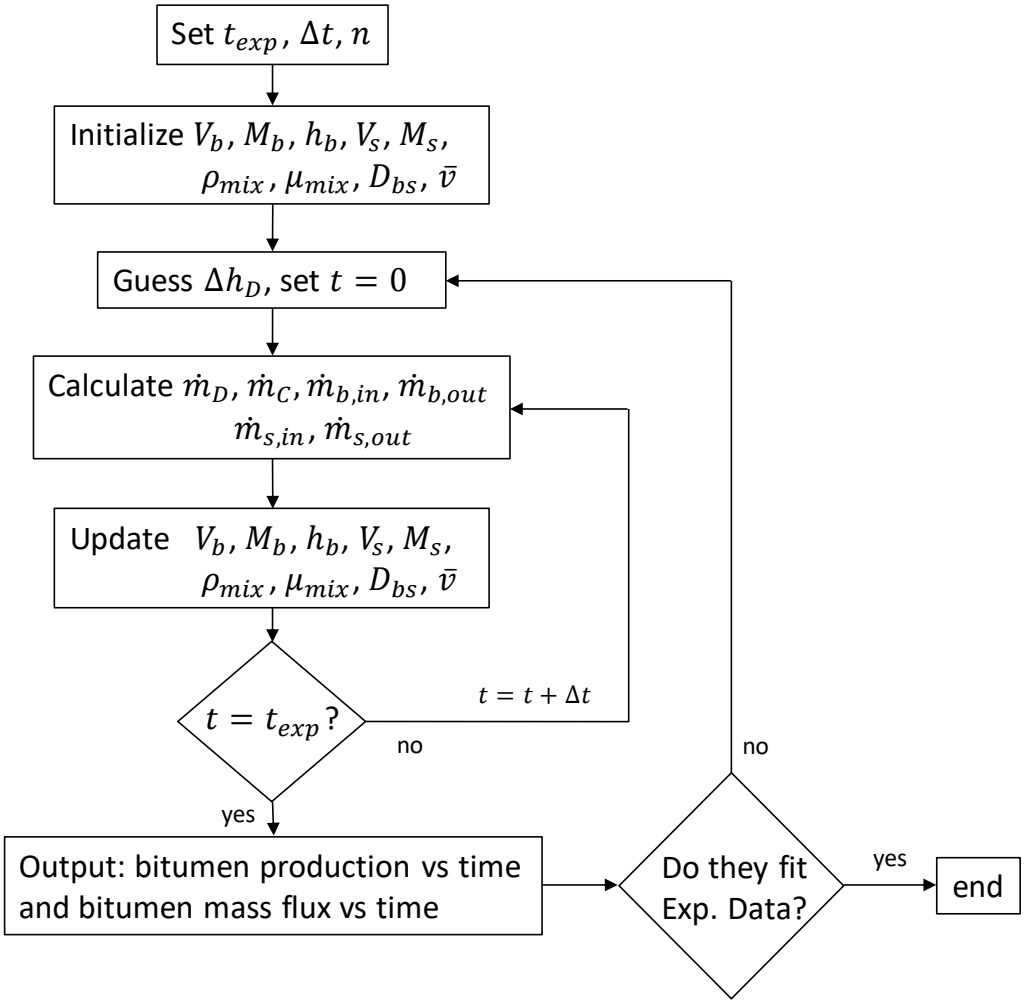

Figure 4.7. Algorithm to fit gravity drainage model to measurements of bitumen production over time.

The choice of the number of blocks and the time step are set to obtain a stable, convergent solution. The model can become unstable if the column thicknesses are too low (number of blocks too high) or the time step is too large. In this case, the initial convective mass flow would exceed the mass

of fluid in the block leading to a negative mass in the block. On the other hand, if the time step is too small, the computation time of the model can become too large for practical applications. Also, if the number of columns is too low, the accuracy of the model will be compromised. For example, a single column cannot represent the change in composition in the solvent layer as it flows from the top to the bottom of the apparatus. Hence, the time step and the number of bitumen columns were constrained with the following criterion:

$$0.03 \leq \frac{\Delta t}{\left(\frac{L}{n}\right)} \leq 0.11 \tag{4.38}$$

The limits of Equation 4.38 were calculated by manually adjusting the number of blocks and the time step until the model lost stability. Within the above criterion, the solution of the model was stable and the total run time was at most 20 seconds.

4.3. Property Models

4.3.1. Density

The densities of the solvent, bitumen, and their mixtures are required inputs for the gravity drainage model. As discussed in Chapter 3, the density of the WC-B-A3 bitumen sample was measured from 50 to 175°C and 0.1 to 10 MPa. The measured densities were fitted using the following empirical correlation (Saryazdi *et al.*, 2013):

$$\rho_b = (A^* - B^* T) \exp\{[F^* \exp(D^* T)](P - 0.1)\} \tag{4.39}$$

where ρ_b is the density of the bitumen in kg/m³, P is the pressure in MPa, T is the temperature in K, and A^*, B^* F^* and $D^*$are fitting parameters. The fitted parameters for the WC-B-A3 bitumen sample is provided in Table 4.1. Equation 4.39 fits the density of bitumen with a maximum absolute deviation of ±0.3 kg/m³.

Table 4.1. Parameters of the bitumen density equation.

Component	A^* **kg/m³**	B^* **kg/(m³K)**	F^* **1/MPa**	D^* **1/K**
WC-B-A3	1196.2	0.63743	0.00014	0.00433

Liquid toluene density was obtained from the NIST Chemistry Book ("NIST chemistry WebBook," 2013). The data was fitted using effective density correlation given by (Saryazdi *et al.*, 2013):

$$\rho_s = (a_1^* + a_2^* T) + (b_1^* + b_2^* T)P \tag{4.40}$$

where P is pressure in MPa, T is temperature in K, and a_1^*, a_2^*, b_1^*, and b_2^* are fluid specific parameters. The toluene parameters were determined following the procedure from Saryazdi *et al.* (2013) and are given in Table 4.2. The correlation fit the measured densities with an absolute deviation of ±0.7 kg/m³.

Table 4.2. Parameters for effective liquid density (Saryazdi *et al.*, 2013)

Component	a_1^* **kg/m³**	a_2^* **kg/(m³·K)**	b_1^* **kg/(m³·MPa)**	b_2^* **kg/(m³·MPa·K)**
Toluene	1150.778	-0.96697	-1.08866	0.006169

The density of the mixture was calculated using mixing rules previously tested on bitumen and toluene mixtures (Ramos-Pallares *et al.*, 2016b; Saryazdi *et al.*, 2013) assuming no excess volume of mixing as follows:

$$\rho_{mix} = \left(\frac{w_s}{\rho_s} + \frac{w_b}{\rho_b}\right)^{-1} \tag{4.41}$$

The density of diluted bitumen mixtures was predicted in previous studies with an accuracy of 1% using the mixing rule described by Equation 4.41 (Saryazdi *et al.*, 2013).

4.3.2. Viscosity

The viscosities of the solvent, bitumen, and their mixtures are required inputs for the gravity drainage model. As discussed in Chapter 3, the viscosity of the WC-B-A3 bitumen sample was measured from 50 to 175°C and 0.1 to 10 MPa. The bitumen viscosity data were fit with the Expanded Fluid Viscosity Model (Motahhari *et al.*, 2013a-c; Ramos-Pallares *et al.*, 2016a; Yarranton and Satyro, 2009). The viscosity of the solvent and the mixtures of bitumen and solvent were also calculated from this model.

In the Expanded Fluid viscosity model, the viscosity of a fluid is calculated as a density dependent departure function from a dilute gas viscosity given by:

$$\mu - \mu_D = 0.165(exp(c_2\beta) - 1) \tag{4.42}$$

where μ_D is the dilute gas viscosity in mPa·s, c_2 is a dimensionless fluid specific parameter and β is a correlating parameter related to the expansion of the fluid given by:

$$\beta = \frac{1}{exp\left(\left(\frac{\rho_s^*}{\rho}\right)^{0.65} - 1\right) - 1} \tag{4.43}$$

where ρ_s^* is the compressed state density in kg/m^3 given by:

$$\rho_s^* = \frac{\rho_s^0}{exp(-c_3 P)} \tag{4.44}$$

and where P is pressure in MPa and ρ_s^0 and c_3 are fluid specific parameters.

The dilute gas viscosity of toluene and WC-B-A3 bitumen was determined from the following empirical correlation:

$$\mu_D = A_0 + B_0 T + E_0 T^2 + F_0 T^3 \tag{4.45}$$

where A_0, B_0, E_0 and F_0 are fitting parameters specific for each pure component (Yaws, 2014) and T is the temperature in K. The dilute gas viscosity of bitumen was estimated using the parameters of the *n*-paraffin compound of the same molecular weight. The contribution of the dilute gas viscosity was negligible for the conditions examined in this thesis.

The parameters ρ_s^0, c_2, and c_3 for bitumen were obtained by fitting Equation 4.42 to experimental data. Solvent parameters were taken from Ramos-Pallares *et al.* (2016b). Both solvent and bitumen parameters are shown in Table 4.3. The correlation fit the bitumen viscosity from 50 to 175°C and pressures from 0.1 to 10 MPa to within ±2.8% with an AARD of 1.1% (Grimaldos, 2018).

Table 4.3. Expanded Fluid model fluid specific parameters.

Component	ρ_s^0 **kg/m³**	c_2	c_3 **10^{-3} MPa^{-1}**
Toluene	1049.6	0.2155	0.14
WC-B-A3	1061.2	0.4905	0.34

The following mixing rules are used in the Expanded Fluid Model to calculate ρ_s^0, c_3 and c_2 for mixtures (Motahhari *et al.*, 2011):

$$\rho_{s,mix}^0 = \left[\sum_{i=1}^{nc}\sum_{j=1}^{nc}\frac{w_i w_j}{2}\left(\frac{1}{\rho_{s,i}^0}+\frac{1}{\rho_{s,j}^0}\right)(1-\theta_{ij})\right]^{-1} \tag{4.46}$$

$$\frac{c_{2,mix}}{\rho_{s,mix}^0} = \sum_{i=1}^{nc}\sum_{j-1}^{nc}\frac{w_i w_j}{2}\left(\frac{c_{2,i}}{\rho_{s,i}^0}+\frac{c_{2,j}}{\rho_{s,j}^0}\right)(1-\theta_{ij}) \tag{4.47}$$

$$c_{3,mix} = \left[\sum_{i=1}^{nc}\frac{w_i}{c_{3,i}}\right]^{-1} \tag{4.48}$$

$$\mu_{D,mix} = \sum_i \frac{x_i \mu_{D,i}}{\sum_j x_j \delta_{ij}} \tag{4.49}$$

$$\delta_{ij} = \frac{\left[1+\left(\mu_{D,i}/\mu_{D,j}\right)^{0.5}\left(MW_j/MW_i\right)^{0.25}\right]^2}{\left[8\left(1+MW_i/MW_j\right)\right]^{0.5}} \tag{4.50}$$

where nc is the number of components in the system and θ_{ij} is a binary interaction parameter that can be calculated using the procedure and equations presented by (Ramos-Pallares et al., 2016a). The binary interaction parameters is given by:

$$\alpha_{ij} = \alpha_{ij}{}^{\circ} - \Delta\alpha_{ij} \tag{4.51}$$

where $\alpha_{ij}°$ is a reference function and $\Delta\alpha_{ij}$ is a departure function. The reference function is given by:

$$\alpha_{ij}° = 0{,}021 \qquad \text{if } \Delta SG_{norm} \leq 0.165 \tag{4.52}$$

$$\alpha_{ij}° = 0{,}038304 - 0{,}10478\Delta SG_{norm} \qquad \text{if } \Delta SG_{norm} > 0.165 \tag{4.53}$$

$$\Delta SG_{norm} = \frac{2\left|SG_i - SG_j\right|}{SG_i + SG_j} \tag{4.54}$$

where ΔSG_{norm} is the normalized specific gravity and SG_i refers to the specific gravity of component *i*. The departure function is given by:

$$\Delta\alpha_{ij} = 0.02756 - 0.1103\Delta(H/C)_{norm} \qquad \text{if } \Delta(H/C)_{norm} \leq 0.25 \tag{4.55}$$

$$\Delta\alpha_{ij} = 0 \qquad \text{if } \Delta(H/C)_{norm} > 0.25 \tag{4.56}$$

$$\Delta(H/C)_{norm} = \frac{2\left|(H/C)_i - (H/C)_j\right|}{(H/C)_i - (H/C)_j} \tag{4.57}$$

where $\Delta(H/C)_{norm}$ is the normalized difference in the hydrogen/carbon ratio of the paired components and $(H/C)_i$ refers to the hydrogen/carbon ratio of component *i*. The expected accuracy of the EF model is between 10 and 14% (Ramos-Pallares *et al.*, 2016a).

4.3.3. Diffusivity

The mutual diffusivity of the bitumen and solvent is a required input for the gravity drainage model. The mutual diffusivity was determined from the following correlation (Grimaldos, 2018):

$$D_{sb} = \frac{AT}{{\mu_{mix}}^n} \tag{4.58}$$

where *n* and *A* are parameters given by:

$$n = \frac{\log \frac{{D_{bs}}^{\infty}}{{D_{sb}}^{\infty}}}{\log \frac{\mu_s}{\mu_b}} \tag{4.59}$$

$$A = \frac{{D_{sb}}^{\infty}}{T} {\mu_b}^{n} \tag{4.60}$$

where ${D_{bs}}^{\infty}$ is the infinite dilution diffusivity of bitumen into solvent and ${D_{sb}}^{\infty}$ is the infinite dilution diffusivity of solvent into bitumen. All diffusivities in this thesis are determined in cm²/s.

The infinite dilution diffusivity of bitumen into solvent ${D_{bs}}^{\infty}$ can be calculated using the Wilke-Chang equation, given by: (Wilke and Chang, 1955)

$$D_{bs}^{\infty} = \frac{7.4 \cdot 10^{-8} \sqrt{\mathrm{MW}_s} T}{\mu_s \check{v}_b^{0.6}} \tag{4.61}$$

where T is the temperature in K, $\check{v}_b$ is the molar volume of the bitumen at normal boiling temperature in cm³/mol and MW_s is the molecular weight of the solvent. The infinite dilution diffusivity of solvent into bitumen ${D_{sb}}^{\infty}$ is given by (Grimaldos, 2018):

$$\frac{D_{sb}^{\infty}}{T} = \frac{2.7 \times 10^{-7}}{{\mu_b}^{0{,}544}} \tag{4.62}$$

The model matched measured concentration profiles to within 2% for bitumen.

CHAPTER FIVE: RESULTS AND DISCUSSION

This chapter presents the results from the gravity drainage experiments of a heavy oil and toluene system. The experimental conditions are summarized and the results for a typical drainage experiment are presented including the mass transfer measured rates, heavy oil recovery rates, and progression of the bitumen profile. Then, the effects of the initial interface angle, gap width (between the glass plates of the Hele-Shaw cell), and solvent injection flow rate are discussed. Finally, the numerical model developed in Chapter 4 is fitted to the measured heavy oil flow rates and the bitumen profiles.

5.1. Data Collected in this Thesis

Gravity drainage experiments were performed with the WC-B-A3 bitumen and toluene. The density and viscosity of the fluids at 20°C are summarized in Table 5.1. Gap widths between the glass plates of the Hele-Shaw cell of 0.5 and 1.0 mm were used to evaluate the effect of capillary forces. Solvent flow rates of 0.1 to 2 cm^3/min were assessed at both gap widths in order to determine the impact of the thickness of the solvent film. The upper limit (2 cm^3/min) was sufficient to investigate the mass transfer controlled drainage mechanism considered in this thesis. Due to the limitations of the injection pump, experiments could not be performed at solvent flow rates below 0.1 cm^3/min. Initial inclination angles from 30 to 45° were considered for the 0.5 mm gap width in order to evaluate the effect of the solvent velocity. Angles below 30° were not evaluated because the initial volume of bitumen in the cell would be low to obtain meaningful experimental results. At an initial inclination angle of 55°, the high velocity of the solvent during gravity drainage caused an erosion effect in the bitumen, leading to high values of bitumen mass flux over time that could no longer be modeled as a diffusion controlled mass transfer process. Hence, results above a 45° initial inclination angle were excluded from the discussion.

Table 5.1. Properties of fluids used for gravity drainage experiments at 20°C.

Fluid	Density, g/cm³	Viscosity, mPa·s
WC-B-A3 Bitumen	1.0093	357,000
Toluene	0.8674	0.602

The data directly measured in a gravity drainage experiment are the mass of the produced fluid (a mixture of bitumen and solvent), the density and bitumen content of the produced fluid, and the progression of the bitumen profile over the course of the experiment. The bitumen production rate is determined from the total production rate and bitumen content of the produced fluid. The bitumen flux is also calculated as follows:

$$n_{b,i} = \frac{\Delta m_{b,i}}{\bar{A}_i \Delta t_i} \tag{5.1}$$

where n_b is the bitumen mass flux in g/cm²·min, Δt is the time interval in min during which a produced fluid sample is collected, Δm_b is the recovered bitumen mass in g during the time interval, $\bar{A}$ is the average area of contact between the solvent and the bitumen during the time interval, and i indicates the sample number. The average area of contact is calculated from the image analysis described in Chapter 3.

5.2. Typical (Base Case) Drainage Experiment

Figure 5.1 shows the cumulative bitumen production, bitumen production rate, bitumen profiles, and bitumen mass flux for a bitumen and toluene system with a gap width of 0.5 mm, an initial interface angle of 35°, and a toluene injection flow rate of 1 cm³/min. The bitumen production rate and bitumen mass flux decreased gradually over time. Possible reasons for this decrease in production rate are discussed later.

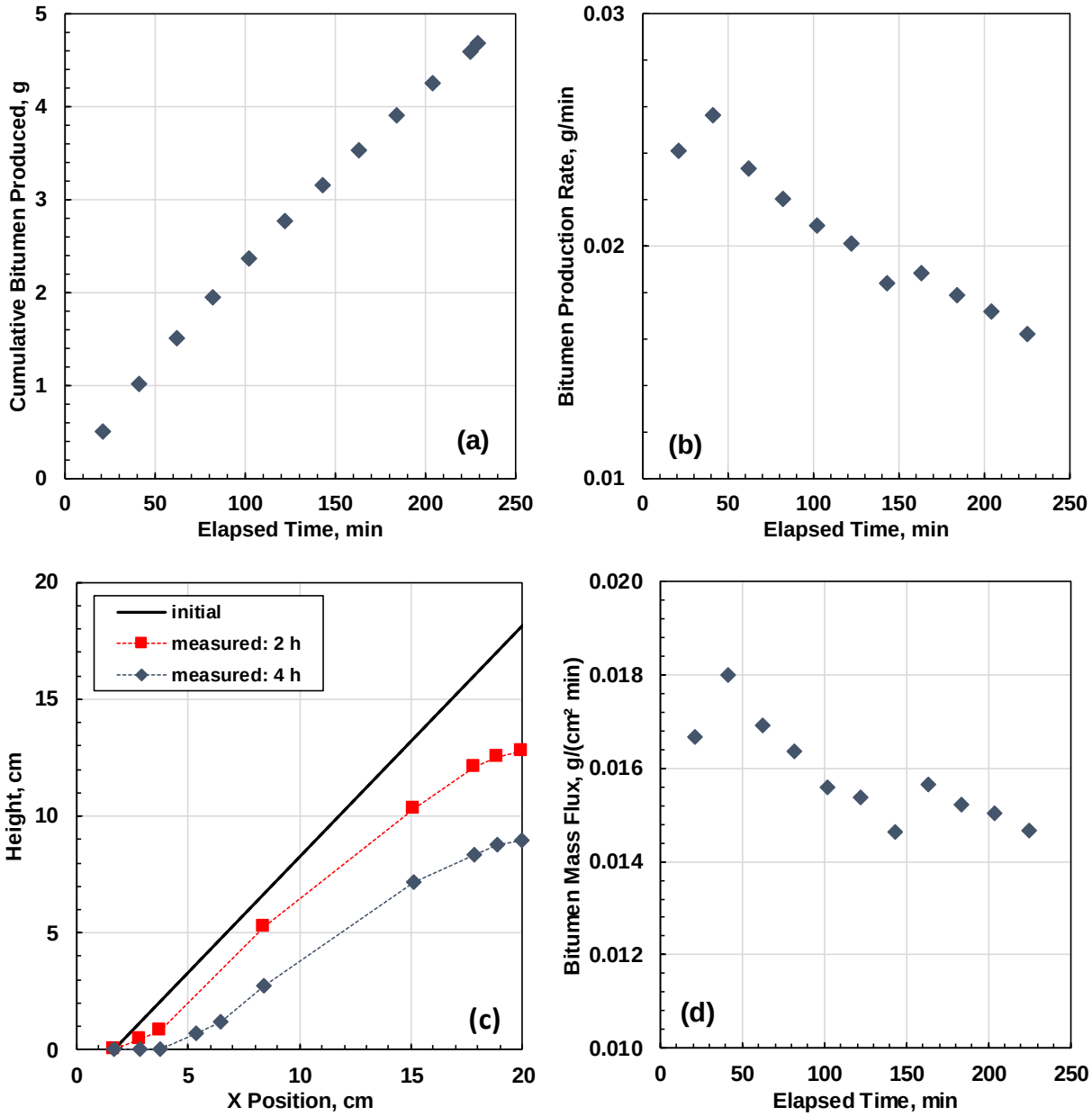

Figure 5.1. Production measurements for the base case gravity drainage experiment (gap width of 0.5 mm, initial angle of inclination of 35° and toluene flow rate of 1 cm³/min): a) cumulative mass of bitumen produced; b) bitumen mass production rate; c), bitumen profiles; d) mass flux.

Figure 5.2a shows the measured bitumen content in the produced fluid over time for the base case experiment. The bitumen content was less than 3.5 wt% consistent with a drainage layer dominated by the convective flow of toluene and with bitumen limited by diffusion into this layer. The

bitumen content decreased over time consistent with the reduced mass flux. Figure 5.2b shows the density of the produced fluid. As expected with such low bitumen contents, the density was near that of toluene (0.867 g/cm³) and decreased over time as the bitumen content decreased. The density was also calculated from the measured bitumen content and the known densities of toluene and the bitumen (1.00 g/cm³) using a regular solution mixing rule (zero excess volume of mixing). Figure 5.2a shows that the calculated densities are within 0.0001 g/cm³ of the measured densities, confirming the consistency of the measurements.

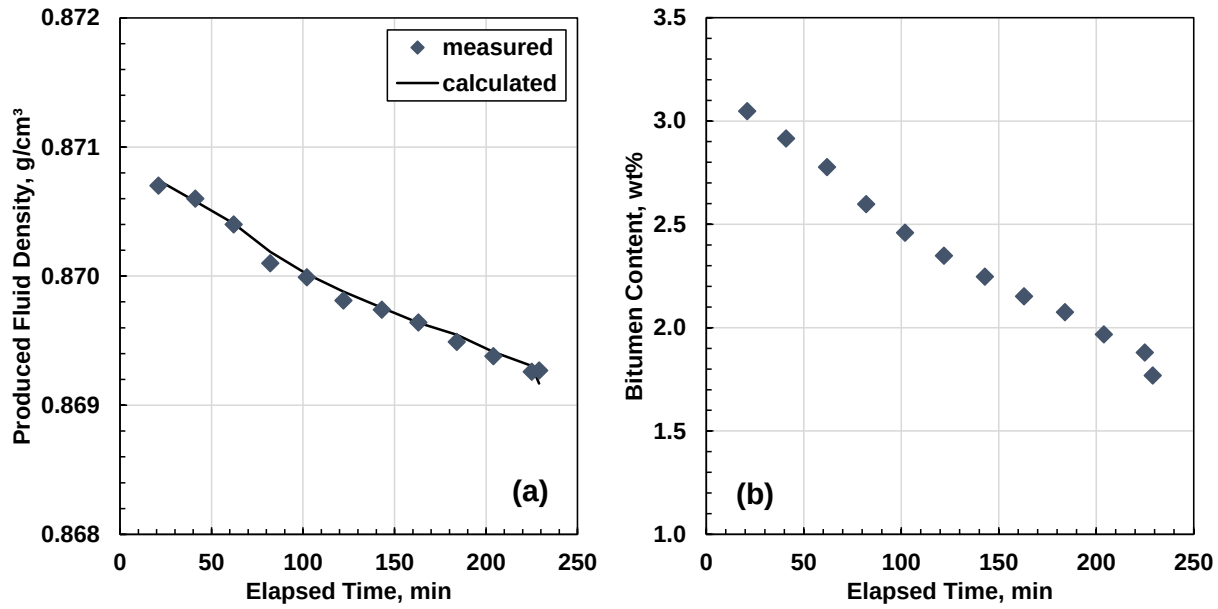

Figure 5.2. Product property measurements from the base case gravity drainage experiment (gap width of 0.5 mm, initial angle of inclination of 35° and toluene flow rate of 1 cm³/min): a) density; b) bitumen content.

5.3. Effect of Experiment Variables on Drainage

The effect of the variables is shown through comparisons of the mass flux. The other measurements compare similarly (see Appendix B).

5.3.1. Gap Width

If capillary forces are a factor in the experiment, the results are expected to depend on the gap width with less capillary effects at wider gaps. Figure 5.3 shows that changing the gap width did not affect the bitumen mass flux at an initial inclination angle of 35° and a toluene flow rate of 0.5 cm^3/min. Similar results were obtained at all the toluene flow rates and inclination angles considered in this thesis. Hence, the capillary forces are considered to be negligible in these experiments. The capillary forces may be negligible because the relevant contacts are between the drainage layer and air (essentially air/toluene) and between bitumen and the drainage layer (bitumen/toluene). For the air/toluene contact, the viscosity of the fluid is low enough for drainage to continue unimpeded. For the bitumen/toluene contact, the interfacial tension is very low giving negligible capillary pressure. The absence of strong capillary forces is what allowed the bitumen to settle under its own weight during the gravity drainage experiments.

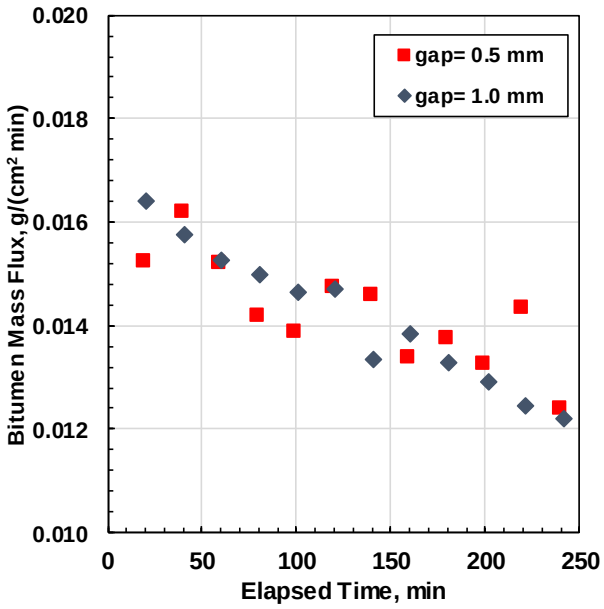

Figure 5.3. Bitumen mass flux over time for gravity drainage experiments with an initial angle of inclination of 35°, toluene flow rate of 0.5 cm^3/min, and gap widths of 0.5 and 1.0 mm. The repeatability of the bitumen flux was ±0.0008 g/(cm^2min) based on a 90% confidence interval.

5.3.2. Initial Angle of Inclination

As presented in Chapter 4, the inclination angle of the bitumen in the Hele-Shaw cell determines the velocity of the solvent film during the process as follows:

$$\bar{v} = \frac{\rho_{mix} g h_s^2 \sin\theta}{3\mu_{mix}} \tag{5.2}$$

where ρ_{mix} is the density of the mixture in g/cm^3, g is gravitational acceleration in cm/s^2, h_s is the film thickness in cm, μ_{mix} is the viscosity of the mixture in g/cm·s and θ is the inclination angle. Therefore, if convection plays a role in the bitumen recovery process, the bitumen mass flux should depend on the inclination angle (velocity). Figure 5.4 shows the bitumen mass flux over time for three different initial inclination angles when all other conditions were kept the same. There is no difference between the recovery rates in the range of 30 and 45°, indicating the angle (or velocity) does not affect the production rate. Hence, the gravity drainage in these experiments must be a diffusive mass transfer and/or creep flow controlled process rather than a convection controlled process.

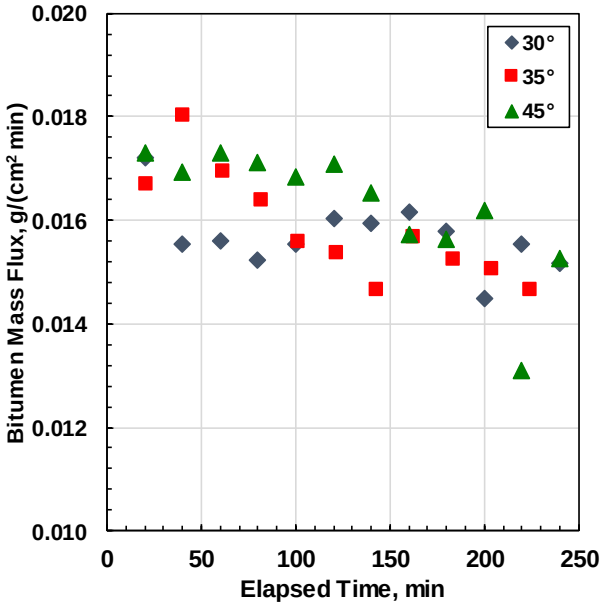

Figure 5.4. Bitumen mass flux over time for gravity drainage experiments with gap width of 0.5 mm, toluene flow rate of 1 cm^3/min and three different initial angles of inclination. The repeatability of the bitumen flux was ±0.0026 g/(cm²min) based on a 90% confidence interval.

5.3.3. Solvent Flow Rate

If the gap width and the initial inclination angle are constant, the solvent flow rate directly affects the drainage layer thickness, as shown in Figure 5.5. The height of the drainage layer is small for a low solvent rate and increases when the solvent rate increases. A sufficiently thick drainage layer will act as a semi-infinite plane for the mass transfer of bitumen into the drainage layer; that is, an infinite acting boundary condition. As long as this condition is met, the mass transfer rate will be independent of the drainage layer thickness. At lower thicknesses, the bitumen concentration reaches the top of the layer (finite acting boundary condition) and the average bitumen concentration within the layer will increase reducing the mass transfer rate.

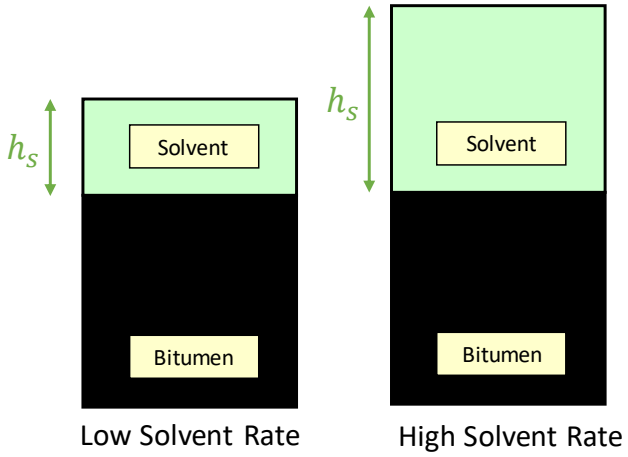

Figure 5.5. Schematic of the change in the drainage layer thickness for different solvent injection rates when all other conditions of the gravity drainage experiment are kept constant.

Figure 5.6 shows the bitumen mass flux over time for a gap width of 0.5 mm (Figure 5.6a) and 1.0 mm (Figure 5.6b) at toluene flow rates from 0.1 to 2 cm³/min. At flow rates of 0.3 cm³/min and above, the bitumen mass flux is independent of the toluene flow rate indicating that the drainage layer acts as a semi-infinite plane. However, at a toluene rates of 0.1 cm³/min, the mass flux decreases substantially indicating that the boundary condition has changed. The mechanism for gravity drainage at toluene flow rates of 0.1 cm³/min will be discussed later in this chapter.

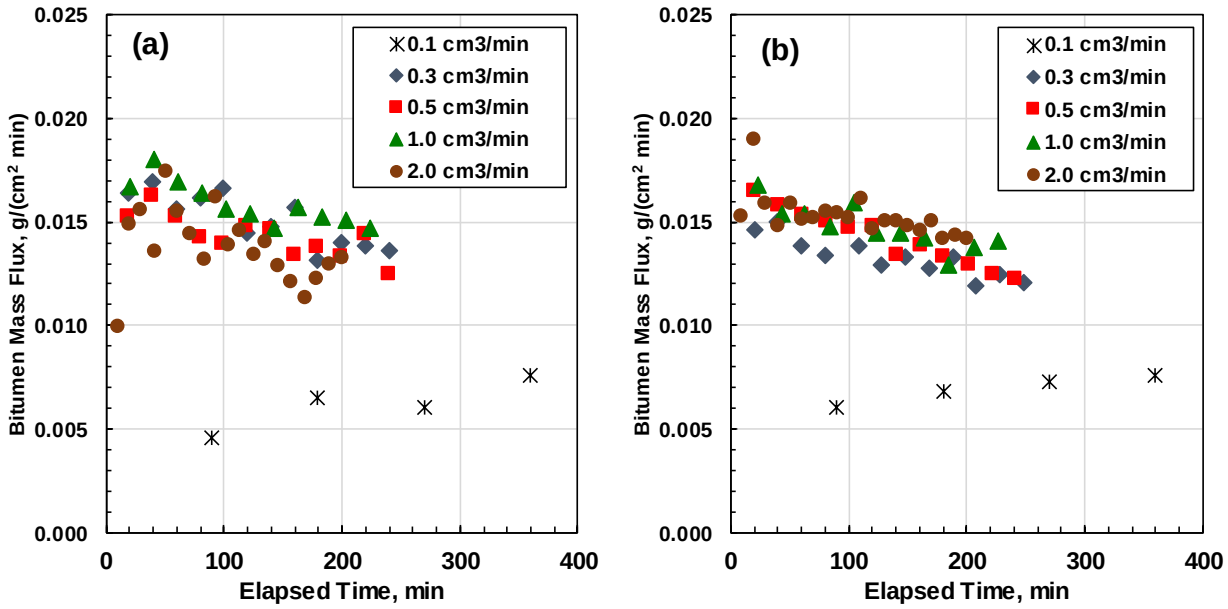

Figure 5.6. Bitumen mass flux over time for gravity drainage experiments with an initial angle of inclination of 35° and toluene flow rates from 0.1 to 2.0 cm³/min: a) 0.5 mm gap width; b) 1.0 mm gap width. The repeatability of the bitumen flux was ±0.0026 g/(cm²min) based on a 90% confidence interval.

5.3.4. Summary

Figure 5.7 compares the bitumen mass flux for all of the experiments in this thesis at flow rates above 0.3 cm³/min. The overall variance was ±0.0026 g/cm²min based on a 90% confidence interval, only slightly higher than the ±0.00255 g/cm²min uncertainty based on repeats. A similar comparison was not possible for density, cumulative production and bitumen production rate because these measurements depended on the bitumen volume in the Hele-Shaw cell. However, these variable must be consistent after accounting for the differences in cell volume when the flux is consistent.

Figure 5.8 compares the bitumen profiles over time for all of the gravity drainage experiments performed at toluene flow rates above 0.3 cm³/min. The overall variance was ±1.7 cm based on a 90% confidence interval, only slightly higher than the ±1.2 cm uncertainty based on repeats. Hence, it was concluded that the gravity drainage process was insensitive to the gap width, angle of inclination, and flow rate at the conditions examined in this thesis (at flow rates above 0.3 cm³/min).

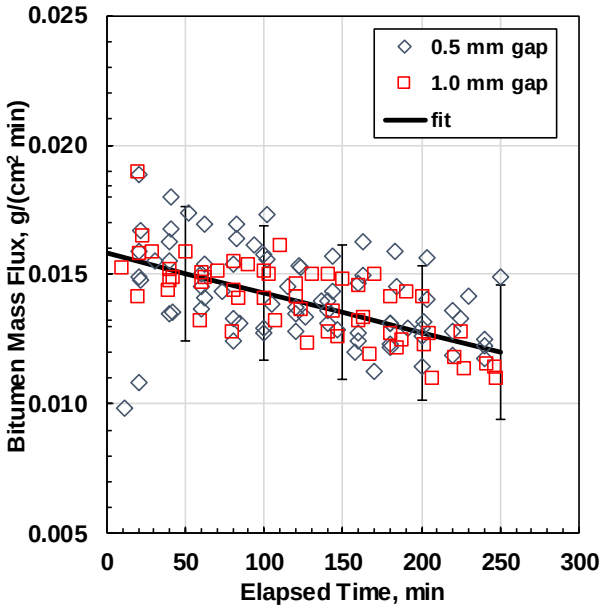

Figure 5.7. Bitumen mass flux over time for gravity drainage experiments with gap widths of 0.5 and 1 mm and toluene flow rates from 0.3 to 2 cm³/min.

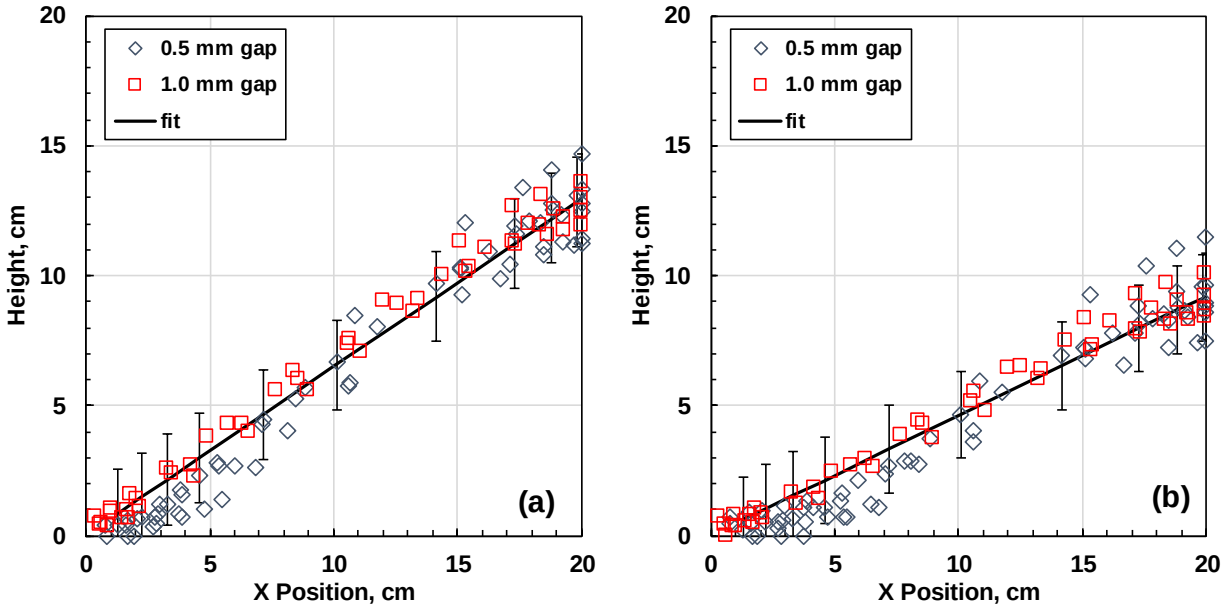

Figure 5.8. Bitumen profiles over time for gravity drainage experiments with gap widths of 0.5 and 1 mm and toluene flow rates from 0.3 to 2 cm3/min. a) after 2 h and b) after 4 h.

5.4. Modeling Gravity Drainage Experiments

5.4.1. Drainage Layer Velocity

The velocity of the drainage layer was investigated with toluene and a teflon spacer set in the Hele Shaw cell to determine the best approach to model the gravity drainage flow rate (see Section 3.3.5). The velocity was assumed to be laminar and was modeled using three approaches:

- falling film flow (Eq. 5.2)
- Darcy's Law (Butler and Mokrys, 1989),
- open channel flow (Tsanis and Leutheusser, 1986).

Darcy flow assumes that the drainage layer flow is equivalent to flow between parallel plates and the velocity is given by:

$$\bar{v} = \frac{\rho_s g B^2 \sin\theta}{12\mu_s} \tag{5.3}$$

The open channel flow assumes a free surface with boundary conditions at the sides and bottom of the channel and the uniform steady state velocity is given by:

$$\bar{v} = \frac{4\rho_s g B^3 \tan\theta}{K_o \mu_s h_s} \frac{\lambda_o^3}{(1+\lambda_o)^2} \tag{5.4}$$

where K_o is a dimensionless value determined from a numerical solution (approximately 60 for the conditions in this thesis) and λ_o is given by:

$$\lambda_o = \frac{2h_s}{B} \tag{5.5}$$

The average velocity is related to the flow rate as follows:

$$\bar{v} = \frac{q_s}{B h_s} \tag{5.6}$$

Equation 5.6 is substituted into Equation 5.4 to obtain the following expression:

$$q_s = \frac{4\rho_s g B^4 \tan\theta}{K_o \mu_s} \frac{\lambda_o^3}{(1+\lambda_o)^2} \tag{5.7}$$

Equation 5.7 is cubic in terms of the drainage layer thickness and is solved numerically. Once the drainage layer thickness is determined the velocity is calculated from Eq. 5.6.

The Reynolds numbers were calculated for all three flow assumptions. The Reynolds number of the falling film was calculated from Eq. 4.5. The Reynolds number for Darcy's law is given by:

$$Re = \frac{D_p \bar{v} \rho_{mix}}{\mu_{mix}} \tag{5.8}$$

where

$$D_p = \frac{2h_s B}{h_s + B} \tag{5.9}$$

and for open channel flow is given by:

$$Re = \frac{4R_h \bar{v} \rho_{mix}}{\mu_{mix}} \tag{5.10}$$

where

$$R_h = \frac{h_s B}{2h_s + B} \tag{5.11}$$

The Reynolds number based on the measurements was less than 350 in all cases confirming laminar flow.

Figures 5.9a and 5.9b compare the measured and modeled drainage layer velocity and thickness, respectively. The approach that best matched the measured drainage layer velocity was the open channel flow model followed by the falling film model. The Darcy's law approach deviated the most from the measured data and incorrectly predicted that the velocity is independent of the drainage layer thickness. At flow rates below 1 cm^3/min, the open channel flow and the falling film approaches predicted similar velocities and film thicknesses. As will be discussed later in this chapter, the velocity of the solvent layer did not have a significant effect on the production of bitumen. Hence, for this thesis, the falling film was used to obtain a simple non-iterative solution. Table 5.2 shows the calculated velocity, film thickness and Reynolds number for all runs performed for this thesis using the falling film approach. The calculated film thicknesses ranged from 0.12 to 0.38 mm and the velocities from 4 to 21 cm/s. Based on Figure 5.9, the actual film thicknesses likely range from 0.2 to 0.6 mm with velocities from 4 to 12 cm/s.

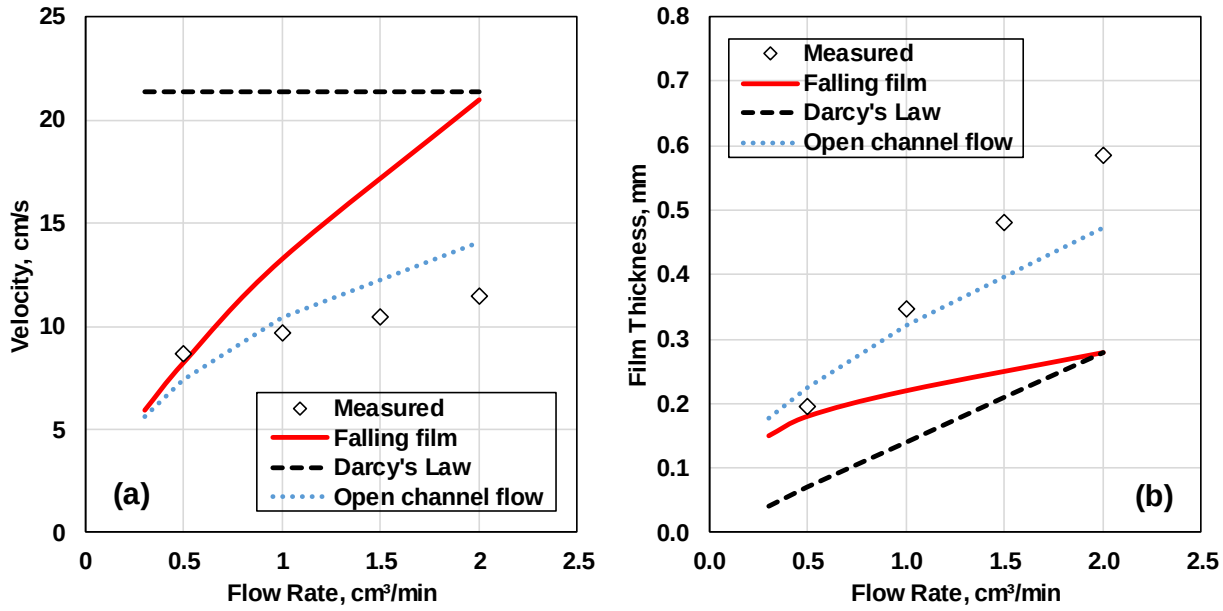

Figure 5.9. Comparison of experimental and modeled velocity and film thickness for a spacer teflon test with a gap width of 0.5 mm and initial angle of inclination of 35°: a) velocity; b) film thickness. The experimental drainage layer heights were calculated from the previously calculated velocity.

Table 5.2. Calculated velocity, film thickness and Reynolds number for gravity drainage experiments performed for this thesis using the falling film approach.

Gap Width mm	Angle °	Inj. Rate cm³/min	Velocity cm/s	Film Thickness mm	Reynolds Number
0.5	35	0.3	5.97	0.149	51
0.5	35	0.5	8.39	0.176	85
0.5	35	1.0	13.31	0.222	170
0.5	35	2.0	21.14	0.280	341
1.0	35	0.3	4.29	0.126	31
1.0	35	0.5	6.03	0.150	52
1.0	35	1.0	9.57	0.188	104
1.0	35	2.0	15.2	0.237	208
0.5	45	1.0	14.28	0.207	170
0.5	30	1.0	12.72	0.233	170

5.4.2. Base Case

Figure 5.10 shows the measured cumulative bitumen production, bitumen production rate, bitumen profiles and bitumen mass flux for a bitumen and toluene system with a gap width of 0.5 mm, an initial interface angle of 35° and a toluene injection flow rate of 1 cm³/min. The measured data are from Figure 5.1. Two versions of the model are shown: one without creep (dotted lines) and one with creep (dashed lines). The models were first tuned to fit the production rate of each experiment by adjusting the effective height of the concentration gradient for diffusion (Δh_D) for each experiment. Then the average effective height was calculated (Δh_D = 0.0247 cm) and used to model all of the experiments in this thesis. The same Δh_D was used for both models. Both models provide similar fits to the production data indicating that creep flow makes a relatively minor contribution to the production. However, the model without creep flow does not match the bitumen profiles while the model with creep does (Figure 5.10c). Hence, creep flow is essential to accurately model the drainage process in these experiments and only the model with creep flow is considered from this point forward.

The model shows a step pattern decrease in the bitumen production rate over time, Figure 5.10b. The step change is generated when one of the bitumen columns runs out of mass. At this point, the mass that diffuses to the solvent phase decreases and generates the step change. The same step change is observed in the bitumen mass flux (Figure 5.10d). When the last column of bitumen runs out of mass, the next column to the right starts transferring bitumen into the solvent layer at a faster rate due to this active column having a slightly bigger height compared to the previous one. Hence, the increase in mass is not equally compensated with a proportional decrease in the area for diffusion, generating the small step increase in the bitumen mass flux. The steps in the model output could be reduced by using a larger number of columns but longer run times would be required.

Figure 5.10b shows that the model partly captures the decrease in bitumen rate over time. The predicted bitumen mass flux is constant. Therefore, the main reason for the decrease in the predicted rate is the decrease in surface area at the interface between the bitumen layer and the solvent layer over time as the bitumen is produced out of the cell. The model underestimates the

mass flux in the first 60 minutes. The mass transfer rate is expected to be higher initially because bitumen is diffusing into pure solvent. The mass transfer rate decreases until a steady state condition is achieved apparently after 60 minutes. The model only applies to steady state and therefore underestimates the initial mass flux.

Overall, the results from Figure 5.10 confirm the validity of the model assumptions. Gravity drainage at the conditions studied in this thesis is dominated by the two described recovery mechanisms. Diffusion of solvent into the bitumen can be neglected because the penetration rate is smaller than the velocity at which the height of the bitumen decreases. The bitumen that diffuses into the solvent is immediately swept away by the solvent layer and the concentration gradient for diffusion remains almost constant over time. The solvent can be approximated as a single flowing layer moving at an average velocity of a falling film down an inclined plane.

Figure 5.11a and 5.11b show, respectively, the bitumen content over time and produced fluid density for the same gravity drainage experiment shown in Figure 5.10. The initial bitumen content and the initial fluid density are underestimated because the initial mass flux is underestimated. The final fluid density is slightly overestimated (maximum of 0.001 g/cm^3) even when the model matches the bitumen content. The maximum deviation is 0.001 g/cm^3 and is less than the measurement error of ±0.006 g/cm^3.

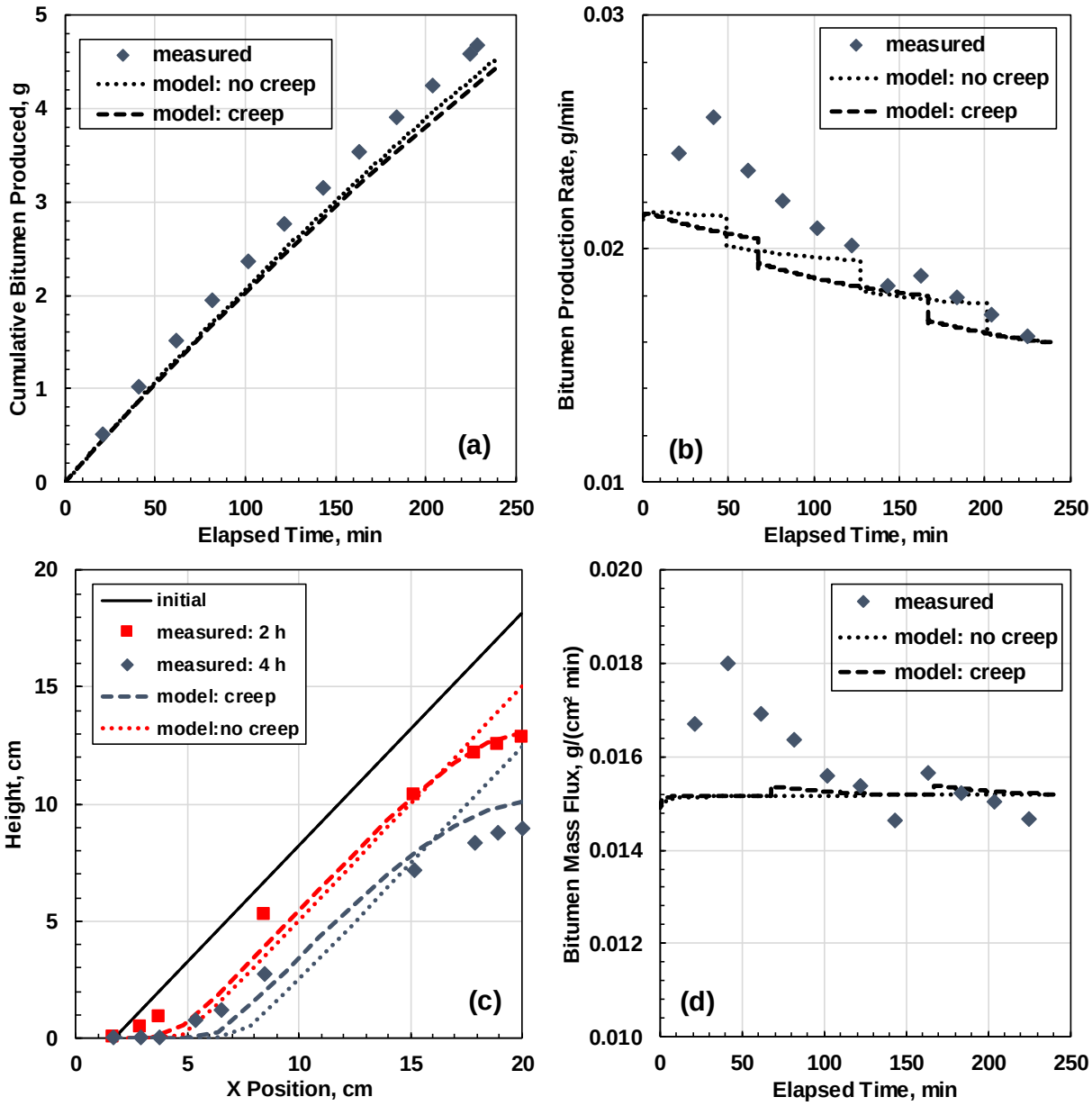

Figure 5.10. Measured and modeled production data for the base case gravity drainage experiment (gap width of 0.5 mm, initial angle of inclination of 35° and toluene flow rate of 1 cm³/min): a) cumulative mass of bitumen produced; b) bitumen mass production rate; c), bitumen profiles; d) mass flux. Dotted and dashed lines are the model without and with bitumen creep, respectively. The repeatabilities of the bitumen flux, cumulative bitumen production, bitumen production rate and height of the bitumen profile were ±0.0026 g/(cm²min), ±0.006 g/min, ±10% and ±1.7 cm, respectively, based on a 90% confidence interval.

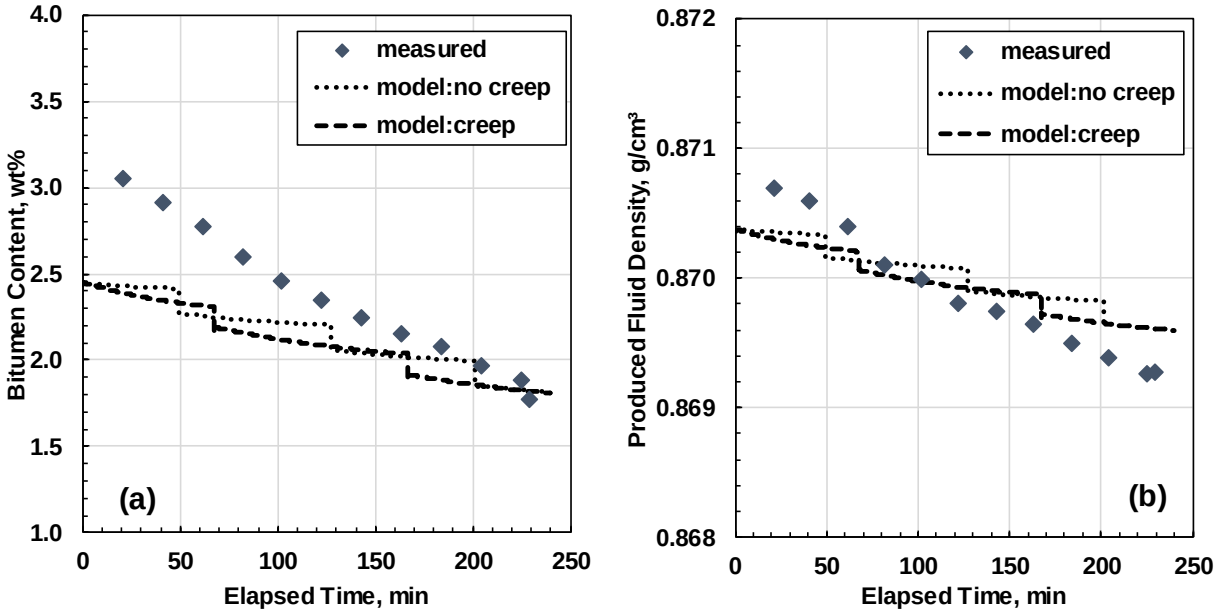

Figure 5.11. Measured and modeled product properties from the base case gravity drainage experiment (gap width of 0.5 mm, initial angle of inclination of 35° and toluene flow rate of 1 cm³/min): a) bitumen content; b) density. Dotted and dashed lines are the model without and with bitumen creep, respectively. The repeatabilities of the bitumen content and the produced fluid density ±0.7 wt% and ±0.006 g/cm³, respectively, based on a 90% confidence interval.

5.4.3. Infinite Acting Diffusion (Toluene Flow Rate > 0.1 cm³/min)

The overall deviations of the model for all of the experiments performed in the infinite acting regime (toluene flow rates above 0.1 cm³/min) are provided in Tables 5.3 and 5.4. The modeling of different gap widths, flow rates, and inclination angles is discussed below. As before, only the mass flux and bitumen profile are considered. In order to compare experimental bitumen profiles with different toluene rates against modeled profiles, the height of the profiles was normalized against the initial height as follows:

$$H = \frac{h_b}{h_{bi}} \tag{5.12}$$

where H is the normalized height of the bitumen phase and h_{bi} and h_b are, respectively, the initial bitumen height and the bitumen height measured at time t at the same horizontal position.

Table 5.3. Deviations of the modeled production related data for gravity drainage experiments performed in the infinite acting regime.

Gap Width mm	Angle degree	Inj. rate cm^3/min	Bitumen Produced		Bitumen Profile	
			AARD %	MARD %	AAD cm	MAD Cm
0.5	35	0.3	11.2	32.5	0.8	1.8
0.5	35	0.5	5.1	7.4	0.8	1.4
0.5	35	1.0	12.4	20.6	0.9	1.7
0.5	35	2.0	4.9	12.7	1.1	2.1
1.0	35	0.3	5.0	10.1	0.5	1.1
1.0	35	0.5	4.2	12.6	0.6	1.8
1.0	35	1.0	5.8	21.9	0.4	0.7
1.0	35	2.0	5.9	13.3	0.5	0.8
0.5	45	1.0	13.6	16.0	1.0	1.6
0.5	30	1.0	6.6	10.9	0.4	1.2

Table 5.4. Deviations of the modeled produced fluid properties for gravity drainage experiments performed in the infinite acting regime.

Gap Width mm	Angle degree	Inj. rate cm^3/min	Bitumen Content		Density	
			AAD wt%	MAD wt%	AAD g/cm^3	MAD g/cm^3
0.5	35	0.3	1.18	2.16	0.0011	0.0025
0.5	35	0.5	1.10	2.19	0.0010	0.0024
0.5	35	1.0	0.45	1.03	0.0004	0.0010
0.5	35	2.0	0.03	0.10	0.0004	0.0005
1.0	35	0.3	2.62	7.53	0.0026	0.0061
1.0	35	0.5	1.23	3.39	0.0013	0.0044
1.0	35	1.0	0.34	1.35	0.0002	0.0007
1.0	35	2.0	0.10	0.53	0.0004	0.0009
0.5	45	1.0	0.32	0.63	0.0001	0.0004
0.5	30	1.0	0.34	0.70	0.0001	0.0004

Gap Width and Flow Rate

Figures 5.12a and 5.12b show the measured and modeled bitumen mass flux for gravity drainage experiments with gap widths of 0.5 and 1.0 mm, respectively, at toluene rates from 0.3 and 2

cm³/min. The modeled flux from diffusion is constant and therefore the only variations in the modeled flux are from creep flow effects. The modeled flux is nearly constant confirming that creep flow has little effect on the bitumen production rate in these experiments. The model predictions are within the experimental error of ±0.0026 g/(cm²min) except for a slight decrease in measured values after the first two hours of gravity drainage. The difference between predictions and experimental measurements are attributed to experimental error and non-steady state behavior at the start of the experiment.

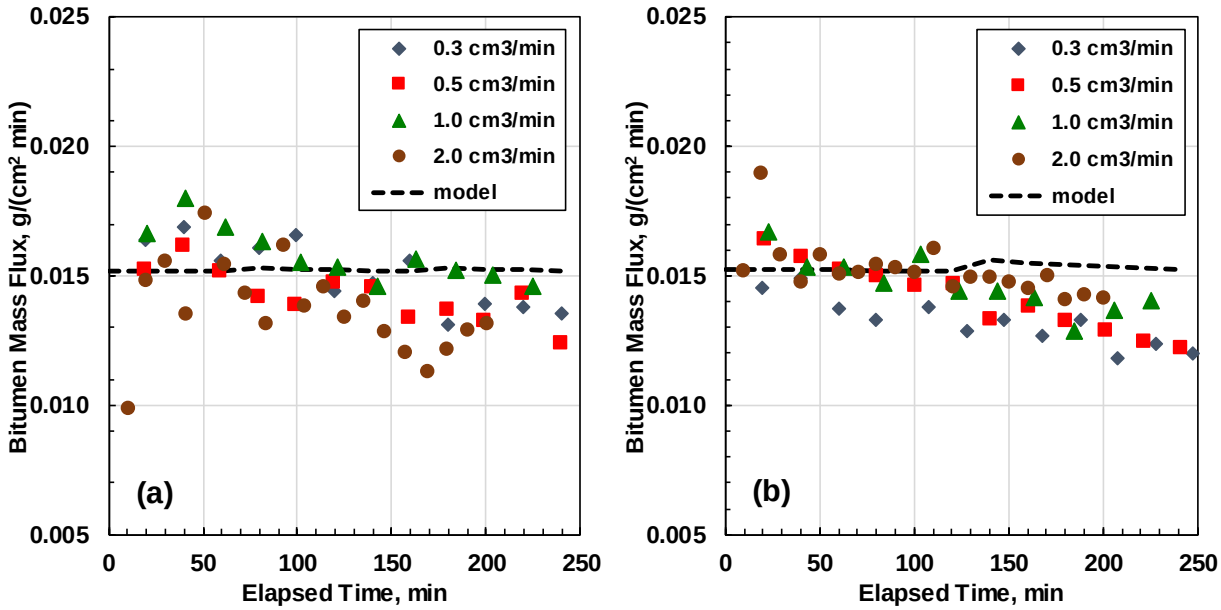

Figure 5.12. Measured and modeled bitumen mass flux over time for gravity drainage experiments with initial angle of inclination 35° and four different toluene flow rates. a) gap width of 0.5 mm and b) gap width of 1.0 mm. The repeatability of the bitumen flux was ±0.0026 g/(cm²min) based on a 90% confidence interval.

Figures 5.13a and 5.13b show the measured and modeled normalized heights over time for gravity drainage experiments with gap widths of 0.5 and 1.0 mm, respectively, at toluene rates from 0.3 and 2 cm³/min. For a gap of 0.5 mm (Figure 5.13a and 5.13c), the model matches the bitumen profile for all flow rates at both times (2 h and 4 h) to within the experimental error of ±1.7 cm (0.09 h/h_i), except for small deviations near the end of the experiment (4 h). For a gap of 1.0 mm

(Figure 5.13b and Figure 5.13d), the model matches the bitumen profiles to within experimental error for all flow rates at both times (2 h and 4 h).

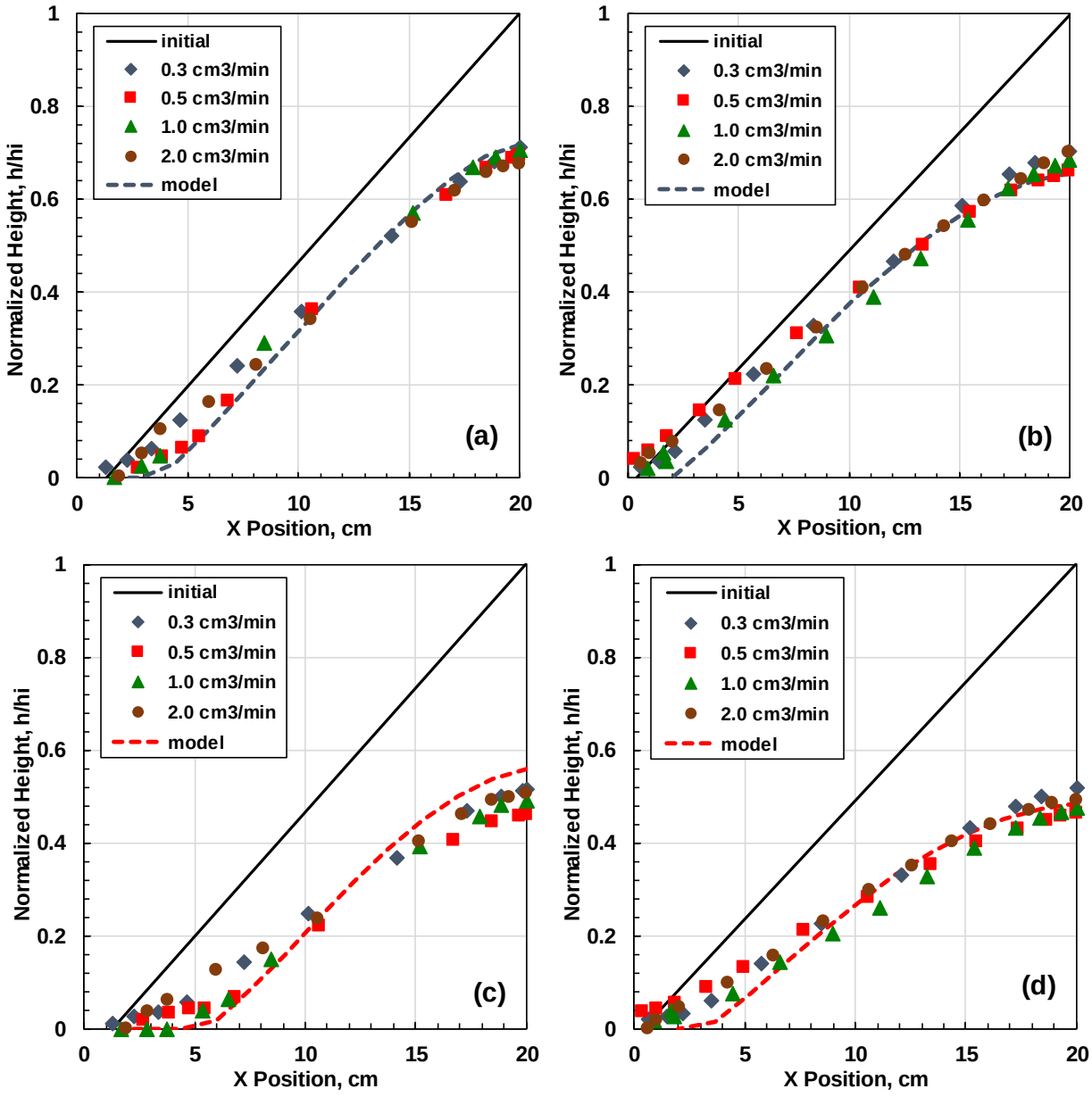

Figure 5.13. Measured and modeled bitumen profiles over time for gravity drainage experiments with initial angle of inclination of 35° and toluene flow rates from 0.3 to 2.0 cm³/min: a) gap width of 0.5 mm after 2 h; b) gap width of 1.0 mm after 2 h; c) gap width of 0.5 mm after 4 h; d) gap width of 1.0 mm after 4 h. The repeatability of the height of the bitumen profile was ±1.7 cm (0.09 h/hi) based on a 90% confidence interval.

Initial Angle of Inclination

Figure 5.14 shows measured and predicted bitumen mass flux, cumulative bitumen production, and bitumen profile for a gravity drainage experiment with initial inclination angle 30°, toluene rate of 1 cm^3/min and gap width of 0.5 mm. The average error in the predicted cumulative bitumen production is 6.6%, within the experimental error of ±10%. The error in the predicted bitumen mass flux is 0.0015 g/(cm^2min), within the experimental error of ±0.0026 g/(cm^2min). The predicted profiles match the measured profiles within the experimental error (±1.2 cm versus ±1.7 cm) with the biggest deviations near the original bitumen contact point with the bottom of the cell. The model predicts that the contact line moves towards the inlet but the measurements show it as a fixed point. It is possible that residual bitumen on the glass plate obscured the movement of the contact line during the measurements.

Figure 5.15 shows the bitumen mass flux, cumulative bitumen production, and bitumen profile over time for a gravity drainage experiment with initial inclination angle 45°, toluene rate of 1 cm^3/min and gap width of 0.5 mm. The error in the predicted cumulative bitumen production is 6.6%, within the experimental error of ±10%. The main difference is again that the model did not match the non-steady state behavior at the start of the experiment. The predicted profiles match the measured profiles within the experimental error (±1.2 cm versus ±1.7 cm) with the biggest deviations near the original bitumen contact point with the bottom of the cell.

Overall, the match of the bitumen mass flux and the bitumen profiles confirms that at toluene rates of 0.3 cm^3/min and above, the drainage process is controlled by mass transfer rate of the bitumen into the solvent and the creep flow of the bitumen. Since the drainage layer acts as a semi-infinite film at these flow rates, the predicted mass transfer rate is not a function of the film thickness or velocity and the bitumen mass fluxes and profiles are the same for all of these experiments.

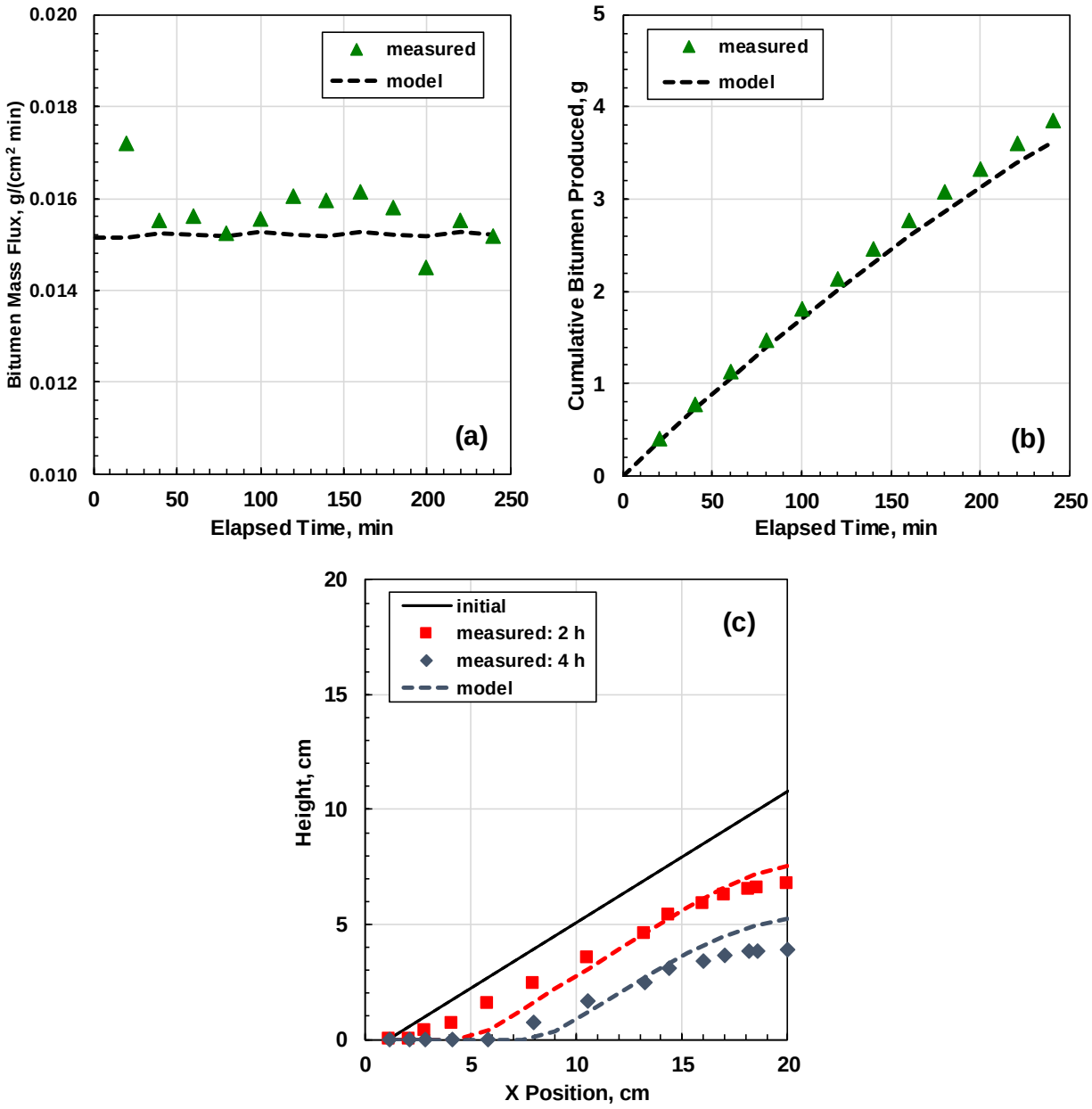

Figure 5.14. Measured and modeled gravity drainage experiment with initial angle of inclination 30°, toluene flow rate of 1 cm³/min, and gap width of 0.5 mm: a) bitumen mass; b) cumulative bitumen production; c) bitumen profile. The repeatabilities of the bitumen flux, cumulative bitumen production, and height of the bitumen profile were ±0.0026 g/(cm²min), ±10%, and ±1.7 cm, respectively, based on a 90% confidence interval.

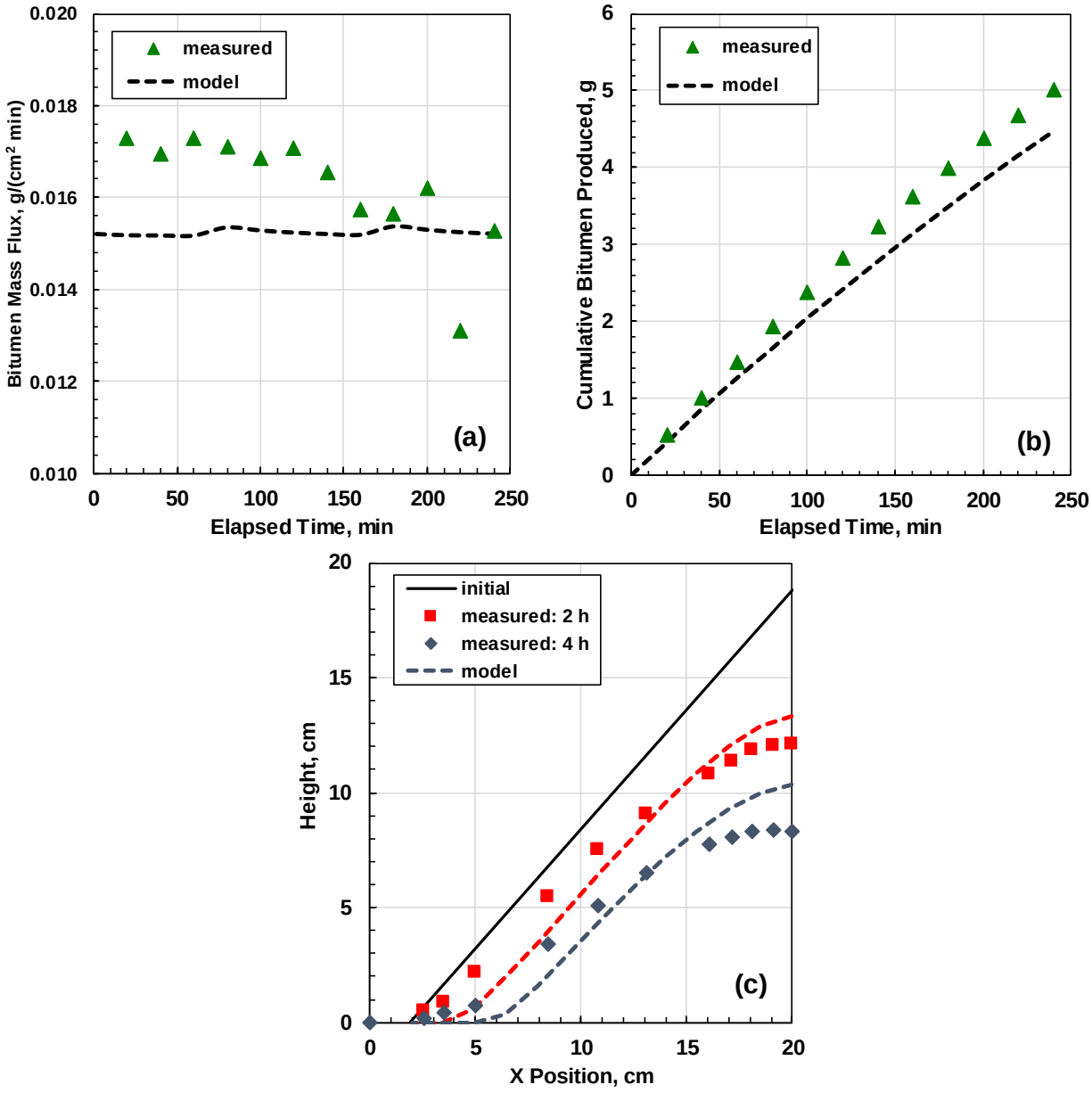

Figure 5.15. Measured and modeled gravity drainage experiment with initial angle of inclination 45°, toluene flow rate of 1 cm³/min, and gap width of 0.5 mm: a) bitumen mass flux; b) cumulative bitumen production; c) bitumen profile. The repeatabilities of the bitumen flux, cumulative bitumen production, and height of the bitumen profile were ±0.0026 g/(cm²min), ±10%, and ±1.7 cm, respectively, based on a 90% confidence interval.

5.4.4. Finite Acting Diffusion (Toluene Flow Rate = 0.1 cm^3/min)

As shown previously in Figure 5.6, a different trend in the mass transfer of bitumen into solvent was seen for both gaps when the toluene injection rate was 0.1 cm^3/min. In these cases, the film thickness is not high enough for the solvent to act as a semi-infinite plane and the boundary condition of the mass transfer system becomes finite. In this case, bitumen can accumulate more in the drainage layer, increasing its viscosity and slowing the drainage rate.

A simplifying hypothesis for this case is that the bitumen production mechanism dominating the process is the creep flow and not the diffusion rate of bitumen into the solvent. To test the hypothesis, the model was run with zero diffusion of bitumen; that is, the only active mass transfer mechanism was the creep flow between the bitumen columns with the bitumen mass by creep flow from the last column (inlet) transferred to the solvent phase. Figures 5.16a and 5.16b show the bitumen mass flux and cumulative bitumen production, respectively, over time for a gravity drainage experiment with an initial angle of inclination 35°, a gap width of 0.5 mm and toluene flow rate of 0.1 cm^3/min. The modeled bitumen mass flux from creep flow alone accounted for less than 5% of the experimental bitumen production disproving the hypothesis and indicating that the dominant mechanism was still diffusion. Similar results were obtained with a 1.0 mm gap width.

Figures 5.16c and 5.17c show the bitumen profile progression for the 0.5 and 1.0 mm gap widths respectively. The modeled profiles are more concave than the measured profiles. The reason for this deviation is that the model does not let the bitumen blocks to move in the x-direction. In the experiment, the bitumen creeps to the left of the initial contact of the bitumen profile with the bottom of the Hele-Shaw cell while in the model the bitumen that moves past this point is immediately produced. Therefore, the shape of the profile does not match near the initial contact point. The same effect is present in all other modeled profiles, but is more obvious in this case where creep flow is the only active mechanism and the bitumen mass fluxes only accounted for a small portion of the total production.

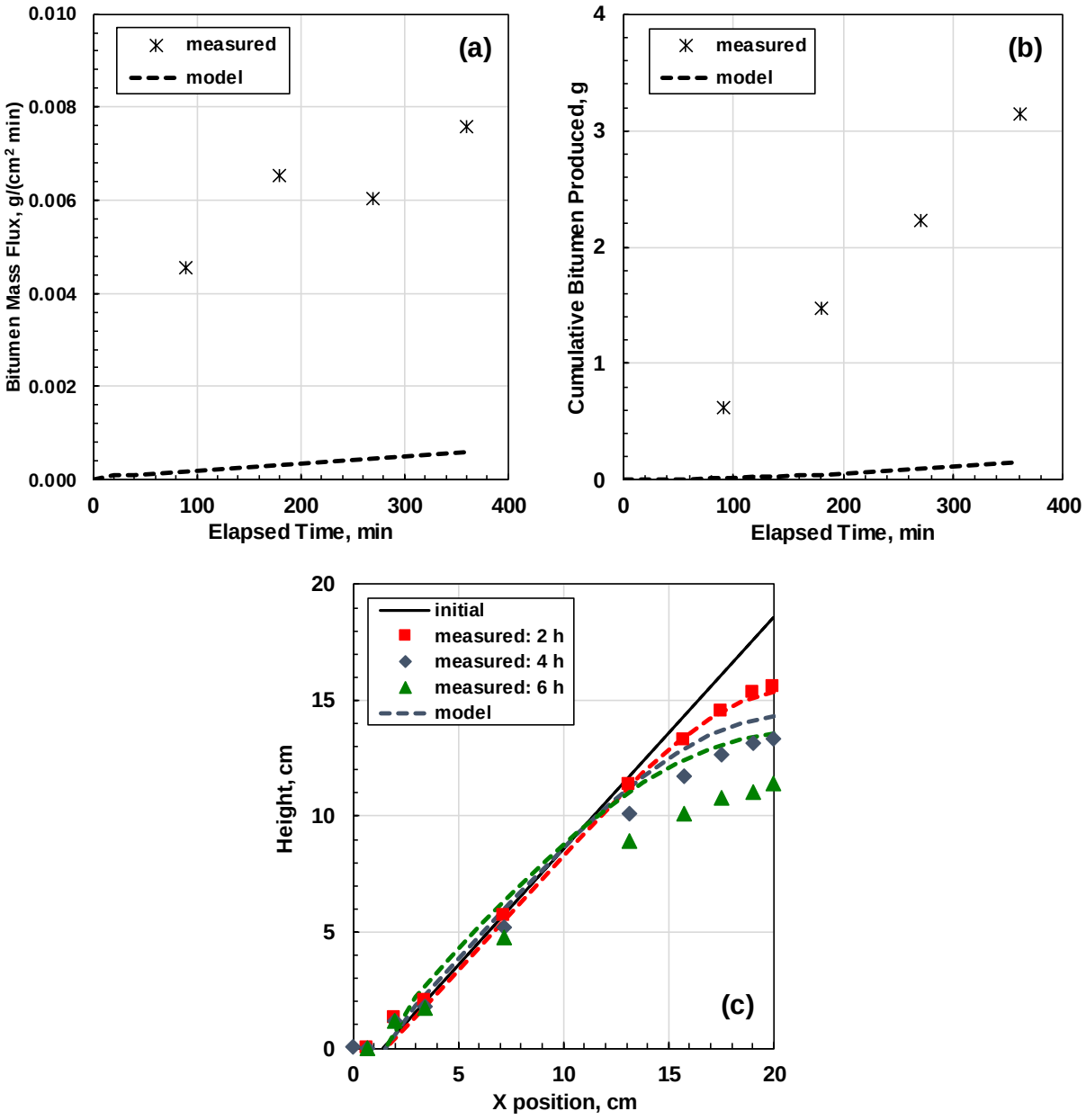

Figure 5.16. Measured and modeled gravity drainage experiment with initial angle of inclination 35°, toluene flow rate of 0.1 cm³/min, and gap width of 0.5 mm: a) bitumen mass flux; b) cumulative bitumen production; c) bitumen profile.

A second hypothesis for this case is that since the solvent layer no longer acts as a semi-infinite plane for diffusion, the average concentration in the solvent layer increases and thus the concentration gradient for mass transfer is smaller and decreases along the interface during gravity drainage. To test the hypothesis, the model was run with both diffusion and creep flow as active mechanisms for mass transfer and the effective height of the concentration gradient for diffusion (Δh_D) was re-adjusted to match the experimental bitumen production.

Figures 5.17a and 5.17b show the bitumen mass flux and cumulative bitumen production, respectively, over time for a gravity drainage experiment with an initial angle of inclination 35°, a gap width of 0.5 mm, and toluene flow rate of 0.1 cm³/min. Figures 5.18a and 5.18b show the same data for a gap width of 1.0 mm. On average, the modeled bitumen mass flux deviates from the measured flux by 0.001 g/(cm²min) for the 0.5 mm gap and by 0.001 g/(cm²min) for the 1.0 mm gap, well within the error of ±0.0026 g/(cm²min). The average error in the modeled bitumen profiles is 0.7 cm, within the experimental error of ±1.7 cm. Deviations in the profile progression depicted in Figures 5.17c and 5.18c are consistent with the deviations in the bitumen production and the bitumen mass flux.

The re-adjusted (Δh_D) for the finite acting diffusion regime depicted in Figures 5.17 and 5.18 was two times higher compared to the one from the infinite acting diffusion regime, confirming that the mass transfer rate is much slower. To appropriately model the finite acting diffusion regime, it is necessary to change the boundary condition and perhaps re-evaluate some of the assumptions of the model. Recommendations to modify the model for these cases are discussed in Chapter 6.

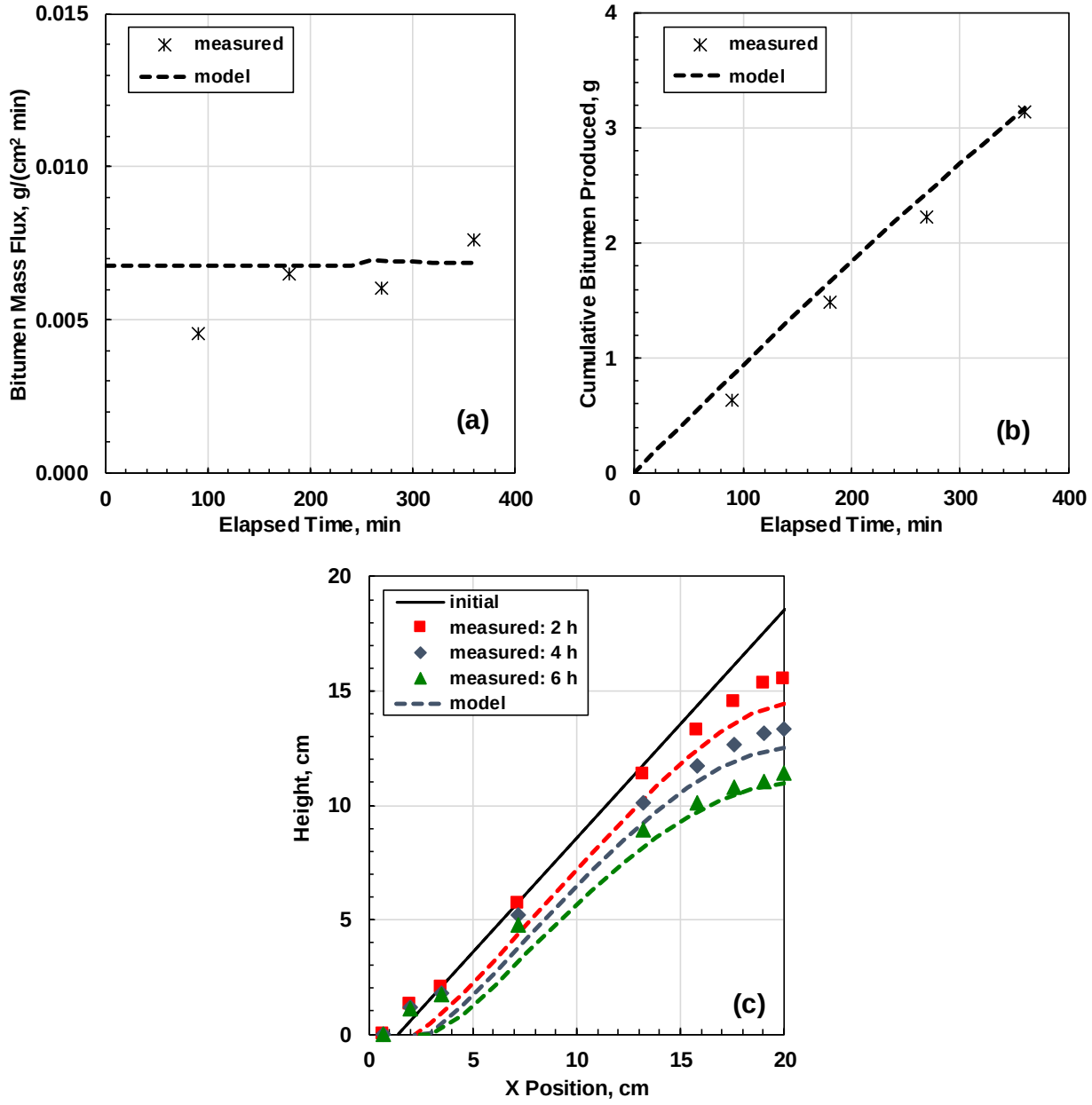

Figure 5.17. Measured and modeled gravity drainage experiment with initial angle of inclination 35°, toluene flow rate of 0.1 cm³/min, and gap width of 0.5 mm: a) bitumen mass flux; b) cumulative bitumen production; c) bitumen profile. The repeatabilities of the bitumen flux and height of the bitumen profile were ±0.0026 g/(cm²min) and ±1.7 cm, respectively, based on a 90% confidence interval.

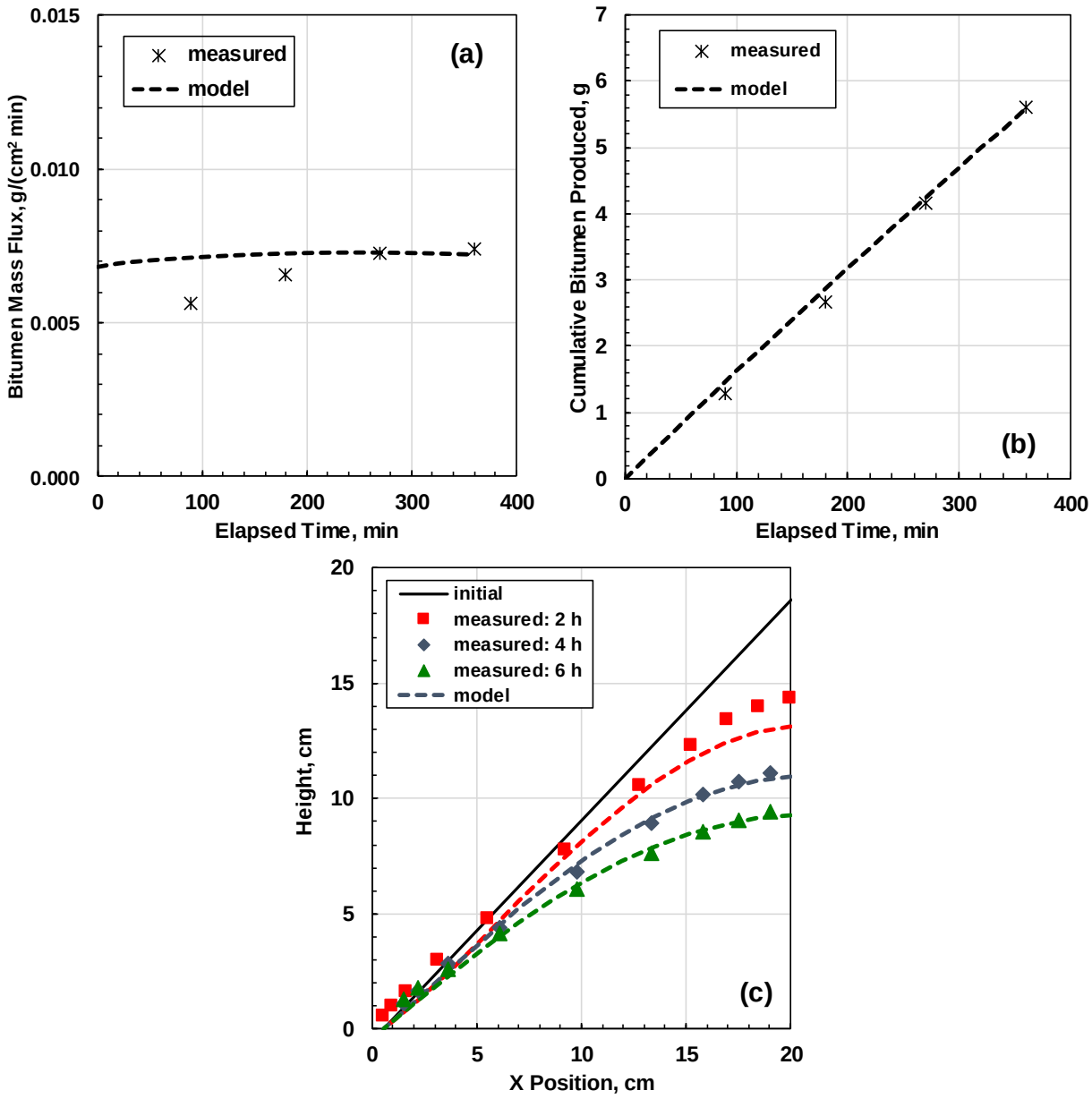

Figure 5.18. Measured and modeled gravity drainage experiment with initial angle of inclination 35°, toluene flow rate of 0.1 cm³/min, and gap width of 1.0 mm: a) bitumen mass flux; b) cumulative bitumen production; c) bitumen profile. The repeatabilities of the bitumen flux and height of the bitumen profile were ±0.0026 g/(cm²min) and ±1.7 cm, respectively, based on a 90% confidence interval.

5.5. Summary

In summary, both experimental results and modeled data confirm that gravity drainage process in a Hele-Shaw cell is controlled by two mechanisms at the conditions investigated in this thesis: the diffusion of bitumen into the drainage layer and the creep flow of the bitumen phase under its own weight. Gravity drainage was successfully approximated as falling film flow with diffusion from bitumen into the falling film. Creep flow was successfully modeled as flow between parallel plates driven by hydrostatic pressure differences. Once fitted to drainage data for a given gap width using a single tuning parameter, the model predicted the production rate, density and bitumen content over time at different flow rates and inclination angles with deviations of 7.4%, 0.1%, and 1%, respectively.

CHAPTER SIX: CONCLUSIONS AND RECOMMENDATIONS

The goals of this thesis were to: 1) design and commission a Hele-Shaw type apparatus to measure mass transfer and drainage rates in heavy oil and solvent systems with controlled geometries, 2) perform gravity drainage experiments for a bitumen and toluene system at ambient conditions, 3) evaluate variables such as the gap width, solvent injection flow rate and initial angle of inclination, and; 4) identify the mass transfer and gravity drainage mechanisms and develop a numerical model for the process. This chapter summarizes contributions and findings of this thesis and recommendations for future work in the area.

6.1. Contributions and Conclusions

The main contributions from this thesis are:

1. The construction and commissioning of a new and novel Hele-Shaw type apparatus to measure recovery rates during gravity drainage experiments for different geometries of bitumen and solvent systems at ambient conditions. The new apparatus consists of a square Hele-Shaw cell that can be rotated, partially filled with bitumen and then rotated back to the horizontal position to create an inclined plane of bitumen. Solvent is injected from the top of the right corner to flow along the bitumen surface, strip out the bitumen, and drain by means of gravity to a sample tube. Recovery rates are measured from the mass and composition (bitumen and solvent content) of the samples. The location of the top of the bitumen surface (bitumen profile) is measured by taking photographs to the interface during the experiments. The apparatus has the flexibility to rotate and the procedure allows to measure recovery rates for different geometries, gap widths and solvent flow rates.
2. The measurement of bitumen recovery rates and bitumen profiles for a system of Western Canadian bitumen and toluene at ambient conditions and different geometries (initial inclination angles between 30 and 45°), injections flow rates (0.1 and 2 cm^3/min) and gap widths (0.5 and 1 mm).

3. The development of a two-dimensional model based on Fick's First Law of diffusion and creep flow between parallel plates and a fitting procedure to match recovery rates of bitumen and bitumen profiles in a Hele-Shaw cell.
4. The demonstration that gravity drainage in a Hele-Shaw cell is governed by a combination of bitumen diffusion into a falling film of solvent and the creep flow of the bitumen under its own weight. The diffusion mechanism was sufficient to match bitumen production rates with the model but the creep flow of the bitumen was required to match the bitumen profiles. The model matched all of the data at two different gap widths (0.5 and 1 mm), initial angles of inclination (30 to 45°) and solvent flow rates (0.3 and 2 ml) using a single fitting parameter.

Some additional conclusions are as follows.

1. The mass transfer between the bitumen and solvent is dominated by the diffusion of bitumen into the solvent and the diffusion of solvent into bitumen can be neglected. First, the diffusivity of solvent into the bitumen is 1-2 magnitudes lower than the diffusivity of bitumen into the solvent. Second, the rate at which the bitumen layer decreased was between 2.5 and 3 cm/h and was much higher compared to the penetration rate of toluene into bitumen of 0.2 cm/day.
2. The drainage of the solvent layer can be represented as a falling film. The falling film model matched the velocity of the draining solvent layer.
3. The bitumen is immediately swept away by the solvent layer and the bitumen concentration gradient in the solvent layer is constant over time once steady state is achieved. This conclusion was demonstrated by the invariance of the bitumen production rate with solvent flow rate and the ability of the model to fit the data at all conditions with a single concentration gradient.
4. The bitumen settled only over several days without solvent injection because the capillary forces acting between the bitumen and air were high enough to significantly retard the creep flow. However, when solvent was added, the contacts became air/solvent and solvent/bitumen. The capillary forces between air and solvent were not enough to affect the flow of the low viscosity solvent layer. The capillary forces between the solvent and

bitumen were negligible or non-existent and therefore the creep flow in the bitumen phase could proceed unimpeded. Although creep flow only has a minor contribution to the bitumen production, it has a major effect on the bitumen profiles over time.

5. At toluene rates of 0.3 cm^3/min and above the drainage layer acts as a semi-infinite film and the predicted mass transfer is independent of the film thickness and velocity of the solvent layer. The measurements confirmed this prediction.
6. Bitumen mass flux was substantially lower at a toluene rate of 0.1 cm^3/min for both gap widths compared to the flux obtained at higher rates, indicating that the boundary condition for the diffusion of bitumen into the solvent is different. In these cases, the film thickness is not high enough for the solvent to act as a semi-infinite plane and the boundary condition of the mass transfer system becomes finite. The bitumen can accumulate more in the drainage layer, increasing the viscosity and slowing the drainage rate. The effective height for mass transfer had to be multiplied by a factor of 2.2 to match the experimental data at these conditions, confirming the hypothesis that the mass transfer rate is smaller compared to the semi-infinite film case.

6.2. Recommendations

Recommendations for future studies are provided below.

1. Investigate gravity drainage in the Hele-Shaw cell at flow rates below 0.1 cm^3/min and determine the concentration gradient required to fit the data at different flow rates. Attempt to correlate this proxy for the mass transfer coefficient to the thickness of the drainage layer.
2. Modify the Hele-Shaw cell apparatus to perform gravity drainage experiments at higher pressures and temperatures. To make this modification, it will be necessary to have an oven available that is large enough to keep the experimental setup inside and to figure out how to: 1) find a way to take photographs of the interface inside the oven; 2) provide the pressure required for the experiments while having a transparent wall to observe the bitumen profiles, and; 3) evaluate if the bitumen used in this thesis is viscous enough not to move before solvent is added at these conditions or use a different sample of bitumen with a higher viscosity.

3. Modify the Hele-Shaw cell apparatus to create a porous medium between the glass plates; that is, create a glass bead bed or a sand pack. With sand packed between the glass plates, it would be possible to perform gravity drainage experiments for porous mediums and study the mechanisms in a system that is closer to the reservoir conditions.
4. Perform gravity drainage with solvents other than toluene to assess the effect of solvent density and viscosity.
5. Perform gravity drainage experiments in systems with asphaltene precipitation (by using solvents different from toluene) to evaluate if the effect of *in-situ* precipitation on the mass transfer, gravity drainage, and bitumen creep flow in the Hele-Shaw cell.
6. Perform gravity drainage experiments with angles higher than 45° to see if the velocity of the solvent layer starts to have an effect on the bitumen production rate. In this case, the solvent flow rates have to be less than 1 cm^3/min to avoid the erosion effect noticed during experiments for this thesis in which the initial angle of inclination was 55° and the toluene flow rate was 1 cm^3/min.
7. Modify the numerical model to account for the movement of the bitumen phase in the x-direction rather than assuming that the mass going out of the last column of bitumen was transferred to the solvent layer and then immediately produced. The modification will allow to have a better representation of the measured bitumen profiles.
8. Implement the open channel flow model to improve the prediction of the velocity and thickness of the draining layer.

REFERENCES

Ahadi, A., and Torabi, F. (2018). Insight into heavy oil recovery of cyclic solvent injection (CSI) utilizing C3H8/CH4 and C3H8/CH4/CO2. *Petroleum*. https://doi.org/10.1016/j.petlm.2018.04.001

Ahmed, T. (2010). Reservoir Engineering Handbook. In *Reservoir Engineering Handbook*.

Akinboyewa, J., Das, S. K., Wu, Y. S., and Kazemi, H. (2010). Simulation of expanding solvent - Steam assisted gravity drainage in a field case study of a bitumen oil reservoir. *SPE - DOE Improved Oil Recovery Symposium Proceedings*.

Al Bahlani, A. M. M., and Babadagli, T. (2008). *A Critical Review of the Status of SAGD: Where Are We and What Is Next?* https://doi.org/10.2118/113283-ms

Alboudwarej, H., Beck, J., Svrcek, W. Y., Yarranton, H. W., and Akbarzadeh, K. (2002). Sensitivity of asphaltene properties to separation techniques. *Energy and Fuels*. https://doi.org/10.1021/ef010213p

Allen, J. C. (1977). *Patent No. 1008361*. Canada.

Allen, J. C., Woodward, C. D., Brown, A., and We, C. H. (1976). *Patent No. 3954141*. USA.

Alshmakhy, A. and Maini, B. (2012). A follow-up recovery method after cold heavy oil production cyclic CO2 injection. *Society of Petroleum Engineers - SPE Heavy Oil Conference Canada 2012*.

Altgelt, K. H., and Boduszynski, M. M. (1994). *Composition and Analysis of Heavy Petroleum Fractions*. Taylor and Francis.

Alvarez, J., and Han, S. (2013). Current overview of Cyclic Steam Injection Process. *Journal of Petroleum Science Research*, (2(3)), 116–127.

Ardali, M., Barrufet, M., and Mamora, D. D. (2012). Laboratory testing of addition of solvents to steam to improve SAGD process. *Society of Petroleum Engineers - SPE Heavy Oil Conference Canada 2012*.

Ardali, M., Kharrat, R., Rostami, B., and Derakhshanfar, M. (2009). Partial movement of asphaltene in presence of connate water in VAPEX process. *Society of Petroleum Engineers - EUROPEC/EAGE Conference and Exhibition 2009*.

Ardali, M., Mamora, D. D., and Barrufet, M. (2010). A comparative simulation study of addition of solvents to steam in SAGD process. *Society of Petroleum Engineers - Canadian Unconventional Resources and International Petroleum Conference 2010*.

Ayodele, O. R., Nasr, T. N., Ivory, J., Beaulieu, G., and Heck, G. (2010). Testing and history matching ES-SAGD (using hexane). *Society of Petroleum Engineers Western North American Regional Meeting 2010 - In Collaboration with the Joint Meetings of the Pacific Section AAPG and Cordilleran Section GSA*.

Badamchi-Zadeh, A., Yarranton, H. W., Maini, B. B., and Satyro, M. A. (2009). Phase behaviour and physical property measurements for VAPEX solvents: Part II. propane, carbon dioxide and athabasca bitumen. *Journal of Canadian Petroleum Technology*. https://doi.org/10.2118/09-03-57

Badamchi-Zadeh, A., Yarranton, H. W., Svrcek, W. Y., and Maini, B. B. (2009). Phase behaviour and physical property measurements for VAPEX solvents: Part I. Propane and athabasca bitumen. *Journal of Canadian Petroleum Technology*. https://doi.org/10.2118/09-01-54

Baltatu, M. E. (1982). Prediction of the Liquid Viscosity for Petroleum Fractions. *Industrial and Engineering Chemistry Process Design and Development*. https://doi.org/10.1021/i200016a034

Bardon, C. P., Karaoguz, D., and Tholance, M. (1986). WELL STIMULATION BY CO//2 IN THE HEAVY OIL FIELD OF CAMURLU IN TURKEY. *Society of Petroleum Engineers of AIME, (Paper) SPE*.

Bayestehparvin, B., Farouq Ali, S. M., and Abedi, J. (2016). Use of solvents with steam-state-of-The-Art and limitations. *Society of Petroleum Engineers - SPE EOR Conference at Oil and Gas West Asia, OGWA 2016*.

Bayestehparvin, B., Farouq Ali, S. M., and Abedi, J. (2019). Solvent-based and solvent-assisted recovery processes: State of the art. *SPE Reservoir Evaluation and Engineering*. https://doi.org/10.2118/179829-PA

Bezaire, G. E., and Markiw, I. A. (1979). Esso resources horizontal hole project at cold lake. *Annual Technical Meeting, PETSOC ATM 1979*.

Bird, R. B, Stewart, W.E, Lightfoot, E.N (2006). Transport Phenomena, Revised 2nd Edition. In *John Wiley and Sons, Inc*. https://doi.org/10.1002/aic.690070245

Blackwell, R. J. (1962). Laboratory Studies of Microscopic Dispersion Phenomena. *Society of Petroleum Engineers Journal*. https://doi.org/10.2118/1483-g

Boak, J., and Palmgren, C. (2007). Preliminary numerical analysis for a naphtha co-injection test during SAGD. *Journal of Canadian Petroleum Technology*.

Boustani, A., and Maini, B. B. (2001). The role of diffusion and convective dispersion in vapour extraction process. *Journal of Canadian Petroleum Technology*, *40*(4), 68–77. https://doi.org/10.2118/01-04-05

BP. (2019). BP Statistical Review of World Energy 2019|68th Edition. *BP World Energy*. https://doi.org/10.2307/3324639

Butler, R. M., Mcnab, G. S., and Lo, H. Y. (1981). Theoretical studies on the gravity drainage of heavy oil during in-situ steam heating. *The Canadian Journal of Chemical Engineering*. https://doi.org/10.1002/cjce.5450590407

Butler, R., and Mokrys, I. J. (1991). A New Process (VAPEX) For Recovering Heavy Oils Using Hot Water And Hydrocarbon Vapour. *Journal of Canadian Petroleum Technology*, *30*(1), 97–106. https://doi.org/10.2118/91-01-09

Butler, R M, and Mokrys, I. (1989). Solvent Analog Model of Steam Assisted Gravity Drainage. *AOSTRA Journal of Research*, Vol. 5, pp. 17–32.

Butler, R M, and Mokrys, L. (1993). Recovery of Heavy Oils Using Vapourized Hydrocarbon Solvents: Further Development of the Vapex Process. *Journal of Canadian Petroleum Technology*, *32*(06), 56–62. https://doi.org/10.2118/93-06-06

Butler, Roger M., and Mokrys, I. J. (1989). Solvent Analog Model of Steam Assisted Gravity Drainage. *AOSTRA Journal of Research*, *5*(1), 17–32.

Cao, K. (2014). *A Numerical Simulation Study of the N-Solv Process*. University of Calgary.

Castellanos-Diaz, O., Hedden, R., and Verlaan, M. L. (2016). Solvent enhanced steam drive: Results from the first field pilot in Canada. *Society of Petroleum Engineers - SPE EOR Conference at Oil and Gas West Asia, OGWA 2016*.

Chen, S., Seib, B., Ben-Zvi, A., and Robinson, T. (2018). Christina lake early rise rate solvent aided process pilot. *Society of Petroleum Engineers - SPE Canada Heavy Oil Technical Conference, CHOC 2018*.

Crank, J. (1975). *The Mathematics of Diffusion*.

Cussler, E. L. (2009). *Difussion: Mass transfer in fluid systems* (3rd ed.; Cambridge University Press, Ed.). Cambridge, UK.

Cuthiell, D., and Edmunds, N. (2013). Thoughts on simulating the VAPEX process. *Journal of Canadian Petroleum Technology*. https://doi.org/10.2118/158499-PA

Das, S. (2005). Diffusion and dispersion in the simulation of Vapex process. *SPE/PS-CIM/CHOA International Thermal Operations and Heavy Oil Symposium Proceedings*.

Das, S.K. (1995). *In-Situ Recovery of Heavy Oil and Bitumen Using Vaporized Hydrocarbon Solvents*. University of Calgary.

Das, S.K., and Butler, R. M. (1994). Effect of Asphaltene Deposition On the Vapex Process: A Preliminary Investigation Using a Hele-Shaw Cell. *Journal of Canadian Petroleum Technology*, *33*(06), 800. https://doi.org/10.2118/94-06-06

Das, S.K, and Butler, R. M. (1994). Investigation of ' VAPEX' process in a packed cell using butane as a solvent. *Canadian SPE/CIM/CANMET International Conference on Recent Advances in Horizontal Well Applications*.

Das, S K. (1997). Vapex : An Efficient Process for the Recovery of Heavy Oil and Bitumen. *SPE International Thermal Operations Symposium*, (September), 232–237. https://doi.org/http://dx.doi.org/10.2118/50941-PA

Das, Swapan K., and Butler, R. M. (1998). Mechanism of the vapor extraction process for heavy oil and bitumen. *Journal of Petroleum Science and Engineering*, *21*(1–2), 43–59. https://doi.org/10.1016/S0920-4105(98)00002-3

Deng, X., Huang, H., Zhao, L., Law, D. H. S., and Nasr, T. N. (2010). Simulating the ES-SAGD process with solvent mixture in Athabasca reservoirs. *Journal of Canadian Petroleum Technology*. https://doi.org/10.2118/132488-PA

Dickson, J. L., Clingman, S., Dittaro, L. M., Jaafar, A. E., Yerian, J. A., and Perlau, D. L. (2011). Design approach and early field performance for a solvent-assisted SAGD pilot at Cold Lake, Canada. *Society of Petroleum Engineers - SPE International Heavy Oil Conference and Exhibition 2011*.

Dickson, J. L., Dittaro, L. M., and Thomas, J. (2013). Integrating the Key Learnings from Laboratory , Simulation , and Field Tests to Assess the Potential for Solvent Assisted - Steam Assisted Gravity Drainage. *SPE Heavy Oil Conference, 2013*, (June), 1–14.

https://doi.org/10.2118/165485-ms

Dickson, J. L., Subramanian, G., Shah, P., Otahal, J. M., Dittaro, L. M., Jaafar, A. E., and Yerian, J. A. (2013). Key learnings from a simulation study of a solvent-assisted SAGD pilot at cold lake. *Society of Petroleum Engineers - SPE Heavy Oil Conference Canada 2013*.

Dittaro, L. M., Jaafar, A. E., Perlau, D. L., Boone, T. J., Yerian, J. A., Dickson, J. L., and Wattenbarger, R. C. (2013). Findings from a solvent-assisted SAGD pilot at cold lake. *Society of Petroleum Engineers - SPE Heavy Oil Conference Canada 2013*.

Dong, M., Huang, S., and Hutchence, K. (2006). Methane pressure-cycling process with horizontal wells for thin heavy-oil reservoirs. *SPE Reservoir Evaluation and Engineering*.

Dunn, S. G., Nenniger, E. H., and Rajan, V. S. V. (1989). A study of bitumen recovery by gravity drainage using low temperature soluble gas injection. *The Canadian Journal of Chemical Engineering*, *67*(6), 978–991. https://doi.org/10.1002/cjce.5450670617

Eastick, R. R., and Mehrotra, A. K. (1990). Viscosity data and correlation for mixtures of bitumen fractions. *Fuel Processing Technology*. https://doi.org/10.1016/0378-3820(90)90021-J

Edmunds, N., and Chhina, H. (2001). Economic optimum operating pressure for SAGD projects in Alberta. *Journal of Canadian Petroleum Technology*. https://doi.org/10.2118/01-12-DAS

El-Haj, R., Lohi, A., and Upreti, S. R. (2009). Experimental determination of butane dispersion in vapor extraction of heavy oil and bitumen. *Journal of Petroleum Science and Engineering*, *67*(1–2), 41–47. https://doi.org/10.1016/j.petrol.2009.02.010

Ely, J. F., and Hanley, H. J. M. (1981). Prediction of Transport Properties. 1. Viscosity of Fluids and Mixtures. *Industrial and Engineering Chemistry Fundamentals*. https://doi.org/10.1021/i100004a004

Energy Fact Book of Natural Resources of Canada. (2018). Retrieved from https://www.nrcan.gc.ca/home

Fadaei, H., Shaw, J. M., and Sinton, D. (2013). Bitumen-toluene mutual diffusion coefficients using microfluidics. *Energy and Fuels*. https://doi.org/10.1021/ef400027t

Gagliano, A. J., Lasalle, D. D., Olivo, J. A., Sabas, R. A., and Farouq, S. M. (1994). Enhanced oil recovery pilot project Catriel Oeste Field. *Proceedings of the SPE Latin American and Caribbean Petroleum Engineering Conference*.

Gates, I. D., and Chakrabarty, N. (2008). Design of the steam and solvent injection strategy in

expanding solvent steam-assisted gravity drainage. *Journal of Canadian Petroleum Technology*.

Ghasemi, M., and Whitson, C. H. (2014). Numerical investigation and integrated optimization of solvent-SAGD process. *Society of Petroleum Engineers - International Petroleum Technology Conference 2014, IPTC 2014 - Innovation and Collaboration: Keys to Affordable Energy*.

Govind, P. A., Das, S., Srinivasan, S., and Wheeler, T. J. (2008). Expanding solvent SAGD in heavy oil reservoirs. *Society of Petroleum Engineers - International Thermal Operations and Heavy Oil Symposium, ITOHOS 2008 - "Heavy Oil: Integrating the Pieces."*

Gray, M. R. (2015). *Upgrading oilsands bitumen and heavy oil* (First). Edmonton, Alberta, Canada: The University of Alberta Press.

Grimaldos, F. (2018). *Mutual Diffusivity of Bitumen and Liquid Hydrocarbons*. University of Calgary.

Gupta, S. C., and Gittins, S. D. (2006). Christina lake solvent aided process pilot. *Journal of Canadian Petroleum Technology*.

Haghighat, P., and Maini, B. B. (2010). Role of asphaltene precipitation in VAPEX process. *Journal of Canadian Petroleum Technology*. https://doi.org/10.2118/134244-PA

Hanley, H. J. M. (1976). Prediction of the viscosity and thermal conductivity coefficients of mixtures. *Cryogenics*. https://doi.org/10.1016/0011-2275(76)90035-7

Hayduk, W., Castaneda, R., Bromfield, H., and Perras, R. R. (1973). Diffusivities of propane in normal paraffin, chlorobenzene, and butanol solvents. *AIChE Journal*. https://doi.org/10.1002/aic.690190432

Horng, T. C., Ajlan, M., Lee, L. L., Starling, K. E., and Ajlan, M. (1988). Generalized Multiparameter Correlation for Nonpolar and Polar Fluid Transport Properties. *Industrial and Engineering Chemistry Research*, *27*(4), 671–679. https://doi.org/10.1021/ie00076a024

James, L. A., Rezaei, N., and Chatzis, I. (2008). VAPEX, warm VAPEX and hybrid VAPEX - The state of enhanced oil recovery for in situ heavy oils in Canada. *Journal of Canadian Petroleum Technology*.

James, Lesley Anne. (2009). Mass Transfer Mechanisms during the Solvent Recovery of Heavy Oil. https://doi.org/10.1017/CBO9781107415324.004

Jia, X., Li, J., and Chen, Z. (2015). Mathermatical modeling of dynamic mass transfer in cyclic solvent injection. *Society of Petroleum Engineers - SPE Canada Heavy Oil Technical Conference 2015, CHOC 2015*.

Jiang, Q., Yuan, J., Russel-Houston, J., Thornton, B., and Squires, A. (2010). Evaluation of recovery technologies for the grosmont carbonate reservoirs. *Journal of Canadian Petroleum Technology*. https://doi.org/10.2118/137779-PA

Jiang, T., Zeng, F., Jia, X., and Gu, Y. (2014). A new solvent-based enhanced heavy oil recovery method: Cyclic production with continuous solvent injection. *Fuel*. https://doi.org/10.1016/j.fuel.2013.07.043

Jimenez, J. (2008). The field performance of sagd projects in canada. *International Petroleum Technology Conference, IPTC 2008*.

Johnson, S. E., Svrcek, W. Y., and Mehrotra, A. K. (1987). Viscosity Prediction of Athabasca Bitumen Using the Extended Principle of Corresponding States. *Industrial and Engineering Chemistry Research*. https://doi.org/10.1021/ie00071a020

Kamari, A., Nikookar, M., and Mohammadi, A. H. (2015). Study of the performance of cyclic steam stimulation (CSS) oil recovery method in a naturally fractured carbonate reservoir. In *Enhanced Oil Recovery: Methods, Economic Benefits and Impacts on the Environment*.

Kantzas, A., and Brook, G. (2002). Preliminary laboratory evaluation of cold and post-cold production methods for heavy oil reservoirs. *Canadian International Petroleum Conference 2002, CIPC 2002*.

Kapadia, R. A., Upreti, S. R., Lohi, A., and Chatzis, I. (2006). Determination of gas dispersion in vapor extraction of heavy oill and bitumen. *Journal of Petroleum Science and Engineering*, *51*, 214–222.

Kapadia, Ronak A., Upreti, S. R., Lohi, A., and Chatzis, I. (2006). Determination of gas dispersion in vapor extraction of heavy oil and bitumen. *Journal of Petroleum Science and Engineering*. https://doi.org/10.1016/j.petrol.2006.01.001

Karmaker, K., and Maini, B. B. (2003). Applicability of Vapor Extraction Process to Problematic Viscous Oil Reservoirs. *Proceedings - SPE Annual Technical Conference and Exhibition*.

Kesler, M. G., and Lee, B. I. (1976). IMPROVE PREDICTION OF ENTHALPY OF FRACTIONS. *Hydrocarbon Processing*.

Khaledi, R., Hamouda, A. A., Dittaro, L. M., and Dakers, A. P. (2014). Results from a Successful Multi-Year Solvent Assisted SAGD Pilot at Cold Lake. *World Heavy Oil Congress 2008,* 1–20.

Kokal, S. L., and Sayegh, S. G. (1990). Gas-Saturated Bitumen Density Predictions Using The Volume-Translated Peng-Robinson Equation Of State. *Journal of Canadian Petroleum Technology*. https://doi.org/10.2118/90-05-07

Léauté, R. P., and Carey, B. S. (2007). Liquid Addition to Steam for Enhancing Recovery (LASER) of bitumen with CSS: Results from the first pilot cycle. *Journal of Canadian Petroleum Technology*.

Léauté, Roland P. (2002). Liquid Addition to Steam for Enhancing Recovery (LASER) of Bitumen with CSS: Evolution of Technology from Research Concept to a Field Pilot at Cold Lake. *SPE International Thermal Operations and Heavy Oil Symposium Proceedings*.

Li, H., Zheng, S., and Yang, D. (2013). Enhanced swelling effect and viscosity reduction of solvent(s)/CO 2/heavy-oil systems. *SPE Journal*. https://doi.org/10.2118/150168-PA

Lim, G. B., Kry, R. P., Harker, B. C., and Jha, K. N. (1995). Cyclic stimulation of cold lake oil sand with supercritical ethane. *Proceedings - SPE International Heavy Oil Symposium*.

Lin, L., Ma, H., Zeng, F., and Gu, Y. (2014). A critical review of the solvent-based heavy oil recovery methods. *Society of Petroleum Engineers - SPE Heavy Oil Conference Canada 2014*.

Lindeloff, N., Pedersen, K. S., Calsep, A. S., Rønningsen, H. P., and Milter, J. (2004). The Corresponding States Viscosity Model Applied to Heavy Oil Systems. *J. Can. Pet. Technol.*, *43*(9), 47–53. https://doi.org/10.2118/2003-150

Luhning, R. W., Das, S. K., Fisher, L. J., Barker, J., Grabowski, J., Engleman, J. R., … Boyle, H. A. (2003). Full scale VAPEX process - Climate change advantage and economic consequences. *Journal of Canadian Petroleum Technology*.

Luo, P., Wang, X., Gu, Y., Zhang, H., and Moghadam, S. (2008). Asphaltene precipitation and its effects on the vapour extraction (VAPEX) heavy oil recovery process. *Society of Petroleum Engineers - International Thermal Operations and Heavy Oil Symposium, ITOHOS 2008 - "Heavy Oil: Integrating the Pieces."*

McKenna, A. M., Donald, L. J., Fitzsimmons, J. E., Juyal, P., Spicer, V., Standing, K. G., …

Rodgers, R. P. (2013). Heavy petroleum composition. 3. Asphaltene aggregation. *Energy and Fuels*. https://doi.org/10.1021/ef3018578

McKenna, A. M., Marshall, A. G., and Rodgers, R. P. (2013). Heavy petroleum composition. 4. Asphaltene compositional space. *Energy and Fuels*. https://doi.org/10.1021/ef301747d

Mehrotra, A. K., and Svrcek, W. Y. (1985). Bitumen Density and Gas Solubility Predictions Using the Peng-Robinson Equation of State. *AOSTRA Journal of Research*.

Mehrotra, Anil K. (1990). Development of mixing rules for predicting the viscosity of bitumen and its fractions blended with toluene. *The Canadian Journal of Chemical Engineering*. https://doi.org/10.1002/cjce.5450680515

Mehrotra, Anil K., and Svrcek, W. Y. (1986). Viscosity of compressed athabasca bitumen. *The Canadian Journal of Chemical Engineering*. https://doi.org/10.1002/cjce.5450640520

Mehrotra, Anil K., and Svrcek, W. Y. (1988). Properties of cold lake bitumen saturated with pure gases and gas mixtures. *The Canadian Journal of Chemical Engineering*. https://doi.org/10.1002/cjce.5450660419

Motahhari, H. R., Schoeggl, F. F., Yarranton, H. W., and Satyro, M. A. (2013). *The Effect of Solvents on the Viscosity of an Alberta Bitumen at In Situ Thermal Process Conditions*. https://doi.org/10.2118/165548-ms

Motahhari, H. R., Schoeggl, F., Satyro, M. A., and Yarranton, H. W. (2011). *Prediction of the Viscosity of Solvent Diluted Live Bitumen at Temperatures up to 175°C*. https://doi.org/10.2118/149405-ms

Motahhari, H., Satyro, M. A., Taylor, S. D., and Yarranton, H. W. (2013). Extension of the expanded fluid viscosity model to characterized oils. *Energy and Fuels*, *27*(4), 1881–1898. https://doi.org/10.1021/ef301575n

Motahhari, H., Satyro, M. A., and Yarranton, H. W. (2011). Predicting the viscosity of asymmetric hydrocarbon mixtures with the expanded fluid viscosity correlation. *Industrial and Engineering Chemistry Research*. https://doi.org/10.1021/ie201415x

Motahhari, H., Schoeggl, F. F., Satyro, M. A., and Yarranton, H. W. (2013). Viscosity prediction for solvent-diluted live bitumen and heavy oil at temperatures up to 175°C. *Journal of Canadian Petroleum Technology*, *52*(5), 376–390.

Motahhari, Hamed reza, and Yarranton, D. H. W. (2013). Development of Viscosity Model for

Petroleum Industry Applications.

Nasr, T. N., and Ayodele, O. R. (2006). New hybrid steam-solvent processes for the recovery of heavy oil and bitumen. *12th Abu Dhabi International Petroleum Exhibition and Conference, ADIPEC 2006: Meeting the Increasing Oil and Gas Demand Through Innovation*.

Nasr, Tawfik N., Beaulieu, G., Golbeck, H., and Heck, G. (2003). Novel expanding solvent-SAGD process "ES-SAGD." *Journal of Canadian Petroleum Technology*.

Nenniger, J. E., and Dunn, S. G. (2018). How fast is solvent based gravity drainage? *Canadian International Petroleum Conference 2008*.

Nenniger, J. E., and Nenniger, E. H. (2005). *Method and Apparatus for Stimulating Heavy Oil Production*.

NIST chemistry WebBook. (2013). *Choice Reviews Online*. https://doi.org/10.5860/choice.43sup-0293

Oballa, V., and Butler, R. (1989). An Experimental Study Of Diffusion In The Bitumen-Toluene System. *Journal of Canadian Petroleum Technology*, *28*(2), 62–69. https://doi.org/10.2118/89-02-03

Oballa, V., and Butler, R. M. (2010). An Experimental Study Of Diffusion In The Bitumen-Toluene System. *Journal of Canadian Petroleum Technology*. https://doi.org/10.2118/89-02-03

Orr, B. (2009). ES-SAGD; Past, present and future. *Proceedings - SPE Annual Technical Conference and Exhibition*.

Pedersen, K. S., and Fredenslund, A. (1987). An improved corresponding states model for the prediction of oil and gas viscosities and thermal conductivities. *Chemical Engineering Science*, *42*(1), 182–186. https://doi.org/10.1016/0009-2509(87)80225-7

Pedersen, K. S., Fredenslund, A., Christensen, P. L., and Thomassen, P. (1984). Viscosity of crude oils. *Chemical Engineering Science*, *39*(6), 1011–1016. https://doi.org/10.1016/0009-2509(84)87009-8

Perkins, T. K., and Johnston, O. C. (1963). A Review of Diffusion and Dispersion in Porous Media. *Society of Petroleum Engineers Journal*. https://doi.org/10.2118/480-pa

Poling, B. E., Prausnitz, J. M., and O'Conell, J. P. (2001). The Properties of Gases and Liquids. In McGraw-Hill (Ed.), *Library* (5th ed.). https://doi.org/10.1300/J111v23n03_01

Poling, Bruce E., Prausnitz, J. M., and O' Connell, J. (2001). The properties of gases and liquids. In *Experimental Thermal and Fluid Science*.

Pourabdollah, K., and Mokhtari, B. (2013). The VAPEX process, from beginning up to date. *Fuel*, Vol. 107, pp. 1–33. https://doi.org/10.1016/j.fuel.2012.12.003

Qazvini Firouz, A., and Torabi, F. (2014). Utilization of carbon dioxide and methane in huff-and-puff injection scheme to improve heavy oil recovery. *Fuel*. https://doi.org/10.1016/j.fuel.2013.10.040

Quiñones-Cisneros, S. E., Zéberg-Mikkelsen, C. K., Baylaucq, A., and Boned, C. (2004). Viscosity modeling and prediction of reservoir fluids: From natural gas to heavy oils. *International Journal of Thermophysics*, *25*(5), 1353–1366. https://doi.org/10.1007/s10765-004-5743-z

Quiñones-Cisneros, Sergio E., Andersen, S. I., and Creek, J. (2005). Density and viscosity modeling and characterization of heavy oils. *Energy and Fuels*. https://doi.org/10.1021/ef0497715

Quiñones-Cisneros, Sergio E., Zéberg-Mikkelsen, C. K., and Stenby, E. H. (2000). The friction theory (f-theory) for viscosity modeling. *Fluid Phase Equilibria*. https://doi.org/10.1016/S0378-3812(00)00310-1

Quiñones-Cisneros, Sergio E., Zéberg-Mikkelsen, C. K., and Stenby, E. H. (2001a). One parameter friction theory models for viscosity. *Fluid Phase Equilibria*. https://doi.org/10.1016/S0378-3812(00)00474-X

Quiñones-Cisneros, Sergio E., Zéberg-Mikkelsen, C. K., and Stenby, E. H. (2001b). The friction theory for viscosity modeling: Extension to crude oil systems. *Chemical Engineering Science*, *56*(24), 7007–7015. https://doi.org/10.1016/S0009-2509(01)00335-9

Quiñones-Cisneros, Sergio E., Zéberg-Mikkelsen, C. K., and Stenby, E. H. (2003). Friction theory prediction of crude oil viscosity at reservoir conditions based on dead oil properties. *Fluid Phase Equilibria*. https://doi.org/10.1016/S0378-3812(03)00263-2

Ramos-Pallares, F. (2017). *The Viscosity and Thermal Conductivity of Heavy Oils and Solvents*. University of Calgary.

Ramos-Pallares, F., Lin, H., Yarranton, H. W., and Taylor, S. D. (2017). Prediction of the liquid viscosity of characterized crude oils by use of the generalized Walther model. *SPE Journal*.

https://doi.org/10.2118/186093-pa

Ramos-Pallares, F., Schoeggl, F. F., Taylor, S. D., Satyro, M. A., and Yarranton, H. W. (2016a). Correction to Predicting the Viscosity of Hydrocarbon Mixtures and Diluted Heavy Oils Using the Expanded Fluid Model. *Energy and Fuels*.

Ramos-Pallares, F., Schoeggl, F. F., Taylor, S. D., Satyro, M. A., and Yarranton, H. W. (2016b). Predicting the Viscosity of Hydrocarbon Mixtures and Diluted Heavy Oils Using the Expanded Fluid Model. *Energy and Fuels*, *30*(5), 3575–3595. https://doi.org/10.1021/acs.energyfuels.5b01951

Ramos-Pallares, F., Schoeggl, F. F., Taylor, S. D., Satyro, M. A., and Yarranton, H. W. (2016c). Predicting the Viscosity of Hydrocarbon Mixtures and Diluted Heavy Oils Using the Expanded Fluid Model. *Energy and Fuels*. https://doi.org/10.1021/acs.energyfuels.5b01951

Rezaei, N., and Chatzis, I. (2007). Incorporation of heat in the VAPEX process: Warm VAPEX. *Canadian International Petroleum Conference 2007, CIPC 2007*.

Rezaei, N., and Chatzis, I. (2008). Warm VPEX; a Thermally-Enhanced Vapor Extraction Process - ABSTRACT. *Canadian International Petroleum Conference*.

Rezaei, N., Mohammadzadeh, O., and Chatzis, I. (2010). Improving the performance of vapor extraction of heavy oil and bitumen using the warm VAPEX process. *Society of Petroleum Engineers - Canadian Unconventional Resources and International Petroleum Conference 2010*.

Rodgers, R. P., and McKenna, A. M. (2011). Petroleum analysis. *Analytical Chemistry*. https://doi.org/10.1021/ac201080e

Rodriguez-Leon, S. L. (2018). *The Stability of Visbroken Heavy Oil Against Asphaltene Precipitation*. University of Calgary.

Salama, D., and Kantzas, A. (2005). Monitoring of diffusion of heavy oils with hydrocarbon solvents in the presence of sand. *SPE/PS-CIM/CHOA International Thermal Operations and Heavy Oil Symposium Proceedings*.

Sarafianos, N. (1986). An analytical method of calculating variable diffusion coefficients. *Journal of Materials Science*. https://doi.org/10.1007/BF01114269

Saryazdi, F., Motahhari, H., Schoeggl, F. F., Taylor, S. D., and Yarranton, H. W. (2013). Density of hydrocarbon mixtures and bitumen diluted with solvents and dissolved gases. *Energy and*

Fuels. https://doi.org/10.1021/ef400330j

Shi, R., and Kantzas, A. (2008). Enhanced heavy oil recovery on depleted long core system by CH 4 and CO 2. *Society of Petroleum Engineers - International Thermal Operations and Heavy Oil Symposium, ITOHOS 2008 - "Heavy Oil: Integrating the Pieces."*

Speight, J. (2007). *The Chemistry and Technology of Petroleum* (4th ed.). Taylor and Francis.

Speight, J. G., and Özüm, B. (2001). Petroleum refining processes. In *Petroleum Refining Processes*. https://doi.org/10.1201/b17048

Stark, S. D. (2013). Cold lake commercialization of the liquid addition to steam for enhancing recovery (LASER) process. *Society of Petroleum Engineers - International Petroleum Technology Conference 2013, IPTC 2013: Challenging Technology and Economic Limits to Meet the Global Energy Demand*.

Sun, X., Dong, M., Zhang, Y., and Maini, B. B. (2015). Enhanced heavy oil recovery in thin reservoirs using foamy oil-assisted methane huff-n-puff method. *Fuel*. https://doi.org/10.1016/j.fuel.2015.07.056

Taylor, G. I. (1954). Diffusion and mass transport in tubes. *Proceedings of the Physical Society. Section B*. https://doi.org/10.1088/0370-1301/67/12/301

Tsanis, I. K., and Leutheusser, H. J. (1986). Hydraulics of laminar open-channel flow. *Journal of Hydraulic Research*. https://doi.org/10.1080/00221688609498542

Wen, Y., Kantzas, A., and Wang, G. J. (2004). Estimation of diffusion coefficients in bitumen solvent mixtures using X-ray CAT scanning and low field NMR. *Canadian International Petroleum Conference 2004, CIPC 2004*.

Wen, Y. W., and Kantzas, A. (2005). Monitoring bitumen-Solvent interactions with low-field nuclear magnetic resonance and X-ray computer-assisted tomography. *Energy and Fuels*. https://doi.org/10.1021/ef049764g

Wilke, C. R., and Chang, P. (1955). Correlation of diffusion coefficients in dilute solutions. *AIChE Journal*. https://doi.org/10.1002/aic.690010222

Yarranton, H. W., Ortiz, D. P., Barrera, D. M., Baydak, E. N., Barré, L., Frot, D., … Oake, J. (2013). On the size distribution of self-associated asphaltenes. *Energy and Fuels*, *27*(9), 5083–5106. https://doi.org/10.1021/ef400729w

Yarranton, H. W., and Satyro, M. A. (2009). Expanded fluid-based viscosity correlation for

hydrocarbons. *Industrial and Engineering Chemistry Research*, *48*(7), 3640–3648. https://doi.org/10.1021/ie801698h

Yarranton, Harvey W., Van Dorp, J. J., Verlaan, M. L., and Lastovka, V. (2013). Wanted dead or live: Crude-cocktail viscosity-a pseudocomponent method to predict the viscosity of dead oils, live oils, and mixtures. *Journal of Canadian Petroleum Technology*. https://doi.org/10.2118/160314-PA

Yaws, C. L. (2014). Transport Properties of Chemicals and Hydrocarbons: Second Edition. In *Transport Properties of Chemicals and Hydrocarbons: Second Edition*. https://doi.org/10.1016/C2013-0-12644-X

Yazdani, A., Alvestad, J., Kjønsvik, D., Gilje, E., and Kowalewski, E. (2012). A parametric simulation study for solvent-coinjection process in bitumen deposits. *Journal of Canadian Petroleum Technology*. https://doi.org/10.2118/148804-PA

Yazdani, Ali, and Maini, B. B. (2005). Effect of Drainage Height and Grain Size on Production Rates in the Vapex Process: Experimental Study. *SPE Reservoir Evaluation and Engineering*, *8*(3), 205–213. https://doi.org/10.2118/89409-pa

Zéberg-Mikkelsen, C. K., Quiñones-Cisneros, S. E., and Stenby, E. H. (2002). Viscosity Prediction of Natural Gas Using the Friction Theory. *International Journal of Thermophysics*. https://doi.org/10.1023/A:1015126022584

Zhang, J., and Kantzas, A. (2014). Gas recharging process study in heavy oil reservoirs. *Society of Petroleum Engineers - SPE Heavy Oil Conference Canada 2014*.

Zhang, X., and Shaw, J. M. (2007). Liquid-phase mutual diffusion coefficients for heavy oil + light hydrocarbon mixtures. *Petroleum Science and Technology*. https://doi.org/10.1080/10916460500411796

Zhang, Xiaohui, Fulem, M., and Shaw, J. M. (2007). Liquid-phase mutual diffusion coefficients for athabasca bitumen + pentane mixtures. *Journal of Chemical and Engineering Data*. https://doi.org/10.1021/je060234j

Zhao, D. W., Wang, J., and Gates, I. D. (2014). Thermal recovery strategies for thin heavy oil reservoirs. *Fuel*. https://doi.org/10.1016/j.fuel.2013.09.023

Zhao, L. (2004). Steam Alternating Solvent Process (Bakersfield 2004). *SPE International Thermal Operations and Heavy Oil Symposium*.

Zhao, L., Nasr, T. N., Huang, H., Beaulieu, G., Heck, G., and Golbeck, H. (2005). Steam alternating solvent process: Lab test and simulation. *Journal of Canadian Petroleum Technology*.

Zhao, Litong. (2007). Steam alternating solvent process. *SPE Reservoir Evaluation and Engineering*.

APPENDIX A

STATISTICAL ANALYSIS OF EXPERIMENTAL RESULTS

This appendix summarizes the main statistical parameters calculated using the data collected in this thesis. To determine the repeatability in terms of absolute error for a set of pairs of measurements, the standard deviation can be determined from the deviations of the pairs of measurements as follows,

$$s = \sqrt{\frac{\sum_{i=1}^{n}(x_i - \overline{x_\iota})^2}{\nu}} \tag{A.1}$$

where s is the standard deviation, x_i is one of the i^{th} pair of measurements, $\overline{x_\iota}$ is the mean of the i^{th} pair of measurements, and ν is the degree of freedom. To determine the repeatability in terms of relative error for a set of pairs of measurements, the standard deviation can be determined from the relative deviations of the pairs of measurements as follows,

$$s = \sqrt{\frac{\sum_{i=1}^{n}(\frac{x_i - \overline{x_\iota}}{\overline{x_\iota}})^2}{\nu}} \tag{A.2}$$

where s is the standard deviation, x_i is one of the i^{th} pair of measurements, $\overline{x_\iota}$ is the mean of the i^{th} pair of measurements, and ν is the degree of freedom. For a single measurement, the error distribution was assumed to be normal and the confidence interval was calculated as follows:

$$CI = \pm z_{(\alpha/2,\nu)} s \tag{A.3}$$

where CI is the confidence interval and 1-α is the confidence level.

The data for the repeat sets of experiments (R1 to R4) in this thesis are provided in Tables A1 to A7. For the R4 repeats, an error was made in the density and bitumen content measurements for one of the repeats. Hence, R4 was only used to determine the repeatability of the mass flux, bitumen production rate, and cumulative bitumen production. Note that although the runs with initial angle of inclination of 55° (R4) were not included in Chapter 5, they are included here for the determination of the repeatability of the experiments. The 90% confidence intervals are summarized in Table A8.

Table A.1. Bitumen mass flux, production rate, and cumulative bitumen production for two gravity drainage experiments with a gap width of 0.5 mm, initial angle of 35° and toluene flow rate of 0.3 cm³/min (R1).

Time min	Bitumen Mass Flux g/cm²min		Bitumen Prod. Rate g/min		Cum. Bit. Prod. g	
20	0.0108	0.0164	0.0242	0.0166	0.33	0.48
40	0.0135	0.0169	0.0244	0.0207	0.75	0.97
60	0.0137	0.0156	0.0221	0.0206	1.16	1.41
80	0.0124	0.0161	0.0221	0.0186	1.53	1.86
100	0.0129	0.0166	0.0222	0.0191	1.91	2.30
120	0.0128	0.0144	0.0190	0.0187	2.29	2.68
140	0.0131	0.0147	0.0191	0.0188	2.66	3.06
160	0.0124	0.0156	0.0199	0.0175	3.01	3.46
180	0.0131	0.0131	0.0165	0.0183	3.38	3.79
200	0.0114	0.0139	0.0171	0.0158	3.70	4.13
220	0.0119	0.0138	0.0166	0.0162	4.02	4.46
240	0.0123	0.0136	0.0161	0.0166	4.35	4.79

Table A.2. Density and bitumen content of product from two gravity drainage experiments with a gap width of 0.5 mm, initial angle of 35° and toluene flow rate of 0.3 cm³/min (R1).

Time min	Density g/cm³		Bitumen Content wt%	
20	0.8763	0.8787	7.44	9.56
40	0.8777	0.8779	8.53	8.79
60	0.8772	0.8769	8.25	7.94
80	0.8769	0.8780	8.02	9.13
100	0.8769	0.8783	7.80	9.04
120	0.8766	0.8781	7.62	8.63
140	0.8762	0.8774	7.41	8.38
160	0.8761	0.8769	7.24	7.99
180	0.8759	0.8767	7.04	7.83
200	0.8755	0.8763	6.92	7.45
220	0.8753	0.8762	6.72	7.29
240	0.8751	0.8756	6.52	6.85

Table A.3. Bitumen mass flux, production rate, and cumulative bitumen production for two gravity drainage experiments with a gap width of 0.5 mm, initial angle of 35° and toluene flow rate of 1.0 cm³/min (R2).

Time min	Bitumen Mass Flux g/cm²min		Bitumen Prod. Rate g/min		Cum. Bit. Prod. g	
20	0.0167	0.0189	0.0241	0.0269	0.51	0.54
40	0.0180	0.0168	0.0256	0.0233	1.02	1.03
60	0.0169	0.0147	0.0233	0.0191	1.51	1.43
80	0.0164	0.0177	0.0220	0.0224	1.95	1.88
100	0.0156	0.0173	0.0209	0.0224	2.37	2.32
120	0.0154	0.0160	0.0201	0.0193	2.77	2.73
140	0.0147	0.0173	0.0184	0.0192	3.16	3.11
160	0.0157	0.0180	0.0188	0.0190	3.53	3.49
180	0.0152	0.0177	0.0179	0.0180	3.91	3.85
200	0.0151	0.0174	0.0172	0.0173	4.25	4.20
220	0.0147	0.0158	0.0162	0.0155	4.59	4.62
240	0.0208	0.0167	0.0228	0.0160	4.68	4.94

Table A.4. Density and bitumen content of product from two gravity drainage experiments with a gap width of 0.5 mm, initial angle of 35° and toluene flow rate of 1.0 cm³/min (R2).

Time min	Density g/cm³		Bitumen Content wt%	
20	0.8707	0.8714	3.05	3.42
40	0.8706	0.8709	2.92	3.15
60	0.8704	0.8710	2.78	2.69
80	0.8701	0.8708	2.60	3.09
100	0.8700	0.8709	2.46	3.10
120	0.8698	0.8704	2.35	2.70
140	0.8697	0.8702	2.25	2.61
160	0.8696	0.8702	2.15	2.52
180	0.8695	0.8700	2.08	2.41
200	0.8694	0.8698	1.97	2.31
220	0.8693	0.8698	1.88	2.21
240	0.8693	0.8697	1.77	2.07

Table A.5. Bitumen mass flux, production rate, and cumulative bitumen production for two gravity drainage experiments with a gap width of 0.5 mm, initial angle of 55° and toluene flow rate of 1.0 cm³/min (R3).

Time min	Bitumen Mass Flux g/cm²min		Bitumen Prod. Rate g/min		Cum. Bit. Prod. g	
20	0.0241	0.0241	0.0286	0.0318	0.57	0.64
40	0.0182	0.0232	0.0203	0.0286	0.98	1.21
60	0.0218	0.0251	0.0229	0.0289	1.44	1.78
80	0.0220	0.0246	0.0218	0.0266	1.87	2.32
100	0.0216	0.0224	0.0201	0.0231	2.27	2.78
120	0.0218	0.0227	0.0190	0.0221	2.65	3.24
140	0.0216	0.0194	0.0178	0.0177	3.01	3.63
160	0.0228	0.0214	0.0176	0.0183	3.36	4.00
180	0.0230	0.0200	0.0166	0.0160	3.69	4.32
200	0.0236	0.0206	0.0160	0.0157	4.02	4.63
220	0.0233	0.0199	0.0149	0.0147	4.31	4.93
240	0.0243	0.0193	0.0146	0.0136	4.61	5.20

Table A.6. Density and bitumen content of product from two gravity drainage experiments with a gap width of 0.5 mm, initial angle of 55° and toluene flow rate of 1.0 cm³/min (R3).

Time min	Density g/cm³		Bitumen Content wt%	
20	0.8705	0.8718	3.36	3.88
40	0.8705	0.8714	2.36	3.53
60	0.8702	0.8714	2.61	3.54
80	0.8700	0.8709	2.48	3.17
100	0.8700	0.8704	2.38	2.76
120	0.8698	0.8701	2.27	2.88
140	0.8697	0.8698	2.16	2.27
160	0.8696	0.8696	2.06	2.10
180	0.8694	0.8695	1.95	2.00
200	0.8693	0.8694	1.88	1.91
220	0.8692	0.8694	1.77	1.81
240	0.8691	0.8691	1.68	1.69

Table A.7. Bitumen mass flux, production rate, and cumulative bitumen production for two gravity drainage experiments with a gap width of 1.0 mm, initial angle of 35° and toluene flow rate of 0.1 cm³/min (R4).

Time	**Bitumen Mass Flux**		**Bitumen Prod. Rate**		**Cum. Bit. Prod.**	
min	**g/cm²min**		**g/min**		**g**	
90	0.0060	0.0056	0.0149	0.0140	1.34	1.26
180	0.0068	0.0065	0.0157	0.0155	2.75	2.66
270	0.0072	0.0072	0.0160	0.0164	4.20	4.14
360	0.0075	0.0074	0.0162	0.0162	5.65	5.59

Table A.8. Summary of confidence intervals for bitumen mass flux, bitumen production rate, bitumen production rate, product density and bitumen content determined from repeated experiments.

Measurement	**Units**	**R1**	**R2**	**R3**	**R4**	**Average**
Bitumen Mass Flux	g/cm²·min	0.0029	0.0022	0.0030	0.0003	0.0021
Bitumen Production Rate	g/min	0.0030	0.0026	0.0036	0.0005	0.0024
Cumulative Bitumen Produced	%	18.8	3.2	17.5	3.8	10.82
Diluted Bitumen Density	g/cm³	0.0011	0.0006	0.0007	-	0.0008
Bitumen Content	wt%	0.97	0.38	0.54	-	0.63

APPENDIX B

This appendix provides experimental and modeling results of bitumen mass flux, cumulative bitumen production and bitumen profiles from the gravity drainage experiments in this thesis.

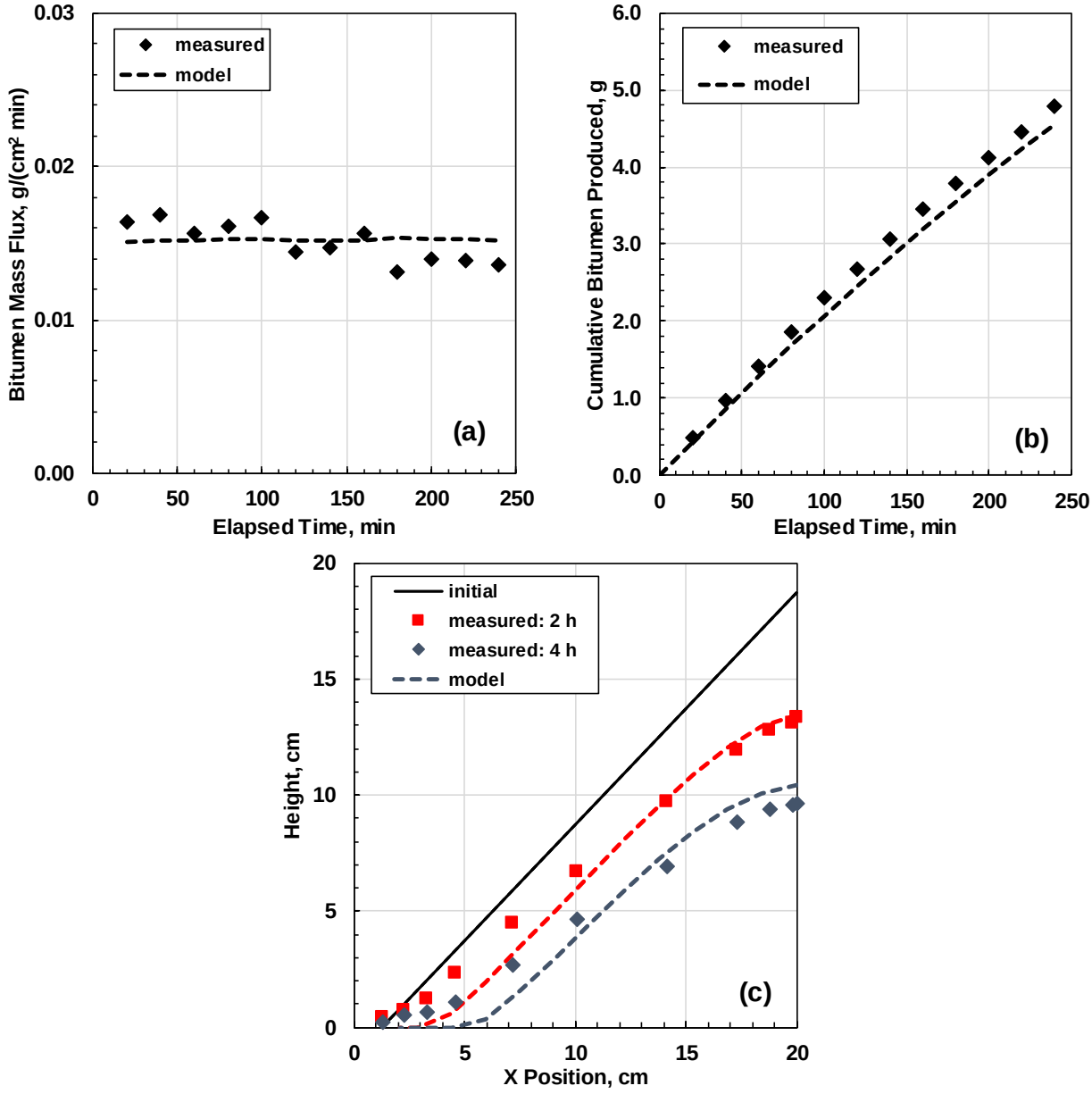

Figure B.1. Measured and modeled gravity drainage experiment with initial angle of inclination 35°, toluene flow rate of 0.3 cm³/min, and gap width of 0.5 mm: a) bitumen mass flux; b) cumulative bitumen production; c) bitumen profile. The repeatabilities of the bitumen flux and height of the bitumen profile were ±0.0026 g/(cm²min) and ±1.7 cm, respectively, based on a 90% confidence interval.

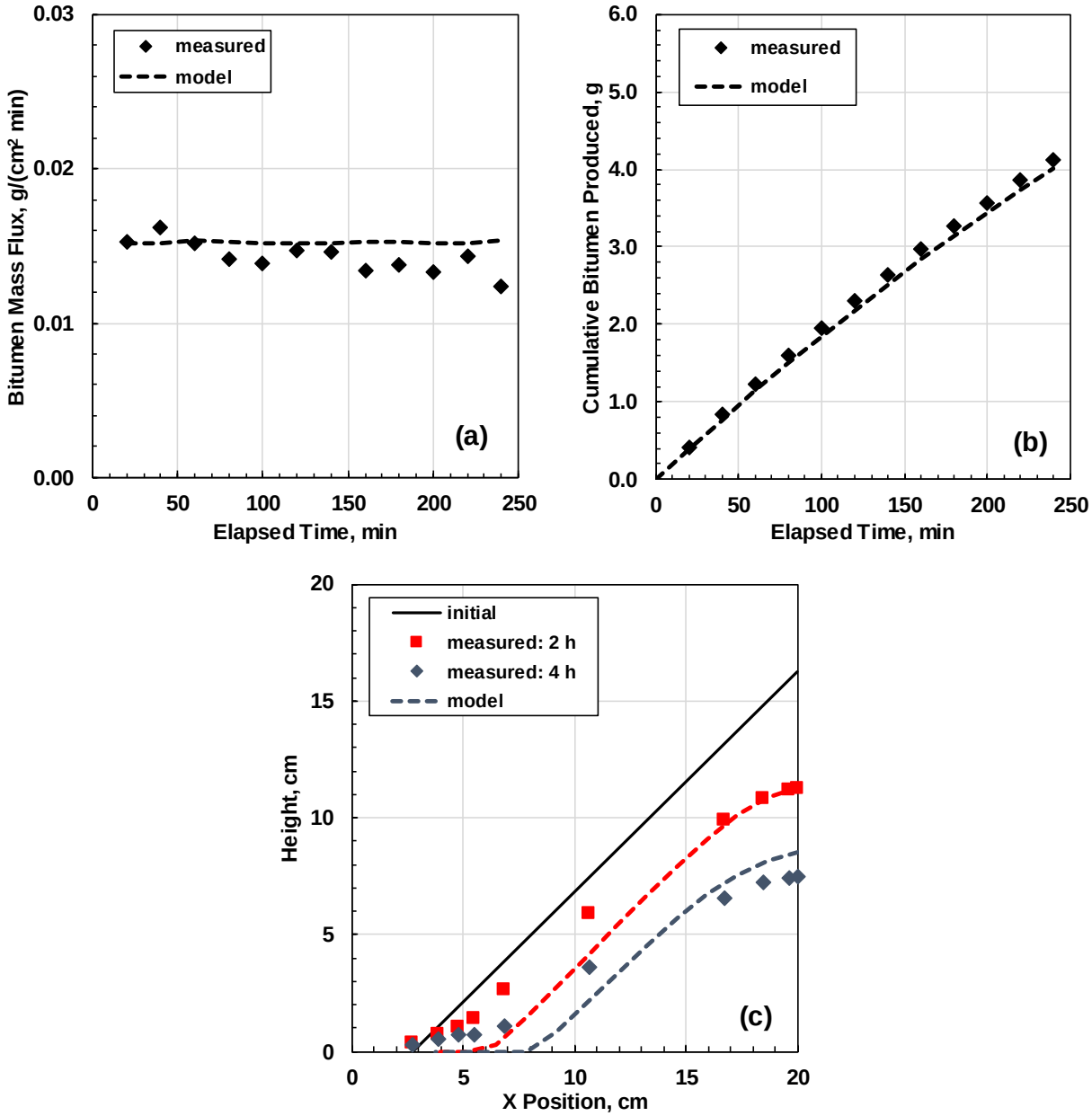

Figure B.2. Measured and modeled gravity drainage experiment with initial angle of inclination 35°, toluene flow rate of 0.5 cm³/min, and gap width of 0.5 mm: a) bitumen mass flux; b) cumulative bitumen production; c) bitumen profile. The repeatabilities of the bitumen flux and height of the bitumen profile were ±0.0026 g/(cm²min) and ±1.7 cm, respectively, based on a 90% confidence interval.

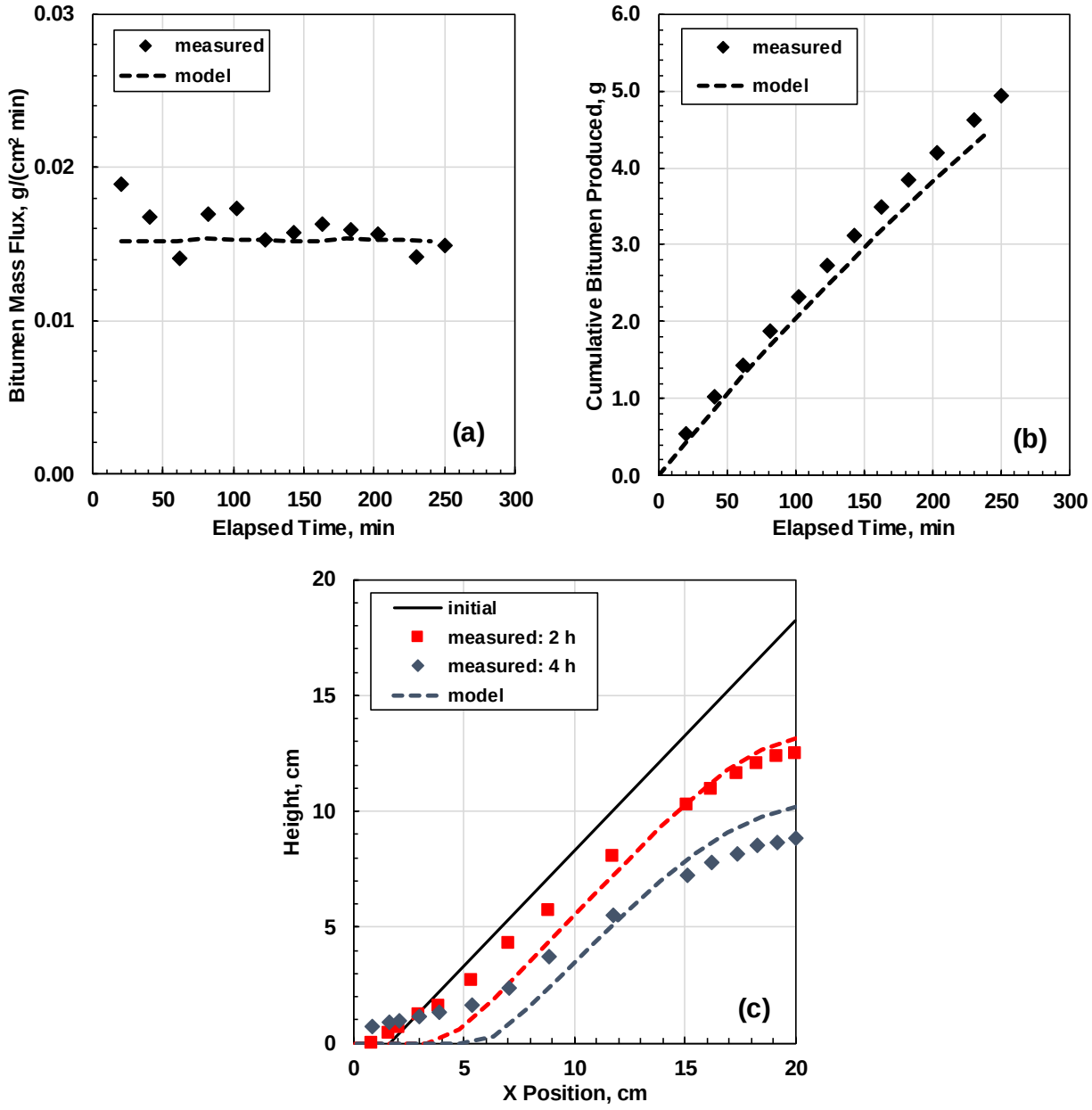

Figure B.3. Measured and modeled gravity drainage experiment with initial angle of inclination 35°, toluene flow rate of 1.0 cm³/min, and gap width of 0.5 mm: a) bitumen mass flux; b) cumulative bitumen production; c) bitumen profile. The repeatabilities of the bitumen flux and height of the bitumen profile were ±0.0026 g/(cm²min) and ±1.7 cm, respectively, based on a 90% confidence interval.

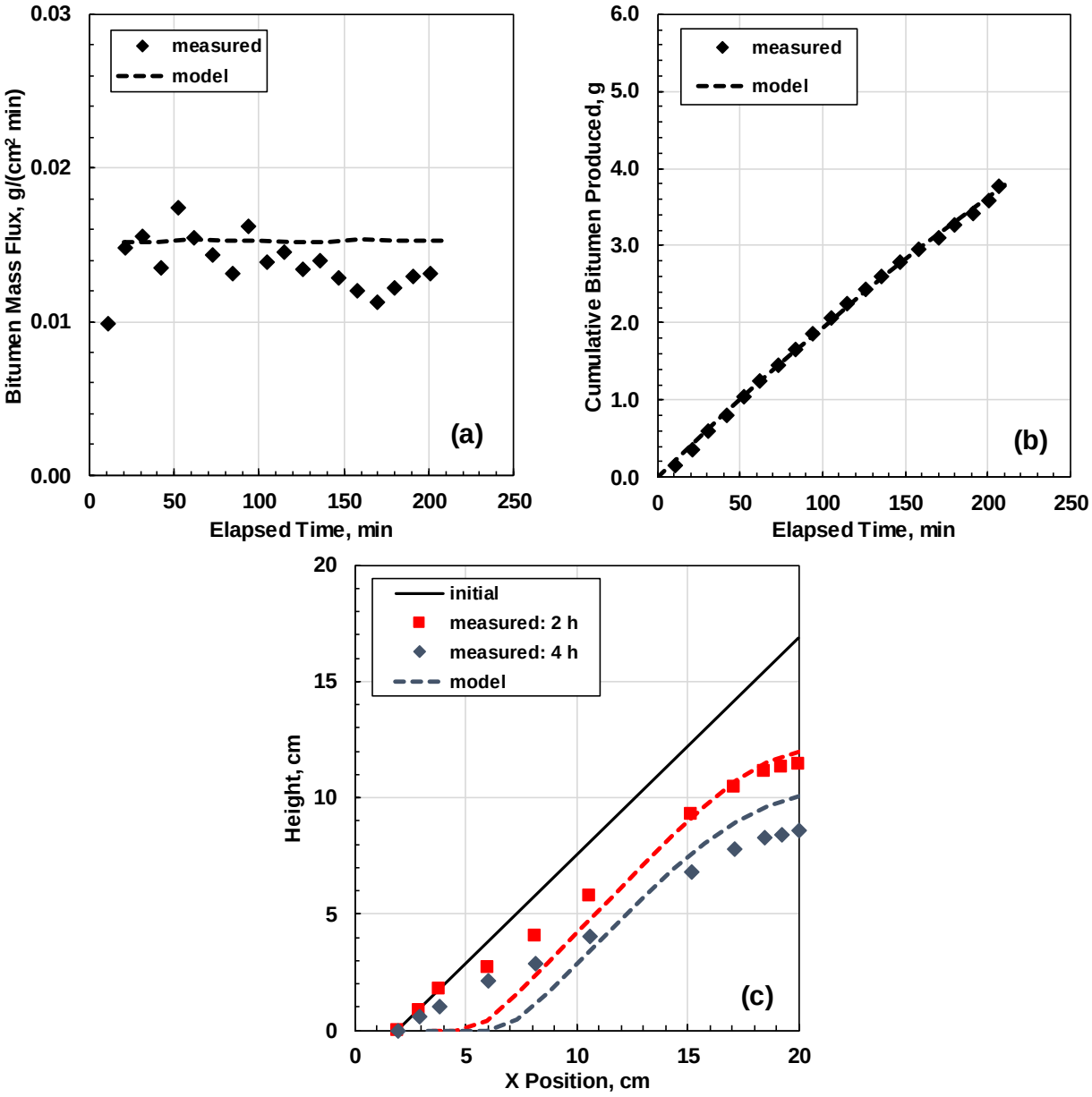

Figure B.4. Measured and modeled gravity drainage experiment with initial angle of inclination 35°, toluene flow rate of 2.0 cm³/min, and gap width of 0.5 mm: a) bitumen mass flux; b) cumulative bitumen production; c) bitumen profile. The repeatabilities of the bitumen flux and height of the bitumen profile were ±0.0026 g/(cm²min) and ±1.7 cm, respectively, based on a 90% confidence interval.

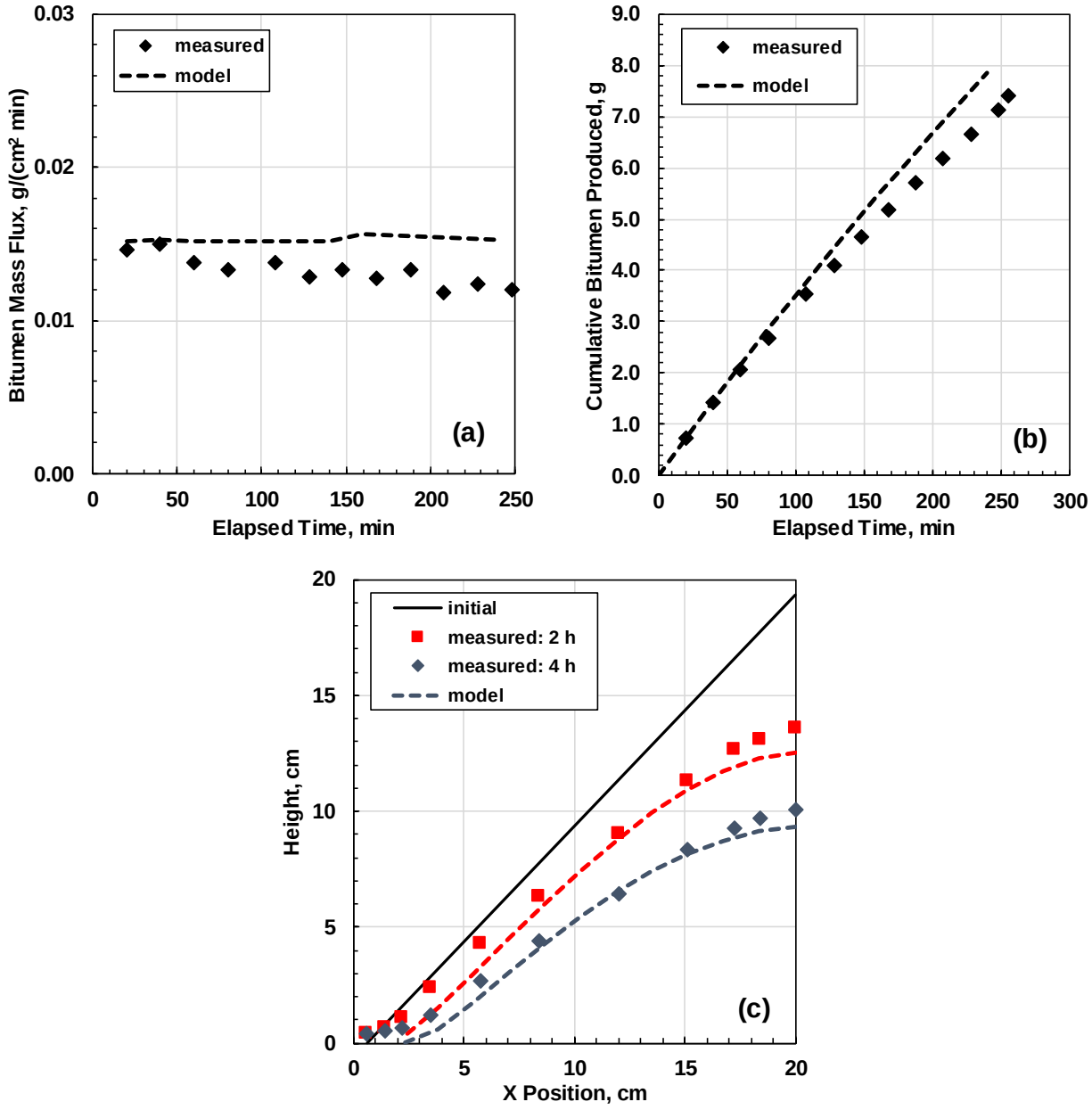

Figure B.5. Measured and modeled gravity drainage experiment with initial angle of inclination 35°, toluene flow rate of 0.3 cm³/min, and gap width of 1.0 mm: a) bitumen mass flux; b) cumulative bitumen production; c) bitumen profile. The repeatabilities of the bitumen flux and height of the bitumen profile were ±0.0026 g/(cm²min) and ±1.7 cm, respectively, based on a 90% confidence interval.

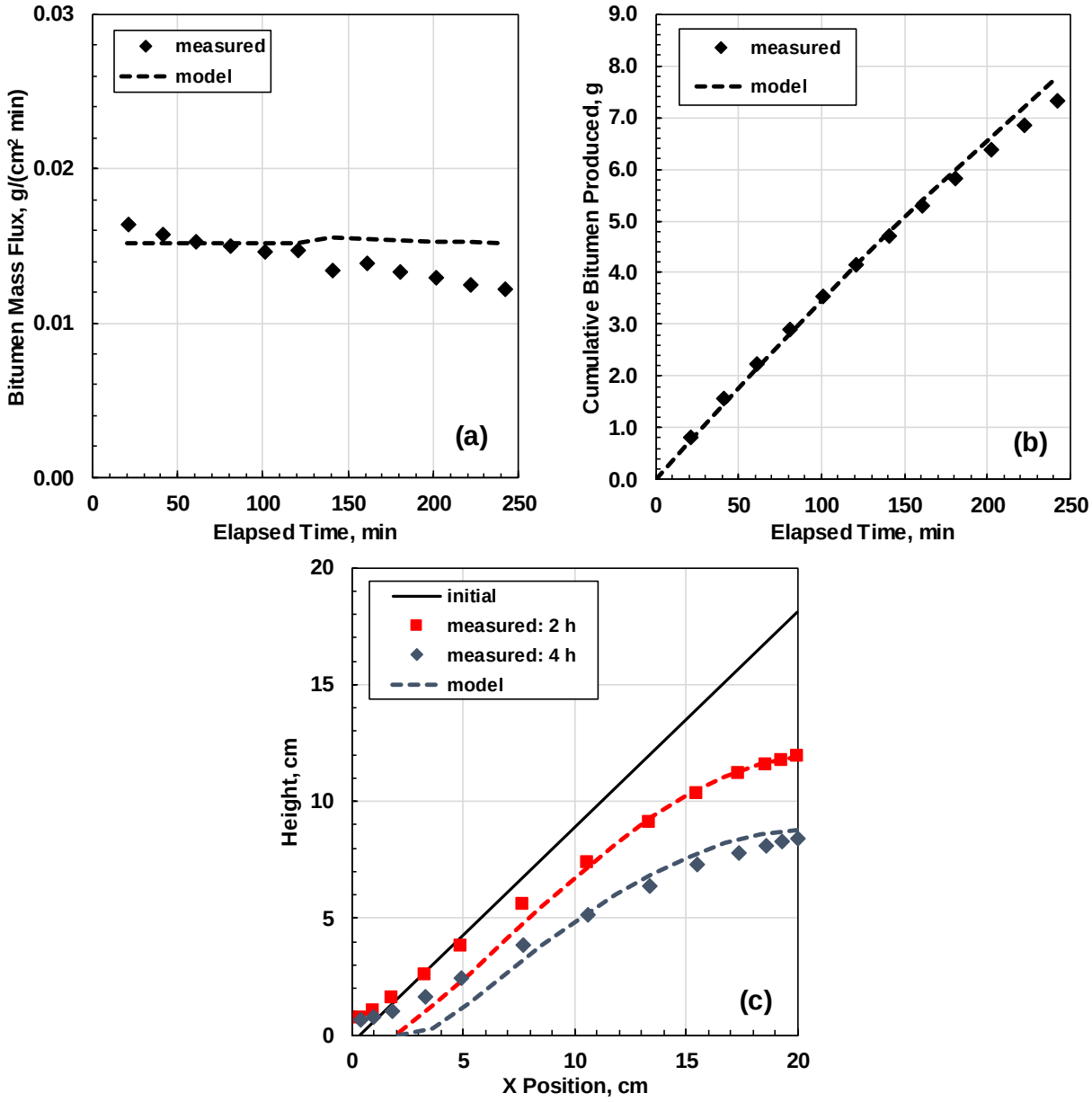

Figure B.6. Measured and modeled gravity drainage experiment with initial angle of inclination 35°, toluene flow rate of 0.5 cm³/min, and gap width of 1.0 mm: a) bitumen mass flux; b) cumulative bitumen production; c) bitumen profile. The repeatabilities of the bitumen flux and height of the bitumen profile were ±0.0026 g/(cm²min) and ±1.7 cm, respectively, based on a 90% confidence interval.

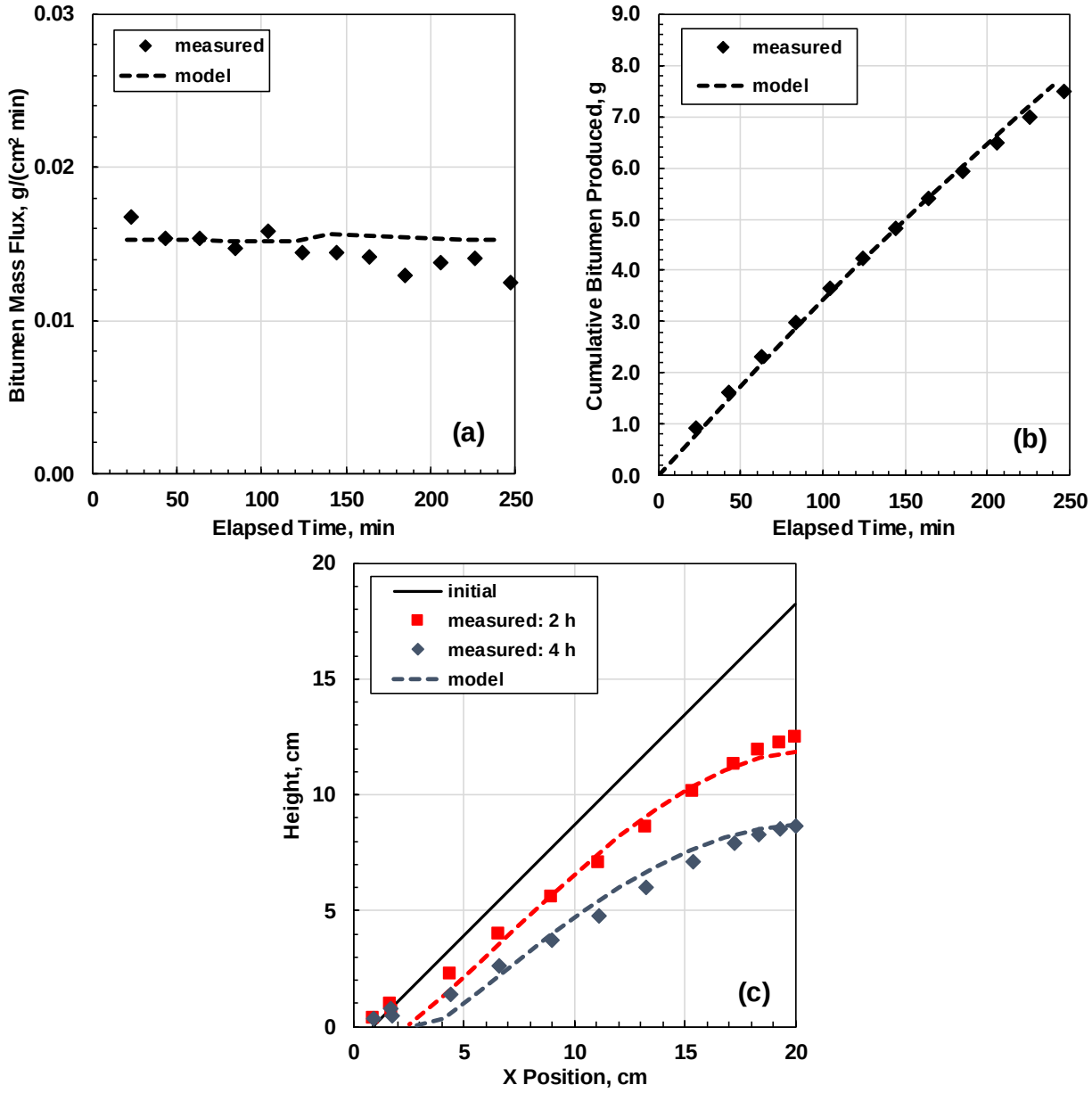

Figure B.7. Measured and modeled gravity drainage experiment with initial angle of inclination 35°, toluene flow rate of 1.0 cm³/min, and gap width of 1.0 mm: a) bitumen mass flux; b) cumulative bitumen production; c) bitumen profile. The repeatabilities of the bitumen flux and height of the bitumen profile were ±0.0026 g/(cm²min) and ±1.7 cm, respectively, based on a 90% confidence interval.

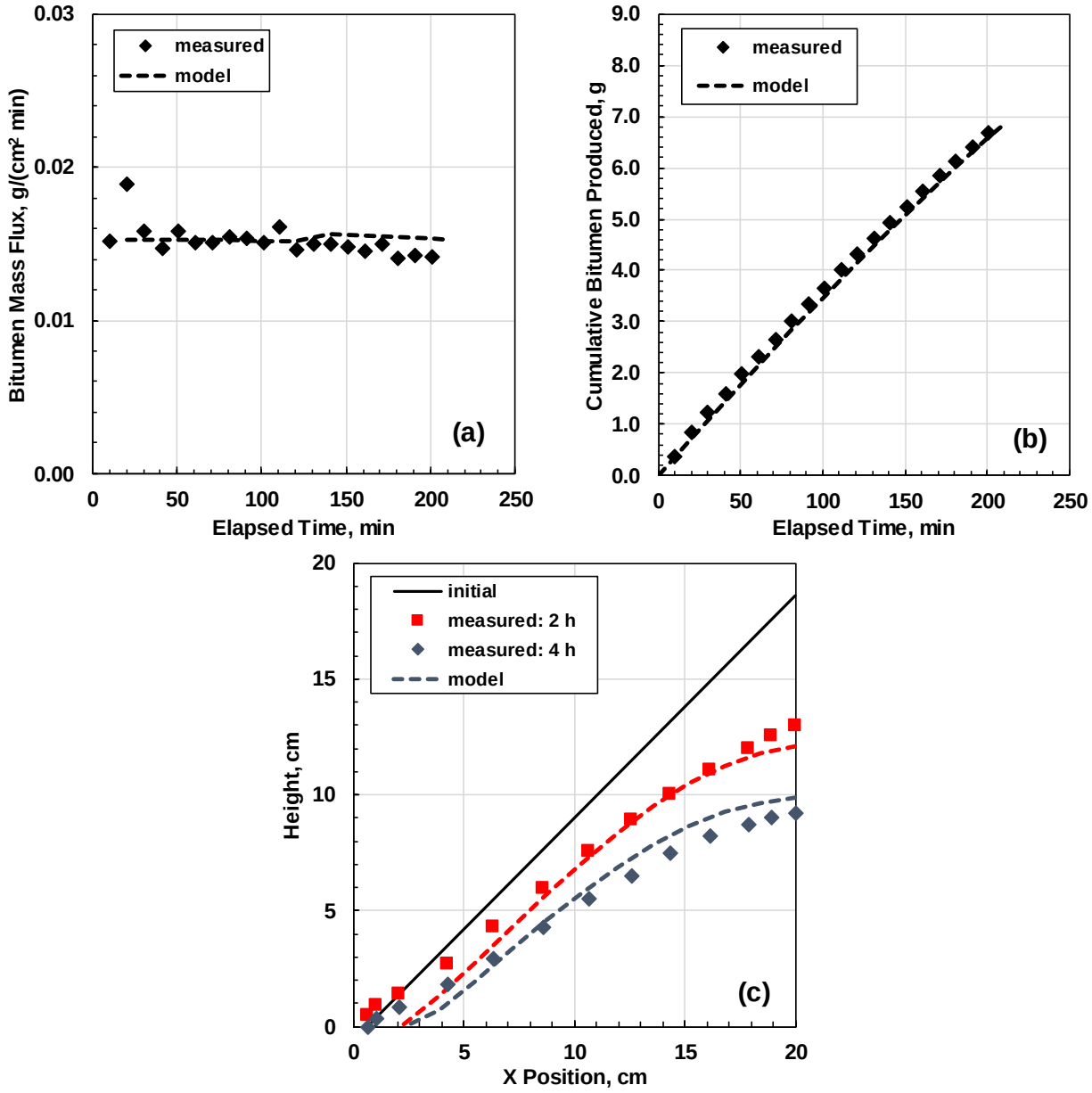

Figure B.8. Measured and modeled gravity drainage experiment with initial angle of inclination 35°, toluene flow rate of 2.0 cm³/min, and gap width of 1.0 mm: a) bitumen mass flux; b) cumulative bitumen production; c) bitumen profile. The repeatabilities of the bitumen flux and height of the bitumen profile were ±0.0026 g/(cm²min) and ±1.7 cm, respectively, based on a 90% confidence interval.